New sources for Kerr and other metrics: rotating relativistic disks with pressure support.

C. Pichon[1,2], **& D. Lynden-Bell**[1]

1 Institute of Astronomy, Madingley Road, Cambridge CB3 0HA
2 CITA,McLennan Labs,University of Toronto,
60 St. George Street,Toronto,Ontario M5S 1A7.

ABSTRACT

Complete sequences of new analytic solutions of Einstein's equations which describe thin super massive disks are constructed. These solutions are derived geometrically. The identification of points across two symmetrical cuts through a vacuum solution of Einstein's equations defines the gradient discontinuity from which the properties of the disk can be deduced. The subset of possible cuts which lead to physical solutions is presented. At large distances, all these disks become Newtonian, but in their central regions they exhibit relativistic features such as velocities close that of light, and large redshifts. Sections with zero extrinsic curvature yield cold disks. Curved sections may induce disks which are stable against radial instability. The general counter rotating flat disk with planar pressure tensor is found. Owing to gravomagnetic forces, there is no systematic method of constructing vacuum stationary fields for which the non-diagonal component of the metric is a free parameter. However, all static vacuum solutions may be extended to fully stationary fields via simple algebraic transformations. Such disks can generate a great variety of different metrics including Kerr's metric with any ratio of a to m. A simple inversion formula is given which yields all distribution functions compatible with the characteristics of the flow, providing formally a complete description of the stellar dynamics of flattened relativistic disks. It is illustrated for the Kerr disk.

keywords: Relativity – methods: analytical – stellar dynamics, disks – quasars
accepted by the Monthly Notices of the Royal Astronomical Society, (1996) **280 (4)**,*1007-1026.*

1. Introduction

The general-relativistic theory of rapidly rotating objects is of great intrinsic interest and has potentially important applications in astrophysics. Following Einstein's early work on relativistic collisionless spherical shells, Fackerell (1968) [10], Ipser (1969) [15] and Ipser & Thorne (1968) [22] have developed the general theory of relativistic collisionless spherical equilibria. The stability of such bodies has been further expanded by Katz (1975) [11]. Here the complete dynamics of flat disk equilibria is developed and illustrated, extending these results to differentially rotating configurations with partial pressure support. A general inversion method for the corresponding distribution functions is presented, yielding a coherent model for the stellar dynamics of these disks. Differentially rotating flat disks in which centrifugal force almost balances gravity can also give rise to relatively long lived configurations with large binding energies. Such objects may therefore correspond to possible models for the latest stage of the collapse of a proto-quasar. Analytic calculations of their structure have been carried into the post Newtonian régime by Chandrasekhar. Strongly relativistic bodies have been studied numerically following the pioneering work on uniformly rotating cold disks by Bardeen & Wagoner [1]. An analytic vacuum solution to the Einstein equations, the Kerr metric [12], which is asymptotically flat and has the general properties expected of an exterior metric

of a rotating object, has been known for thirty years, but attempts to fit an interior solution to its exterior metric have been unsatisfactory. A method for generating families of self-gravitating rapidly rotating disks purely by geometrical methods is presented. Known vacuum solutions of Einstein's equations are used to produce the corresponding relativistic disks. One family includes interior solutions for the Kerr metric.

1.1. Background

In 1919 Weyl [26] and Levi-Civita gave a method for finding all solutions of the axially symmetric Einstein field equations after imposing the simplifying conditions that they describe a static vacuum field. Bìcák, Lynden-Bell and Kalnajs (1993) [3]- - here-after refered as BLK – derived complete solutions corresponding to counter rotating pressure-less axisymmetric disks by matching exterior solutions of the Weyl- Levi-Civita type on each side of the disk. For static metrics, the vacuum solution was obtained via line superposition of fictitious sources placed symmetrically on each side of the disk by analogy with the classical method of images. The corresponding solutions describe two counter-rotating stellar streams. This method will here be generalised, allowing *true rotation* and radial pressure support for solutions describing self-gravitating disks. These solutions provide physical sources (interior solutions) for stationary axisymmetric gravitational fields.

1.1.1. Pressure Support via Curvature

In Newtonian theory, once a solution for the vacuum field of Laplace's equation is known, it is straightforward to build solutions to Poisson's equation for disks by using the method of mirror images. In general relativity, the overall picture is similar. In fact, it was pointed out by Morgan & Morgan (1969) [18] that for pressureless counter rotating disks in Weyl's co-ordinates, the Einstein equation reduces essentially to solving Laplace's equation. When pressure is present, no global set of Weyl co-ordinates exists. The condition for the existence of such a set of co-ordinates is that $T_{RR} + T_{zz} = 0$. On the disk itself, this is satisfied only if the radial eigenvalue of the pressure tensor, p_R, vanishes (T_{zz} vanishes provided the disk is thin). When p_R is non-zero, vacuum co-ordinates of Weyl's type still apply both above and below the disk, but as two separate co-ordinate patches. Consider global axisymmetric co-ordinates (R', ϕ', z') with $z' = 0$ on the disk itself. For $z' > 0$, Weyl's co-ordinates R, ϕ, z may be used. In terms of these variables, the upper boundary of the disk $z' = 0^+$ is mapped onto a given surface $z = f(R)$. On the lower patch, by symmetry, the disk will be located on the surface $z = -f(R)$. Thus in Weyl co-ordinates, the points $z = f(R)$ on the upper surface of the disk must be identified with the points $z = -f(R)$ on the lower surface. The intrinsic curvature of the two surfaces that are identified match by symmetry. The jump in the extrinsic curvature gives the surface distribution of stress-energy on the disk. A given metric of Weyl's form is a solution of the empty space Einstein equations, and does not give a complete specification of its sources (for example, a Schwarzschild metric of any given mass can be generated by a static spherical shell of any radius). With this method, all physical properties of the source are entirely characterised once it is specified that the source lie on the surface $z = \pm f(R)$ and the corresponding extrinsic curvature (i.e. its relative layout within the embedding vacuum spacetime) is known. The freedom of choice of ν in the Weyl metric corresponds to the freedom to choose the density of the disk as a function of radius. The supplementary degree of freedom involved in choosing the surface of section $z = f(R)$ corresponds classically to the choice of the radial pressure profile.

1.1.2. Rotating Disks

For rotating disks, the dragging of inertial frames induces strongly non-linear fields outside the disk which prohibit the construction of a vacuum solution by superposition of the line densities of fictitious sources. nevertheless, in practise quite a few vacuum stationary solutions have been given in the literature, the most famous being the Kerr metric. Hoenselaers, Kinnersley & Xanthopoulos (1979) [13,14](HKX hereafter) have also given a discrete method of generating rotating solutions from known static Weyl solutions. The disks are derived by taking a cut through such a field above all singularities or sources and identifying it with a symmetrical cut through a reflection of the source field. This method applies directly to the non-linear fields such as those generated by a rotating metric of the Weyl-Papapetrou type describing stationary axisymmetric vacuum solutions. The analogy with electromagnetism is then to consider the field associated

with a known azimuthal vector potential A_ϕ, the analog of $g_{t\phi}/g_{tt}$. The jump in the tangential component of the corresponding B-field gives the electric current in the plane, just as the jump in the t,ϕ component of the extrinsic curvature gives the matter current.

The procedure is then the following: for a given surface embedded in curved space-time and a given field outside the disk, the jump in the extrinsic curvature on each side of the mirror images of that surface is determined in order to specify the matter distribution within the disk. The formal relationship between extrinsic curvatures and surface energy tensor per unit area was introduced by Israel and is described in details by Misner Thorne Wheeler (1973) p 552. [19] Plane surfaces and non-rotating vacuum fields (*i.e.*the direct counterpart of the classical case) were investigated by BLK and led to pressureless counter-rotating disks. Any curved surface will therefore produce disks with some radial pressure support. Any vacuum metric with $g_{t\phi} \neq 0$ outside the disk will induce rotating disks.

Figure 1.1: Symbolic representation of a section $z = \pm f(R)$ through the $g_{t\phi}$ field representing the upper and lower surface of the disk embedded in two Weyl-Papapetrou fields. The isocontours of $\omega(R,z)$ correspond to a measure of the amount of rotation in the disk.

In section 2, the construction scheme for rotating disks with pressure support is presented. In section 3, the properties of these disks are analysed, and a reasonable cut, $z = f(R)$, is suggested. Section 4 describes stellar equilibria which have the corresponding anisotropic stress energy tensors, while section 5 derives the properties of the limiting counter-rotating disks. This method is then first applied to warm counter rotating disks in section 6; the dominant energy condition given for Curzon disks by Chamorow *et. al.*(1987) [5], and Lemos ' solution for the self - similar Mestel disk with pressure support are recovered. In section 7, the Kerr disk is studied and the method for producing general HKX disks is sketched.

2. Derivation

The jump in extrinsic curvature of a given profile is calculated and related to the stress energy tensor of the matter distribution in the corresponding self gravitating relativistic disk.

2.1. The Extrinsic Curvature

The line element corresponding to an axisymmetric stationary vacuum gravitational field is given by the Weyl-Papapetrou (WP) metric

$$ds^2 = -\,e^{2\,\nu}\,(dt - \omega\,d\phi)^2 + e^{2\,\zeta - 2\,\nu}\,\left(dR^2 + dz^2\right) + R^2 e^{-2\,\nu}\,d\phi^2, \tag{2.1}$$

where (R,ϕ,z) are standard cylindrical co-ordinates, and ν, ζ and ω are functions of (R,z) onlygeometric units $G = c = 1$ are used throughout this paper. Note that this form is explicitly symmetric under simultaneous change of ϕ and t. The vacuum field induces a natural metric on a 3-space-like $z = f(R)$ surface

$$\begin{aligned} d\,\sigma^2 = g_{\alpha\beta}\,\frac{\partial x^\alpha}{\partial x^a}\frac{\partial x^\beta}{\partial x^b}dx^a dx^b &\equiv g_{\alpha\beta}\,h^\alpha_a h^\beta_b\,dx^a dx^b, \\ &\equiv \gamma_{ab}\,dx^a\,dx^b, \end{aligned} \tag{2.2}$$

where $\{x^a\}$ are the co-ordinates on the embedded hypersurface $z = f(R)$, $\{x^a\} = (t,R,\phi)$, and $\{x^\alpha\} = (t,R,z,\phi)$ are Weyl's co-ordinates for the embedding spacetime. Here, γ_{ab} stands for the embedded metric, and h^α_a is given by

$$h^\alpha_a = \frac{\partial x^\alpha}{\partial x^a} = \begin{bmatrix} 1 & 0 & 0 & 0 \\ 0 & 1 & 0 & f' \\ 0 & 0 & 1 & 0 \end{bmatrix}, \tag{2.3}$$

where hereafter a prime, $(\ )'$, represents the derivative with respect to R. The line element is then

$$d\sigma^2 = -\,e^{2\,\nu}\,(dt-\omega\,d\phi)^2 + R^2 e^{-2\,\nu} d\phi^2 + e^{2\,\zeta-2\,\nu}\,\left(1+f'^2\right)\,dR^2. \tag{2.4}$$

Let the upward pointing normal N_μ to the surface $z=f(R)$ be

$$N_\mu = \frac{\partial}{\partial x^\mu}\left[z-f\,(R)\right] = (0,-f',0,1)\,. \tag{2.5}$$

The normalised normal is therefore

$$n_\mu = \frac{N_\mu}{\sqrt{N_\alpha N^\alpha}} = \frac{N_\mu}{\sqrt{g^{\alpha\beta}N_\beta N_\alpha}} = \frac{N_\mu}{\sqrt{1+f'^2}} e^{\zeta-\nu}. \tag{2.6}$$

The extrinsic curvature tensor K is given in its covariant form by

$$K_{ab} = n_\mu\left(\partial_a h^\mu_b + \Gamma^\mu_{\alpha\,\beta}\,h^\alpha_a\,h^\beta_b\right), \tag{2.7}$$

where $\partial_a h^\mu_b = \partial h^\mu_b/\partial x^a$. Eq. (2.6) and (2.3) together with the Christoffel symbols for the Weyl metric lead to the computation of K , the extrinsic curvature of that surface embedded in the Weyl Papapetrou metric:

$$K_{tt} = -\frac{e^{\nu-\zeta}}{\sqrt{1+f'^2}}\left(\frac{\partial\nu}{\partial N}\right)e^{4\nu-2\zeta}, \tag{2.8a}$$

$$K_{RR} = -\frac{e^{\nu-\zeta}}{\sqrt{1+f'^2}}\left(\frac{f''}{1+f'^2}+\frac{\partial\,(\nu-\zeta)}{\partial N}\right)\left(1+f'^2\right), \tag{2.8b}$$

$$K_{\phi t} = -\frac{e^{\nu-\zeta}}{\sqrt{1+f'^2}}\left[\frac{\partial\left[\nu+\frac{1}{2}\log(\omega)\right]}{\partial N}\right]\omega e^{4\nu-2\zeta}, \tag{2.8c}$$

$$K_{\phi\phi} = -\frac{e^{\nu-\zeta}}{\sqrt{1+f'^2}}\left[\left(\frac{f'}{R}+\frac{\partial\nu}{\partial N}\right)R^2 e^{-2\zeta}+e^{4\nu-2\zeta}\omega^2\frac{\partial\left[\nu-\log(\omega)\right]}{\partial N}\right], \tag{2.8d}$$

where the notation $\partial/\partial N \equiv (\partial/\partial z - f'\partial/\partial R)$ has been used.

2.2. The Stress Energy Tensor

The stress energy tensor per unit surface τ^a_b is the integral of of the stress energy tensor carried along the normal to the surface $z=f(R)$. In a locally Minkowskian frame co-moving with the mean flow of the disk, the corresponding orthonormal tetrad is

$$e^{(0)}_i = e^\nu\,(1,0,-\omega)\,, \tag{2.9a}$$

$$e^{(1)}_i = e^{\zeta-\nu}\sqrt{1+f'^2}\,(0,1,0)\,, \tag{2.9b}$$

$$e^{(2)}_i = Re^{-\nu}\,(0,0,1)\,, \tag{2.9c}$$

so that

$$d\,s^2 = \eta_{(a)(b)}\left(e^{(a)}_i d\,x^i\right)\left(e^{(b)}_j d\,x^j\right), \tag{2.10}$$

with $\eta_{(a)(b)} = \mathrm{Diag}(-1,1,1)$. In that frame,

$$\left[\tau^{(a)(b)}\right]_0 = \begin{bmatrix}\varepsilon & 0 & 0\\ 0 & p_{_R} & 0\\ 0 & 0 & p_\phi\end{bmatrix}. \tag{2.11}$$

After a Lorentz transformation to a more general frame in which the flow is rotating with relative velocity V in the ϕ direction, this stress becomes

$$\tau^{(a)(b)} = \frac{1}{1-V^2}\begin{bmatrix}\varepsilon+p_\phi V^2 & 0 & (p_\phi+\varepsilon)\,V\\ 0 & \left(1-V^2\right)p_{_R} & 0\\ (p_\phi+\varepsilon)\,V & 0 & p_\phi+\varepsilon V^2\end{bmatrix}. \tag{2.12}$$

2.3. The Discontinuity Equations

Israel (1964) [16] has shown that Einstein's equations integrated through a given surface of discontinuity can be re-written in terms of the jump in extrinsic curvature, namely

$$\tau_b^a = \frac{1}{8\pi}\,[K_b^a - K_a^a\,\delta_b^a]_-^+ \equiv \mathcal{L}_b^a. \tag{2.13}$$

where $[\quad]_-^+$ stands for $(\quad)$ taken on $z = f(R)$ minus $(\quad)$ taken on $z = -f(R)$. This tensor $\mathcal{L}_b^a$ is known as the Lanczos tensor.

In the tetrad frame (2.9), the Lanczos tensor given by Eqs. (2.13) and (2.8) reads

$$\mathcal{L}^{(a)(b)} = \frac{e^{\nu-\zeta}}{4\pi\sqrt{1+f'^2}} \begin{bmatrix} \frac{f''}{1+f'^2} + \frac{f'}{R} + \frac{\partial(2\nu-\zeta)}{\partial N} & 0 & \frac{\partial\omega}{\partial N}\frac{e^{2\nu}}{2R} \\ 0 & -\frac{f'}{R} & 0 \\ \frac{\partial\omega}{\partial N}\frac{e^{2\nu}}{2R} & 0 & -\frac{f''}{1+f'^2} + \frac{\partial\zeta}{\partial N} \end{bmatrix}. \tag{2.14}$$

Identifying the stress energy tensor $\tau^{(a)(b)}$ with the tetrad Lanczos tensor $\mathcal{L}^{(a)(b)}$ according to Eq. (2.13), and solving for $p_{_R}\,, p_\phi\,, \varepsilon$ and V yields

$$V = \frac{R\,e^{-2\nu}}{\partial\omega/\partial N}\left[\left(\frac{f'}{R} + 2\frac{\partial\nu}{\partial N}\right) - Q\right], \tag{2.15a}$$

$$\varepsilon = \frac{e^{\nu-\zeta}}{4\pi\sqrt{1+f'^2}}\left[\frac{Q}{2} + \left(\frac{f''}{1+f'^2} + \frac{f'}{2R} + \frac{\partial\,(\nu-\zeta)}{\partial N}\right)\right], \tag{2.15b}$$

$$p_\phi = \frac{e^{\nu-\zeta}}{4\pi\sqrt{1+f'^2}}\left[\frac{Q}{2} - \left(\frac{f''}{1+f'^2} + \frac{f'}{2R} + \frac{\partial\,(\nu-\zeta)}{\partial N}\right)\right], \tag{2.15c}$$

$$p_{_R} = \frac{e^{\nu-\zeta}}{4\pi\sqrt{1+f'^2}}\left(\frac{-f'}{R}\right), \tag{2.15d}$$

where

$$Q \equiv \sqrt{\left(\frac{f'}{R} + 2\frac{\partial\nu}{\partial N}\right)^2 - \frac{e^{4\nu}}{R^2}\left(\frac{\partial\omega}{\partial N}\right)^2}. \tag{2.16}$$

All quantities are to be evaluated along $z = f(R)$. Eq. (2.15) gives the form of the most general solution to the relativistic rotating thin disk problem provided the expressions for $\varepsilon, p_\phi, p_{_R}$ are physically acceptable.

3. Physical properties of the warm disks

Physical properties of interest for these disks are derived and related to the choice of profile $z = f(R)$ compatible with their dynamical stability.

Defining the circumferential radius R_c, proper radial length $\tilde{R}$, and a synchronised proper time τ_* by

$$R_c = R\,e^{-\nu}\,, \tag{3.1a}$$

$$\tilde{R} = \int \sqrt{1+f'^2}\,e^{\zeta-\nu}\,dR\,, \tag{3.1b}$$

$$\tau_* = \int_{(\mathcal{T})} e^{\nu}\left(1 - \omega\frac{d\phi}{dt}\right)dt\,, \tag{3.1c}$$

where the integral over dR is performed at $z = f(R)$ and that over dt is performed along a given trajectory $(\mathcal{T})$, the line element on the disk (2.4) reads

$$d\,\sigma^2 = -\not{d}\tau_*^2 + d\tilde{R}^2 + R_c^2 d\phi^2. \tag{3.2}$$

For circular flows ($\not{d}\tau_* = e^\nu[1-\omega d\phi/dt]\,dt$), V may be re-written as

$$V = R_c\,\frac{d\phi}{\not{d}\tau_*}. \tag{3.3}$$

Equation (3.3) is inverted to yield the angular velocity of the flow as measured at infinity:

$$\Omega \equiv \frac{d\phi}{dt} = \frac{Ve^\nu/R_c}{1+\omega Ve^\nu/R_c}. \tag{3.4}$$

Similarly, the covariant specific angular momentum h of a given particle reads in terms of these variables

$$h \equiv \frac{p_\phi}{\mu} = \gamma_{t\,\phi}u^t + \gamma_{\phi\,\phi}u^\phi = \frac{1}{\sqrt{1-V^2}}\left(R_cV + \omega\, e^\nu\right), \tag{3.5}$$

where μ is the rest mass of the particle. The covariant specific energy ϵ of that particle reads

$$\epsilon \equiv -\frac{p_t}{\mu} = -\gamma_{t\,\phi}u^\phi - \gamma_{t\,t}u^t = \frac{e^\nu}{\sqrt{1-V^2}}\,. \tag{3.6}$$

which gives the central redshift, $1+z_c = \exp(-\nu)$. The velocity of zero angular momentum observers (so called ZAMOs) follows from Eq. (3.5):

$$V_z = -\frac{\omega e^\nu}{R_c}\,. \tag{3.7}$$

With these observers, the cuts $z = f(R)$ may be extended inside ergoregions where the dragging of inertial frames induces apparent superluminous motions as measured by locally static observers. The circumferential radius R_z as measured by ZAMOs is Lorentz contracted with respect to R_c, becoming

$$R_z \equiv \sqrt{g_{\phi\phi}} = R_c\left[1-V_z^2\right]^{1/2}, \tag{3.8}$$

while the velocity flow measured by ZAMOs is

$$V_{/z} = \frac{V-V_z}{1-VV_z}\,. \tag{3.9}$$

The total angular momentum of the disk H follows from the asymptotic behaviour of the vacuum field ω at large radii, $\omega \to -2H/r$. Define the binding energy of the disk ΔE as the difference between the baryonic rest mass M_0 and the total mass-energy of the disk M as measured from infinity given by $\nu \to -M/r$:

$$\Delta E = M_0 - M. \tag{3.10}$$

M is also given by the Tolman formula, but corresponds, by construction, to the mass of the line source for the vacuum field. The baryonic rest mass can be expressed as

$$M_0 \equiv \int \Sigma\,\sqrt{-g}\,U^\mu dS_\mu = \int \frac{\left[1-\omega\Omega\right]^{-1}}{\sqrt{1-V^2}}\,\Sigma\,2\pi R_c d\tilde{R}\,, \tag{3.11}$$

where the baryonic energy density Σ can be related to the energy density ε through some yet unspecified equation of state or the knowledge of a distribution function.

3.1. Constraints on the internal solutions

The choice of the profile $z = f(R)$ is open, provided that it leads to meaningful physical quantities. Indeed it must lead to solutions which satisfy $\varepsilon \geq 0$, $p_{_R} \geq 0$, $p_\phi \geq 0$, and $V \leq 1$ while the dominant energy condition implies also that $\varepsilon \geq p_\phi$ and $\varepsilon \geq p_{_R}$. These translate into the following constraints on f

$$\varepsilon \geq 0 \quad \Rightarrow \quad \sqrt{\mathcal{N}^2 - \mathcal{O}^2} + (\mathcal{N} - 2\mathcal{Z}) \geq 0\,; \tag{3.12a}$$

$$0 \leq V \leq 1 \quad \Rightarrow \quad \mathcal{N} \geq \mathcal{O} \text{ and } \mathcal{O} \geq 0\,; \tag{3.12b}$$

$$0 \leq p_\phi \leq \varepsilon \quad \Rightarrow \quad 4\mathcal{Z}\,\mathcal{N} \geq \left(\mathcal{O}^2 + 4\mathcal{Z}^2\right) \text{ and } \mathcal{N} \geq 2\mathcal{Z}\,; \tag{3.12c}$$

$$0 \leq p_{_R} \leq \varepsilon \quad \Rightarrow \quad f' \leq 0 \text{ and } -2f'/R \leq \sqrt{\mathcal{N}^2 - \mathcal{O}^2} + (\mathcal{N} - 2\mathcal{Z})\,; \tag{3.12d}$$

given

$$\mathcal{N} \equiv \frac{f'}{R} + 2\frac{\partial \nu}{\partial N}\,, \quad \mathcal{O} \equiv \frac{e^{2\nu}}{R}\frac{\partial \omega}{\partial N}\,, \quad \text{and} \quad \mathcal{Z} \equiv \left(\frac{\partial \zeta}{\partial N} - \frac{f''}{1+f'^2}\right)\,. \tag{3.13}$$

The existence of a solution satisfying this set of constraints can be demonstrated as follows: in the limit of zero pressure and counter-rotation (*i.e.* $\mathcal{O} \to 0, \mathcal{N} \to 2\partial\nu/\partial z$, and $\mathcal{Z} \to \partial\zeta/\partial z$), any cut $z = \text{Const} \equiv b \gg m$ satisfies Eqs. (3.12). By continuity, there exist solutions with proper rotation and partial pressure support. In practise, all solutions given in sections 6 and 7 satisfy the constraints (3.12). Note that in the limit of zero radial pressure, Eq. (3.12*b*) implies $\partial/\partial z\,[\omega/R + \exp 2\nu] \leq 0$.

3.2. Ansatz for the profile

In the following discussion, the section $z = f(R)$ is chosen so that the corresponding radial pressure gradient balances a given fraction of the gravitational field which would have occurred had there been no radial pressure within the disk. This choice 'bootstraps' calculations for all relevant physical quantities in terms of a single degree of freedom (*i.e.* this fraction η), rather than a complete functional. This gives

$$\frac{\partial p_{_R}}{\partial \tilde{R}} = -\frac{\eta}{(1-V^2)}\frac{\partial \nu}{\partial \tilde{R}}\left[\varepsilon + p_{_R} + V^2\,(p_\phi - p_{_R})\right]\,. \tag{3.14}$$

On the r.h.s. of Eq. (3.14), $p_{_R}$ is put to zero and V, p_ϕ, ε are re-expressed in terms of ζ, ν, ω via Eqs. (2.15) with $f' = f'' = 0$ and $z = \text{Const}$. On the l.h.s. of Eq. (3.14), $p_{_R}$ is chosen according to Eq. (2.15*d*). In practise, this Ansatz for f is a convenient way to investigate a parameter space which is likely to be stable with respect to ring formation as discussed in the next subsection. In principle, a cut, f, could be chosen so as to provide a closed bounded symmetrical surface containing all fictitious sources. Indeed, by symmetry no flux then crosses the $z = 0$ plane beyond the cut, and the energy distribution is therefore bound to the edge of that surface: this corresponds to a finite pressure supported disk. It turns out that in general this choice is not compatible with all the constraints enumerated in the previous section. More specifically, the positivity of p_ϕ fails for all finite disk models constructed. The Ansatz described above gives for instance an upper bound on the height of that surface when assuming that all the support is provided by radial pressure. This height is in turn not compatible with positive azimuthal pressure at all radii.

3.3. Stability

To what extent are the equilibria studied in the previous sections likely to be stable under the action of disturbances? The basic instabilities can be categorised as follows:

dynamical instabilities, which are intrinsic to the dynamical parameters of the disks, grow on an orbital time scale, and typically have drastic effects on the structure of the system.

secular instabilities, which arise owing to dissipative mechanisms such as viscosity or gravitational radiation, grow on a time scale which depends on the strength of the dissipative mechanism involved, and slowly drive the system along a sequence of dynamical equilibria.

Amongst dynamical instabilities, kinematical instabilities correspond to the instability of circular orbits to small perturbations, and collective instabilities arises from the formation of growing waves triggered by the self-gravity of the disk. Rings, for instance, will be generated spontaneously in the disk if the local radial pressure is insufficient to counteract the self-gravity of small density enhancements. Even dynamically stable non-axisymmetric modes may drive the system away from its equilibrium by radiation of gravitational waves which will slowly remove angular momentum from the disk. For gaseous disks, viscosity and photon pressure will affect the equilibria. Radiative emission may disrupt or broaden the disk if the radiation pressure exceeds the Eddington limit. The energy loss by viscosity may induce a radial flow in the disk. However, the disks discussed in this paper have anisotropic pressures inappropriate for gaseous disks and the accurate description of the latter two processes requires some prescription for the dissipative processes in the gas. The scope of this section is therefore restricted to a simple analysis of the dynamical instabilities.

Turning briefly to the corresponding Newtonian problem, Toomre (1963) [24] gave the local criterion for radial collective instability of stellar disks,

$$\sigma_{_R} \geq \frac{3.36 G \Sigma_0}{\kappa}, \tag{3.15}$$

where Σ_0 is the local surface density, σ_R^2 the radial velocity dispersion, and κ the epicyclic frequency of the unperturbed stars. This criterion is derived from the first critical growing mode of the dispersion relation for radial waves. The corresponding critical wavelength is Jeans length $\sim\ 2\sigma_R^2/G\Sigma_0$.

For the relativistic disks described in this paper, spacetime is locally flat, which suggests a direct translation of Eq. (3.15) term by term. The constraints that stability against ring formation places on these models will then be addressed at least qualitatively via the Newtonian approach. The proper relativistic analysis is left to further investigation. The relativistic surface density generalising Σ_0 is taken to be the co-moving energy density ε given by Eq. (2.15b). The radial velocity dispersion $\sigma_{_R}^2$ is approximated by $p_{_R}/\varepsilon$. The epicyclic frequency is calculated in the appendix. Putting Eqs. (D.4) and (D.5) into Eq. (3.15) give another constraint on f for local radial stability of these disks. Note that the kinematical stability of circular orbits follows from Eq. (D.3) by requiring κ^2 to be positive.

4. Stellar dynamical equilibria for rotating super-massive disks

The method described in section 2 will generally induce rotating disks with anisotropic pressures ($p_\phi \neq p_R$). These objects may therefore be described in the context of stellar dynamics. It should be then checked that there exist a stellar equilibria compatible with a given vacuum field and a given cut $z = f(R)$.

4.1. Distribution functions for rotating super-massive disks

Here a general procedure to derive all distribution functions corresponding to a specified stress energy tensor is presented for disks with non-zero mean rotation (a more direct derivation for counter-rotating disk is given in Appendix B). The detailed description of the dynamics of the disk follows.
In Vierbein components, the stress energy tensor reads

$$T^{(\alpha\beta)} = \int\int \frac{f_\star\left(\epsilon,h\right)\, P^{(\alpha)}\, P^{(\beta)}}{P^{(t)}}\, dP^{(R)} dP^{(\phi)}\,, \tag{4.1}$$

where $f_\star(\epsilon,h)$ is the distribution of stars at position R,ϕ with momentum $P^{(R)}, P^{(\phi)}$. For a stationary disk, it is a function of the invariant of the motion ϵ, h. Now for the line element (2.4):

$$d\sigma^2 = -\, e^{2\,\nu}\left(dt - \omega\, d\phi\right)^2 + e^{2\,\zeta - 2\,\nu}\, \left(1 + f'^2\right)\, dR^2 + R^2 e^{-2\,\nu}\, d\phi^2, \tag{4.2}$$

the Vierbein momenta read

$$P^{(\phi)} = e^{\nu}\, R^{-1}\left(h - \omega\,\epsilon\right)\,, \tag{4.3a}$$
$$P^{(t)} = e^{-\nu}\,\epsilon\,, \tag{4.3b}$$
$$P^{(R)} = \left[\epsilon^2 e^{-2\nu} - e^{2\nu}\, R^{-2}\, \left(h - \omega\,\epsilon\right)^2 - 1\right]^{1/2}\,. \tag{4.3c}$$

Calling $\chi = h/\epsilon$ and $\vartheta = 1/\epsilon^2$, Eqs. (4.3) becomes

$$P^{(\phi)} = e^{\nu}\, R^{-1}\, \vartheta^{-1/2}\, \left(\chi - \omega\right)\,, \tag{4.4a}$$
$$P^{(t)} = e^{-\nu}\, \vartheta^{-1/2}\,, \tag{4.4b}$$
$$P^{(R)} = \vartheta^{-1/2}\, \left[e^{-2\nu} - e^{2\nu}\, R^{-2}\, \left(\chi - \omega\right)^2 - \vartheta\right]^{1/2}\,. \tag{4.4c}$$

In terms of these new variables, the integral element $dP^{(\phi)} dP^{(R)}$ becomes

$$dP^{(\phi)} dP^{(R)} = \left|\frac{\partial P^{(\phi)}\, \partial P^{(R)}}{\partial\chi\, \partial\vartheta}\right| d\chi\, d\vartheta = \frac{e^{-\nu} R^{-1}\, \vartheta^{-2}\, d\chi\, d\vartheta}{2\sqrt{e^{-2\nu} - e^{2\nu}\, R^{-2}\, \left(\chi - \omega\right)^2 - \vartheta}}\,. \tag{4.5}$$

Given Eq. (4.5) and Eq. (4.3b), Eq. (4.1) may be rewritten as

$$T^{(\alpha\beta)} = \int\int P^{(\alpha)}\, P^{(\beta)}\, \frac{f_\star\left(\epsilon,h\right)\, R^{-1}\, \vartheta^{-3/2}\, d\chi\, d\vartheta}{2\sqrt{e^{-2\nu} - e^{2\nu}\, R^{-2}\, \left(\chi - \omega\right)^2 - \vartheta}}\,. \tag{4.6}$$

In particular,

$$R\, T^{(tt)}\, e^{2\nu} = \int\int \frac{f_\star\left(\epsilon,h\right)\, \vartheta^{-5/2}\, d\chi\, d\vartheta}{2\sqrt{e^{-2\nu} - e^{2\nu}\, R^{-2}\, \left(\chi - \omega\right)^2 - \vartheta}}\,, \tag{4.7a}$$
$$R^2\, T^{(t\phi)} = \int\int \left(\chi - \omega\right)\, \frac{f_\star\left(\epsilon,h\right)\, \vartheta^{-5/2}\, d\chi\, d\vartheta}{2\sqrt{e^{-2\nu} - e^{2\nu}\, R^{-2}\, \left(\chi - \omega\right)^2 - \vartheta}}\,, \tag{4.7b}$$
$$R^3\, T^{(\phi\phi)}\, e^{-2\nu} = \int\int \left(\chi - \omega\right)^2\, \frac{f_\star\left(\epsilon,h\right)\, \vartheta^{-5/2}\, d\chi\, d\vartheta}{2\sqrt{e^{-2\nu} - e^{2\nu}\, R^{-2}\, \left(\chi - \omega\right)^2 - \vartheta}}\,. \tag{4.7c}$$

Note that given Eqs. (4.7), $T^{(RR)}$ follows from the equation of radial support. Note also that

$$R_c\left(T^{(tt)} - T^{(\phi\phi)} - T^{(RR)}\right) = \int\int \frac{f_\star\left(\epsilon,h\right)\, e^{-\nu}\, \vartheta^{-3/2}\, d\chi\, d\vartheta}{2\sqrt{e^{-2\nu} - e^{2\nu}\, R^{-2}\, \left(\chi - \omega\right)^2 - \vartheta}}\,, \tag{4.8}$$

or equivalently,

$$T^{(tt)} - T^{(\phi\phi)} - T^{(RR)} = \int\int \frac{f_\star(\epsilon, h)}{P^{(t)}}\, dP^{(\phi)}\, dP^{(R)}\,. \tag{4.9}$$

Equation (4.9) yields the total gravitating mass. It is known as Tolman's formulae and can be derived directly from the relation $P^\mu P_\mu = -1$ and Eq. (4.1).
Let

$$F(\chi, R) = \frac{1}{2}\int \frac{f_\star(\epsilon, h)\,\vartheta^{-5/2}\,d\vartheta}{\sqrt{e^{-2\nu} - e^{2\nu}\,R^{-2}\,(\chi-\omega)^2 - \vartheta}} = \int_1^{\mathcal{Y}} \frac{f_*(\chi,\vartheta)\;d\vartheta}{2\sqrt{\mathcal{Y}-\vartheta}}\,, \tag{4.10}$$

$$\text{where}\quad f_*(\chi,\vartheta) = f_\star(\epsilon,h)\,\vartheta^{-5/2}\,,\quad \text{and}\quad \mathcal{Y}(R,\chi) = e^{-2\nu} - e^{2\nu}\,R^{-2}\,(\chi-\omega)^2\,. \tag{4.11}$$

The set of Eqs. (4.7) becomes

$$R\,T^{(tt)}\,e^{2\nu} = \int F(\chi,R)\;d\chi = Re^{-2\nu}\int \bar{F}(v_\phi,R)\;dv_\phi\,, \tag{4.12a}$$

$$R^2\,T^{(t\phi)} = \int F(\chi,R)\;(\chi-\omega)\;d\chi = R^2e^{-4\nu}\int v_\phi\,\bar{F}(v_\phi,R)\;dv_\phi\,, \tag{4.12b}$$

$$R^3\,T^{(\phi\phi)}\,e^{-2\nu} = \int F(\chi,R)\;(\chi-\omega)^2\;d\chi = R^3e^{-6\nu}\int v_\phi^2\,\bar{F}(v_\phi,R)\;dv_\phi\,. \tag{4.12c}$$

The *r.h.s* of Eqs. (4.12) was re-expressed convinienlty in terms of the new variable $v_\phi \equiv e^\nu(\chi-\omega)/R_c$, and the new function $\bar{F}(v_\phi,R) \equiv F(\chi = R_c v_\phi e^{-\nu}+\omega, R)$ in order to stress the analogy with the classical identities. Note that in the limit of zero pressures, v_ϕ reduces to V, the geodesic velocity of stars on circular orbits. In Eq. (4.12), the dragging of inertial frames requires to fix simultaneously three moments of the velocity distribution to account for the given energy density, pressures and rotation law. This third constraint does not hold in the corresponding Newtonian problem, nor for static relativistic disks as described in appendix B. Any positive function $F(\chi,R)$ satisfying the moment constraints Eqs. (4.12) corresponds to a possible choice. For instance the parametrisation is carried in Appendix C for $\bar{F}$ distributions corresponding to powers of Lorentzians in azimuthal momenta. Let $\tilde{F}(\chi,\mathcal{Y}) = F(\chi,R)$, where $\mathcal{Y}(R,\chi)$ is given by Eq. (4.11). Written in terms of $\tilde{F}$, the integral equation Eq. (4.10) is solved for f_* by an Abel transform

$$f_*(\chi,\vartheta) = \frac{2}{\pi}\int_1^{\vartheta}\left(\frac{\partial\tilde{F}}{\partial\mathcal{Y}}\right)_\chi \frac{d\mathcal{Y}}{\sqrt{\vartheta-\mathcal{Y}}}\,. \tag{4.13}$$

The latter integration may be carried in R space and yields

$$f_\star(\epsilon,h) = \frac{2}{\epsilon^4\pi}\int_{\mathcal{R}_e}^{\mathcal{R}_p}\left(\frac{\partial F}{\partial R}\right)_\chi \frac{dR}{\sqrt{-\left(P^{(R)}\right)^2}} - \frac{2}{\epsilon^4\pi}\int_{\mathcal{R}_a}^{\infty}\left(\frac{\partial F}{\partial R}\right)_\chi \frac{dR}{\sqrt{-\left(P^{(R)}\right)^2}}\,, \tag{4.14}$$

where $P^{(R)}$ is given by Eq. (4.3*c*) as a function of R, ϵ, and h. Here F is chosen to satisfy Eq. (4.12) which specifies the stress energy components $T^{(\alpha\beta)}$. The integration limits correspond to two branches: the first branch is to be carried between $\mathcal{R}_e(h)$, the inner radius of a star on a "parabolic" orbit with momentum h, and $\mathcal{R}_p(h,\epsilon)$, the perigee of a star with invariants (h,ϵ); the second branch contributes negatively to Eq. (4.14) and corresponds to radii larger than $\mathcal{R}_a(h,\epsilon)$, the apogee of a star with invariants (h,ϵ). Note that the derivative in Eq. (4.14) is taken at constant reduced momentum $\chi = h/\epsilon$. This inversion procedure is illustrated on Fig. 7.5. All properties of the flow follow in turn from $f_\star(\epsilon,h)$. For instance, the rest mass surface density, Σ, may be evaluated from the detailed "microscopic" behaviour of the stars, leading to an estimate of the binding energy of the stellar cluster.

Figure 4.1: sketch for the effective potential $Y(R)$ as a function of radius. The horizontal line corresponds to the energy level $1/\epsilon^2$, the absisse line corresponds to the escape energy $1/\epsilon^2 = 1$. The ordinate axis corresponds to $\mathcal{R}_e(h,\epsilon)$, the inner radius of a star on a "parabolic" orbit with momentum h, the left vertical line corresponds to $\mathcal{R}_p(h,\epsilon)$, the perigee of a star with invariants (h,ϵ); the right vertical line corresponds to $\mathcal{R}_a(h,\epsilon)$, the apogee of a star with invariants (h,ϵ). The area between the curve $Y = Y(R)$ and the lines $Y = 1/\epsilon^2$ and $R = \mathcal{R}_e$ are shaded, defining three regions from left to right. The middle region does not contribute to Eq. (4.14). The equation $Y = 1/\epsilon^2$ has two roots corresponding to $\mathcal{R}_p(h,\epsilon)$ and $\mathcal{R}_a(h,\epsilon)$, while $Y = 1$ has two roots corresponding to infinity and $\mathcal{R}_e$. The sign of the slope of $Y(R)$ gives the sign of the contribution for each branch in Eq. (4.14).

4.2. A simple equation of state

An equation of state for these rotating disks with planar anisotropic pressure tensors is alternatively found directly while assuming (somewhat arbitrarily) that the fluid corresponds to the superposition of two isotropic flows going in opposite directions. In other words, the anisotropy of the pressures measured in the frame co-moving with the mean flow V is itself induced by the counter rotation of two isotropic streams. (These counter rotating streams are described in more details in the next section.) In each stream, it is assumed that the pressure is isotropic and that the energy is exchanged adiabatically between each volume element. The detailed derivation of the corresponding relationship between the surface density and the pressure of each stream is given in Appendix A. The above set of assumption yields the following prescription for Σ :

$$\Sigma = \frac{\varepsilon - p_\phi - p_{_R} + \sqrt{(\varepsilon - p_\phi - p_{_R})\,(\varepsilon - p_\phi + 3p_{_R})}}{2\sqrt{1-V_0^2}}, \tag{4.15}$$

where $V_0 = \sqrt{(p_\phi - p_{_R})/(\varepsilon + p_{_R})}$ is the counter rotating velocity measured in the frame co-moving with V which induces $p_\phi \neq p_{_R}$. In the classical limit, $\Sigma \to (\varepsilon - p_\phi)/\sqrt{1-V_0^2}$. The binding energy of these rotating disks is computed from Eq. (4.15) together with Eqs. (3.11) and (2.15).

5. Application: warm counter-rotating disks

For simplicity, warm counter-rotating solutions are presented first, avoiding the non-linearities induced by the dragging of inertial frames. These solutions generalise those of BLK, while implementing partial pressure support within the disk. Formally this is achieved by putting $\omega(R,z)$ identically to zero in Eq. (4.2); the metric for the axisymmetric static vacuum solutions given by Weyl is then recovered:

$$ds^2 = -e^{2\,\nu}\,dt^2 + e^{2\,\zeta - 2\,\nu}\,\left(dR^2 + dz^2\right) + R^2\,e^{-2\,\nu}d\phi^2, \tag{5.1}$$

where the functions $\zeta(R,z)$ and $\nu(R,z)$ are generally of the form (cf. Eq. (BLK 2.21))

$$\nu = -\int \frac{W\,(b)\;db}{\sqrt{R^2 + (|z| + b)^2}}, \tag{5.2a}$$

$$\zeta = \int\int W\,(b_1)\,W\,(b_2)\,Z\,(b_1,b_2)\;db_1\,db_2, \tag{5.2b}$$

with Z given by

$$Z = -\frac{1}{2r_1r_2}\left\{1 - \left(\frac{r_2 - r_1}{b_2 - b_1}\right)^2\right\} \geq 0\,. \tag{5.3}$$

Here b_1 and b_2 are the distances of two points below the disk's center and r_1 and r_2 are the distances measured from these points to a point above the disk. Below the disk, Z is given by reflection with respect

to the plane $z = 0$. When the line density of fictitious sources is of the form $W(b) \propto b^{-m}$ (Kuzmin-Toomre), or $W(b) \propto \delta^{(m)}(b)$ (Kalnajs-Mestel), the corresponding functions ζ, ν have explicitly been given in Bìcák, Lynden-Bell & Pichon (1994) [4]. For the metric of Eq. (5.1), the Lanczos tensor (2.14) reads

$$\begin{bmatrix} \mathcal{L}^{(t)(t)} \\ \mathcal{L}^{(R)(R)} \\ \mathcal{L}^{(\phi)(\phi)} \end{bmatrix} = \frac{e^{\nu-\zeta}}{4\pi\sqrt{1+f'^2}} \begin{bmatrix} \frac{f''}{1+f'^2} + \frac{f'}{R} + \frac{\partial(2\nu-\zeta)}{\partial N} \\ \frac{-f'}{R} \\ \frac{-f''}{1+f'^2} + \frac{\partial\zeta}{\partial N} \end{bmatrix}. \tag{5.4}$$

Consider again counter-rotating disks made of two equal streams of stars circulating in opposite directions around the disk center. The stress energy tensor is then the sum of the stress energy tensor of each stream:

$$\tau^{(a)(b)} = \begin{bmatrix} \varepsilon & 0 & 0 \\ 0 & p_{_R} & 0 \\ 0 & 0 & p_\phi \end{bmatrix} = \frac{2}{1-V_0^2} \begin{bmatrix} \varepsilon_0 + p_0\, V_0^2 & 0 & 0 \\ 0 & \left(1-V_0^2\right) p_0 & 0 \\ 0 & 0 & p_0 + \varepsilon_0 V_0^2 \end{bmatrix}, \tag{5.5}$$

the pressure p_0 in each stream being chosen to be isotropic in the plane. Subscript $(\quad)_0$ represents quantities measured for one stream. Expressions for ε, p_ϕ and $p_{_R}$ follow from identifying Eqs. (5.5) and (5.4) according to Eq. (2.13). Solving for ε_0, V_0, and p_0 in Eq. (5.5), given Eq. (5.4) and (2.13) gives

$$\varepsilon_0 = \frac{e^{\nu-\zeta}}{4\pi\sqrt{1+f'^2}} \left[\frac{f''}{1+f'^2} + \frac{\partial\left(\nu-\zeta\right)}{\partial N}\right], \tag{5.6a}$$

$$p_0 = \frac{e^{\nu-\zeta}}{8\pi\sqrt{1+f'^2}} \left[\frac{-f'}{R}\right], \tag{5.6b}$$

$$V_0^2 = \left(\frac{\partial\zeta}{\partial N} - \frac{f''}{1+f'^2} + \frac{f'}{R}\right) \left(\frac{f''}{1+f'^2} + \frac{\partial\left(2\nu-\zeta\right)}{\partial N}\right)^{-1}. \tag{5.6c}$$

The above solution provides the most general counter rotating disk model with pressure support. Indeed, any physical static disk will be characterised entirely by its vacuum field ν and its radial pressure profile $p_{_R}$, which in turn defines $W(b)$ and $f(R)$ uniquely according to Eqs. (5.6b) and (BLK 2.33). The other properties of the disk are then readily derived.

The angular frequency and angular momentum of these disks follow from Eq. (3.5), (3.4) on putting ω to zero and V to V_0. The epicyclic frequency κ given by Eq. (D.4) may be recast as

$$\kappa^2 = \frac{e^\nu}{R_c^3} \frac{dh^2}{d\tilde{R}}, \tag{5.7}$$

which relates closely to the classical expression $\kappa^2 = R^{-3} dh^2/dR$.

The Ansatz given by Eq. (3.14) for $z = f(R)$ becomes, after the substitutions $\varepsilon \to \varepsilon_0$, $V \to V_0$, $p_\phi \to 0$,

$$\left(f'/R\right)' = -\eta \frac{\partial\nu}{\partial R} \left[\frac{\partial\nu}{\partial z} - \frac{1}{2}\frac{\partial\zeta}{\partial z}\right], \tag{5.8a}$$

$$= \eta \frac{\partial\nu}{\partial R}\frac{\partial\nu}{\partial z} \left[R\frac{\partial\nu}{\partial R} - 1\right], \tag{5.8b}$$

where z is to be evaluated at b. Equation (5.8b) follows from Eq. (5.8a) given the $\binom{R}{z}$ component of the Einstein equation outside the disk.

The equation of state for a relativistic isentropic 2D flow of counter-rotating identical particles is derived in appendix A while relating the perfect fluid stress energy tensor of the flow to the most probable distribution function which maximises the Boltzmann entropy. It reads

$$\varepsilon_0 = 2\, p_0 + \frac{\Sigma}{1 + p_0/\Sigma}. \tag{5.9}$$

Solving for Σ gives

$$\Sigma = \frac{1}{2}\left[\varepsilon_0 - 2\,p_0 + \sqrt{\varepsilon_0 - 2\,p_0}\,\sqrt{\varepsilon_0 + 2\,p_0}\right], \tag{5.10}$$

which in the classical limit gives $\Sigma \to \varepsilon_0 - p_0$. The binding energy of these counter rotating disks is computed here from Eq. (5.10) together with Eqs. (3.11) and (5.6). Alternatively, it could be computed by constructing distribution functions using the inversion described in Appendix B.

6. Examples of warm counter-rotating disks

6.1. Example 1 : The Self-similar disk

The symmetry of the self-similar disk allows one to reduce the partial differential equations corresponding to Einstein's field equations to an ordinary differential equation with respect to the only free parameter $\theta = \arctan(R/z)$ (Lemos, 89 [17]) . Lemos' solution may be recovered and corrected by the method presented in sections 2 and 4. Weyl's metric in spherical polar co-ordinates (ρ, χ, ϕ) defined in terms of (R, z, ϕ) by $\rho = \sqrt{(}R^2 + z^2)$ and $\cot(\chi) = z/R$ is

$$d\sigma^2 = -e^{2\nu}d\tau^2 + \rho^2\left[e^{-2\nu}\,\sin^2(\chi)\,d\phi^2 + e^{2\zeta-2\nu}\left(\frac{d\rho}{\rho^2}^2 + d\chi^2\right)\right]. \tag{6.1}$$

A self-similarity argument led Lemos to the metric

$$ds^2 = -r^{2n}e^N dt^2 + r^{2k}\left[e^{2P-N}\,d\phi^2 + e^{Z-N}\left(\frac{dr}{r^2}^2 + d\theta^2\right)\right], \tag{6.2}$$

where P, N, and Z are given by

$$P(\theta) = \log\left[\sin(k+n)\;\theta\right], \tag{6.3a}$$

$$N(\theta) = \frac{4n}{k+n}\log\left[\cos(k+n)\;\theta/2\right], \tag{6.3b}$$

$$Z(\theta) = \frac{8n^2}{(k+n)^2}\log\left[\cos(k+n)\;\theta/2\right] + 2\log(k+n). \tag{6.3c}$$

Here the ϕ's in both metrics have already been identified since they should in both case vary uniformly in the range $[0, 2\pi[$. The rest of the identification between the two metrics follows from the transformation

$$\chi = (n+k)\;\theta, \tag{6.4a}$$

$$\rho = r^{n+k}, \tag{6.4b}$$

$$\tau = t, \tag{6.4c}$$

with the result that ν and ζ take the form:

$$2\nu = N + 2n\log(r), \tag{6.5a}$$

$$2\zeta = Z - 2\log(n+k). \tag{6.5b}$$

This can be written in terms of the new variables given in Eqs. (6.4) as

$$\zeta = \frac{4n^2}{(k+n)^2}\log\left(\frac{\chi}{2}\right), \tag{6.6a}$$

$$\nu = \frac{2n}{(k+n)^2}\log\left(\frac{\chi}{2}\right) + \frac{n}{k+n}\log(\rho). \tag{6.6b}$$

The procedure described earlier may now be applied. In order to preserve the self-similarity of the solution and match Lemos' solution, $f(R)$ is chosen so that

$$f'(R) = \text{const.} = \cot(\bar{\eta}) \quad \text{say.} \tag{6.7}$$

Then

$$\frac{\partial}{\partial N} \equiv \left(\frac{\partial}{\partial z} - f' \frac{\partial}{\partial R} \right) = -\frac{1}{\rho \sin(\bar{\eta})} \frac{\partial}{\partial \bar{\eta}}. \tag{6.8}$$

Putting Eqs. (6.6) and Eq. (6.8) into Eq. (2.15) gives

$$\begin{bmatrix} \varepsilon \\ p_{_R} \\ p_\phi \end{bmatrix} = \frac{r^{-k}}{4\pi} \left[\cos\left(\frac{\bar{\eta}}{2}\right) \right]^{\frac{2n(k-n)}{(k+n)^2}} \begin{bmatrix} \cot(\bar{\eta}) + \frac{2n\,k}{(k+n)^2} \tan(\eta/2) \\ -\cot(\bar{\eta}) \\ \frac{2n^2}{(k+n)^2} \tan(\bar{\eta}/2) \end{bmatrix}, \tag{6.9}$$

with $\bar{\eta}$ to be evaluated at $(n+k)\,\pi/2$. The above equations are in accordance with the solution found by Lemos by directly integrating the Einstein field equations.

6.2. Example 2: The Curzon disk

Figure 6.1: the "Toomre Q number" $Q = \sigma_{_R}\kappa/(3.36\Sigma_0)$ is plotted here as a function of circumferential radius R_c for different compactness parameter $\alpha = b/M$ when $\eta = 1/25$.

The Curzon disk is characterised by the following pair of Weyl functions:

$$\nu = -\alpha/r, \qquad \zeta = -\alpha^2 R^2/\left(2\,r^4\right), \tag{6.10}$$

with $r = \sqrt{R^2 + f^2}$, given the dimensionless parameter $\alpha = M/b$ (recall that $G \equiv c \equiv 1$), all lengths being expressed in units of b. This disk is the simplest example of the Kuzmin-Toomre family, where $W(b) \propto \delta(b)$. It also corresponds to the building block of the expansion given in Eqs. (5.2). Equations (5.4) and (5.5) then imply

Figure 6.2: the binding energy over the rest mass $\Delta E/M_0$ for Curzon disks, plotted against the compactness parameter $\alpha = b/M$ for different ratios p_0/ε_0 fixed by $\eta = 0.01, 0.16, \cdots, 0.7$.

$$\begin{bmatrix} \varepsilon \\ p_{_R} \\ p_\phi \end{bmatrix} = \frac{e^{-\frac{\alpha}{r}\left(1-\frac{\alpha\,R^2}{2r^3}\right)}}{4\pi b\sqrt{1+f'^2}} \begin{bmatrix} \frac{f''}{1+f'^2} + \frac{f'}{R} + \frac{\alpha}{r^6}\left\{2f\left(r^3 - \alpha\,R^2\right) + \left[\alpha\left(R^2 - f^2\right) - 2r^3\right] Rf'\right\} \\ \frac{-f'}{R} \\ -\frac{f''}{1+f'^2} + \frac{\alpha^2}{r^6}\left[2R^2 f - \left(R^2 - f^2\right) Rf'\right] \end{bmatrix}. \tag{6.11}$$

The weak energy conditions $\varepsilon \geq 0$, $\varepsilon + p_{_R} \geq 0$, and $\varepsilon + p_\phi \geq 0$ which follow are in agreement with those found by Chamorow *et al.*(1987) [5]. Their solution was derived by direct integration of Einstein's static equations using the harmonic properties of the supplementary unknown needed to avoid the patch of Weyl metric above and below the disk. The cut $z = f(R)$ corresponds to the imaginary part of the complex analytic function, the existence of which follows from the harmonicity of that new function.

The Ansatz (3.14) leads here to the cut

$$f\,(R) = b\,+\,\frac{\eta}{2}\left[\frac{b\,m^2}{4\,(b^2+R^2)}\,-\,\frac{2b\,m^3\,\left(4b^2+7R^2\right)}{105\,(b^2+R^2)^{5/2}}\right]\,. \tag{6.12}$$

In Fig. 6.1, the ratio of the binding energy of these Curzon disks (which is derived from Eqs. (3.11), (5.10),(6.11) and (6.12)) over the corresponding rest mass M_0 is plotted with respect to the compactness parameter b/M_0 for different ratios p_0/ε_0 measured at the origin. The relative binding energy decreases in the most compact configurations because these contain too many unstable orbits ($\kappa^2 < 0$). A maximum ratio of about 5 % is reached.

7. Examples of rotating disks and an internal solution for the Kerr metric

The problem of constructing disks with proper rotation and partial pressure support is more complicated but physically more appealing than that of counter rotating solutions. It is now illustrated on an internal solution for the Kerr metric, and a generalisation of the solutions constructed by BLK and BLP to *warm rotating* solutions is sketched.

7.1. A Kerr internal solution

The functions (ν, ζ, ω) for the Kerr metric in Weyl-Papapetrou form expressed in terms of spheroidal co-ordinates ($R = s\sqrt{(x^2 \mp 1)(1-y^2)},\ z = sxy$) are given by

$$e^{2\nu} = \frac{-m^2 + s^2\,x^2 + a^2\,y^2}{(m + s\,x)^2 + \ a^2\,y^2}, \tag{7.1}$$

$$e^{2\zeta} = \frac{-m^2 + s^2\,x^2 + a^2\,y^2}{s^2\ (x^2 \mp y^2\ )}, \tag{7.2}$$

and

$$\omega = -\frac{2\,a\,m\ (m + s\,x)\ \left(1-y^2\right)}{-m^2 + \ s^2\,x^2 + a^2\,y^2}, \tag{7.3}$$

where $s = (\pm(m^2 - a^2))^{1/2}$. Here $\pm$ corresponds to the choice of prolate (+), or oblate (−) spheroidal co-ordinates corresponding to the cases $a < m$ and $a > m$ respectively. In this set of co-ordinates, the prescription given in section 2 leads to completely algebraic solutions. The normal derivative to the surface $z = f(R)$ reads (when $a > m$)

$$(\partial/\partial N) = N\,(x,y)\,(\partial/\partial x) + N\,(y,x)\,(\partial/\partial y)\,, \tag{7.4}$$

where

$$N\,(x,y) = \left(x^2-1\right)\left[y/s + x\ \ \left(y^2-1\right)\ f'/R\right]/\left(x^2-y^2\right).$$

Differentiating Eqs. (7.1) through (7.3) with respect to x and y together with Eq. (7.4) leads via Eqs. (2.15) to all physical characteristics of the Kerr disk in terms of the Kerr metric parameters m and a, and the function $z = f(R)$ which must be chosen so as to provide relevant pressures and energy distributions according to Eqs. (3.12). (Bìcák & Ledvinka (1993) [2] have constructed independently a cold Kerr solution when $a < m$.) On the axis $R = 0$, $f \equiv b$, and $f'' \equiv -c$, while Eqs. (3.12) imply $f' = 0$ at $(x = b/s,\ y = 1)$. This in turn implies

$$(p_\phi)_0 = (p_{_R})_0 = \frac{c}{4\pi}\sqrt{\frac{a^2+b^2-m^2}{a^2+(b+m)^2}}, \tag{7.5a}$$

$$(\varepsilon)_0 = \frac{1}{4\pi}\sqrt{\frac{a^2+b^2-m^2}{a^2+(b+m)^2}}\left[\frac{2m\left[(b+m)^2-a^2\right]}{\left(a^2+(b+m)^2\right)\left(a^2+b^2-m^2\right)} - c\right], \tag{7.5b}$$

Figure 7.1: the azimuthal velocity (a), the radial pressure (b), the ratio of radial over azimuthal pressure and the relative fraction of Kinetic Support (d) namely $\varepsilon V^2/(\varepsilon V^2 + p_\phi + p_{_R})$ for the $a/m = 0.5$ Kerr disk as a function of circumferential radius R_c, for a class of solutions with decreasing potential compactness, $b/m = 1.1, 1.2 \cdots 1.7$, and relative radial pressure support $\eta/m = 1/5 + 2(b/m - 1)/5$.

Figure 7.2: as in Fig. 7.1 with $a/m = 0.95$, $\eta/m = 1/15 + (b-1)/5$. Note the large relative kinetic support.

Figure 7.3: the azimuthal velocity (a), the azimuthal pressure (b), the relative fraction of Kinetic Support (c), namely $\varepsilon V^2/(\varepsilon V^2 + p_\phi)$ and the angular momentum (d) for the $a/m = 10$ zero radial pressure Kerr disk as a function of circumferential radius R_c, for a class of solutions with decreasing potential compactness $b/m = 210, 260 \cdots 510$. The first curve corresponds to a cut which induces negative azimuthal pressure (tensions).

where $(\quad)_0$ stands for $(\quad)$ taken at $R = 0$. The constraint that all physical quantities should remain positive implies

$$b \geq \sqrt{m^2 - a^2}, \tag{7.6a}$$

$$c \leq 2m \frac{(b+m)^2 - a^2}{\left(a^2 + (b+m)^2\right)(a^2 + b^2 - m^2)}. \tag{7.6b}$$

Equation (7.6a) is the obvious requirement that the surface of section should not enter the horizon of the fictitious source. Similarly, ergoregions will arise when the cut $z = f(R)$ enter the torus

$$\left(\frac{z}{m}\right)^2 + \left(\frac{R}{m} - \frac{a}{m} + \frac{1}{2}\frac{m}{a}\right)^2 = \left(\frac{1}{2}\frac{m}{a}\right)^2. \tag{7.7}$$

The analysis may be extended beyond the ergoregion via the ZAMO frame. The characteristics of these frames are given by Eq. (3.7), (3.8) and (3.9). The central redshift

$$1 + z_c = e^{-\nu} = \frac{(m+b)^2 + a^2}{b^2 + a^2 - m^2}, \tag{7.8}$$

can be made very large for such models constructed when $b \to \sqrt{m^2 - a^2}$.

On Fig. 7.1, Fig. 7.2 and Fig. 7.3, some characteristics of these Kerr disks with both $a > m$ and $a < m$ are illustrated. For simplicity, pressure is implemented via the cut (6.12). These disks present anisotropy of the planar pressure tensor ($p_\phi \neq p_{_R}$). The anisotropy follows from the properties of the ω vacuum field which gives rise to the circular velocity curve. Indeed, in the outer part of the disk, the specific angular momentum h tends asymptotically to a constant. The corresponding centrifugal force is therefore insufficient to counter-balance the field generated by the ν function. As this construction scheme generates such equilibria, the system compensates by increasing its azimuthal pressure away from isotropy. When $a > m$, and $\eta = 0$ the height of the critical cut corresponding to the last disk with positive pressures everywhere scales like $a\,(a^2 - m^2)^{1/2}$ in the range $2 \leq a/m \leq 20$. Note that this limit is above that of the highly relativistic motions which only occurs when b tends asymptotically to the Kerr horizon $(a^2 - m^2)^{1/2}$. The binding energy which follows Eq. (4.15) reaches values as high as one tenth of the rest mass for the most compact configurations. The inversion method described in section 4.1 was carried for the Kerr disks and yields distribution functions which characterise completely the equilibria as illustrated on Fig. 7.5. It was assumed that the velocity distribution of stars at radius R was a modified squared Lorentzian, as discussed in Appendix C and shown on Fig. 7.4. Note that disks with low rotation support present in their outer parts two distinct maxima, one of which is counter rotating, in agreement with the assumptions yielding the equation of state Eq. (4.15).

Figure 7.4: Parametrization of the number of star with velocity v_ϕ at radius R as a squared Lorentzian (as discussed in Appendix C) for the Kerr disk. The corresponding radius is appended on each curve. The left panel correspond to $a = 0.2$ while the right panel corresponds to $a = 0.8$. The pressure law is given in the caption of Fig. 7.5 where the corresponding distribution function is illustrated.

Figure 7.5: the isocontours of the distribution function for the Kerr disk as a function of the reduced momentum $\chi = h/\epsilon$, and the relative eccentricity of the orbit $\bar{e}_c = (\epsilon - \epsilon_\chi)/(1 - \epsilon_\chi)$ where ϵ_χ is the energy of circular orbits with reduced momentum χ. The four panels correspond to $a = 0, 0.1, 0.2, 0.3, 0.4$ from left to right and top to bottom, while the pressure law was chosen to correspond to the cut $f(R) = -4(4+7R^2)/(525(1+R^2)^{5/2}) + (16+15R^2)/(10(1+R^2))$ corresponding to a tepid disk. The figures are centered on the inner parts of the disk to illustrate the relative shift of the maximum number of stars towards larger angular momentum for faster rotating disks. The inversion assumed a squared Lorentzian for the distribution in angular velocity as discussed in Appendix C and illustrated on Fig. 7.4.

7.2. Other rotating solutions

The rotating disk models given in section 2 require prior knowledge of the corresponding vacuum solutions. However, while studying the symmetry group of the stationary axially symmetric Einstein Maxwell equations, Hoenselaers, Kinnersley & Xanthopoulos (1979) [13,14] found a method of generating systematically complete families of stationary Weyl-Papapetrou vacuum metrics from known static Weyl solutions. Besides, the decomposition of the Weyl potential ν_0 into line densities provides a direct and compact method of finding solutions to the static field. The N+1 rank zero HKX transform is defined as follows: let ν_0 and ζ_0 be the seed Weyl functions given by Eqs. (5.2). HKX define the $N \times N$ matrix $\mathbf{\Gamma}$ parameterised by N twist parameters α_k and N poles, a_k, $k = 1, \cdots N$ as

$$\left(\Gamma^{\pm}\right)_{k,k'} = i\,\alpha_k\,\frac{e^{\beta_k}}{r_k}\left[\frac{r_k - r_{k'}}{a_k - a_{k'}} \pm 1\right], \tag{7.9}$$

with $r_k = r(a_k) = \sqrt{R^2 + (z - a_k)^2}$ and $\beta_k = \beta(a_k)$, β being a function satisfying (7.11a) below. Defining $\mathbf{r} = \mathrm{Diag}(r_k)$, they introduce the auxiliary functions

$$D^{\pm} = \left|\mathbf{1} + \mathbf{\Gamma}^{\pm}\right|, \text{ and } L_{\pm} = 2D^{\pm}\,\mathrm{tr}\left[\left(\mathbf{1} + \mathbf{\Gamma}^{\pm}\right)^{-1}\mathbf{\Gamma}^{\pm}\,\mathbf{r}\right],$$
$$\omega_{\pm} = D^{+} \pm e^{2\nu_0} D^{-}, \text{ and } \mathcal{M}_{\pm} = \varpi\,\omega_{\pm} + 2\left(L_{+} \mp e^{2\nu_0} L_{-}\right),$$

which lead to the Weyl-Papapetrou potentials

$$e^{2\nu} = e^{2\nu_0}\,\Re\left[\frac{D^{-}}{D^{+}}\right], \tag{7.10a}$$

$$e^{2\zeta} = k e^{2\zeta_0}\,\Re\left[D^{-} D^{+^*}\right], \tag{7.10b}$$

$$\omega = 2\Im\left[\frac{\mathcal{M}_{+}^{*}\left(\omega_{+} + \omega_{-}\right) - \mathcal{M}_{-}\left(\omega_{+} + \omega_{-}\right)^{*}}{\left|\omega_{+}\right|^2 - \left|\omega_{-}\right|^2}\right], \tag{7.10c}$$

where $\Re$ and $\Im$ stand respectively for the real part and the imaginary part of the argument and $(\ )^*$ represents the complex conjugate of $(\ )$. k is a constant of integration which is fixed by the boundary conditions at infinity. The two yet unspecified function β and ϖ satisfy:

$$\nabla\beta\left(a_k\right) = \frac{1}{r_k}\left(\left[z - a_k\right]\nabla + R\,\mathbf{e}_\phi \times \nabla\right)\nu_0, \tag{7.11a}$$

$$\nabla\varpi = R\,\mathbf{e}_\phi \times \nabla\nu_0, \tag{7.11b}$$

Figure 7.6: the azimuthal velocity for the a/κ_Y zero radial pressure Yamazaki disk as a function of circumferential radius R_c, for a class of solutions with decreasing potential compactness $b/\kappa_Y = 3.6, 3.8, \cdots 5$. κ_Y is the natural unit of distance in these disks as defined by Yamazaki's Eq. (Y-2) [27].

where $\nabla = (\partial/\partial R, \partial/\partial z)$ and $\mathbf{e}_\phi$ is the unit vector in the ϕ direction. The linearity of these equations suggests again that solutions should be sought in terms of the line density, $W(b)$, characterising ν_0, namely

$$\beta(a_k) = \int \frac{W(b)}{a_k}\left[\frac{R^2+(z-b-a_k)^2}{R^2+(z-b)^2}\right]^{\frac{1}{2}} db, \tag{7.12a}$$

$$\varpi = \int \frac{W(b)(b-z)}{\sqrt{R^2+(z-b)^2}}\, db. \tag{7.12b}$$

It is therefore a matter of algebraic substitution to apply the above procedure and construct all non-linear stationary vacuum fields of the Papapetrou form from static Weyl fields. Following the prescription described in section 2, the corresponding disk in real rotation is then constructed. The requirement for the physical source to be a disk is in effect a less stringent condition on the regularity of the vacuum metric in the neighbourhood of its singularity because only the half space which does not contain these singularities is physically meaningful. A suitable Ehlers transformation on $D_-/D+$ ensures asymptotic flatness at large distance from the source.

To illustrate this prescription consider the vacuum field given by Yamazaki (1981) [27]. This field arises from 2 HKX rank zero transformation on the Zipoy-Voorhess [25] static metric given by

$$\nu_0 = \tfrac{1}{2}\delta \log\frac{(x-1)}{(x+1)}, \tag{7.13a}$$

$$\zeta_0 = \tfrac{1}{2}\delta^2 \log\frac{(x-1)}{(x^2-y^2)}, \tag{7.13b}$$

in prolate spheroidal co-ordinates. It corresponds to a uniform line density between $\pm\delta$. The functions β and ϖ follow from Eqs. (7.12). Choosing poles $a_k,\ k = 1, 2$ at the end of the rod $\pm\delta$, leads to

$$\beta(a_\pm) = \tfrac{1}{2}\delta \log\frac{x^2-1}{[x \mp y]^2}, \tag{7.14a}$$

$$\varpi = 2\delta y. \tag{7.14b}$$

Equations (7.10) together with (7.13) and (7.11) characterize completely the three Weyl-Papapetrou metric functions $\nu, \zeta,$ and ω; all physical properties of the corresponding disks follow. For instance, Fig. 7.6 gives the zero radial pressure velocity curve of the Yamazaki disk spanning from the Schwarzschild ($\delta = 1/2$) metric when $\alpha_1 = \alpha_2$.

More generally, the extension of this work to the construction of disks with planar *isotropic* pressures should be possible by requiring that Eq. (2.15c) is identically equal to Eq. (2.15d) given Eq. (7.10).

8. Conclusion

The general counter rotating disk with partial pressure support has been presented. The suggested method for implementing radial pressure support also applies to the construction of stationary axisymmetric disk with rotation but requires prior knowledge of the corresponding vacuum solution. In this manner, a disk-like source for the Kerr field has been constructed orbit by orbit. The corresponding distribution reduces to a Keplerian flow in the outer part of the disk and presents strong relativistic features in the inner regions such as azimuthal velocities close to that of light, large central redshift and ergoregions. The disk itself is likely to be stable against ring formation and the ratio of its binding energy to rest mass can be as large as 1:10. The broad lines of how to construct all rotating disks arising from HKX-transforming the corresponding counter rotating model into a fully self-consistent model with proper rotation and partial pressure support has been sketched. It should be a simple matter to implement this method with the additional requirement that the pressure remains isotropic with a sensible polytropic index. One could then analyse the fate of a sequence of gaseous disks of increasing compactness and relate it to the formation and evolution of quasars at high redshift. Alternatively, the inversion method described in section 4.1 yields a consistent description of the detailed dynamics for all disks in terms of stellar dynamics.

References

1. Bardeen, J. *"A variational principle for rotating stars in general relativity."* ApJ 162, 71-95 (1970).
2. Bìcák, J. & Ledvinka, T. *"Relativistic disks as sources of the Kerr metric."* Phys Rev D 71, 1669-1672 (1993).
3. Bìcák, J. Lynden-Bell, D. et al. *"Relativistic disks as sources of static vacuum spacetimes." Phys Rev D 47, 4334-4343 (1993).*
4. *Bìcák J, Lynden-Bell, D & Pichon C."Relativistic discs and flat galaxy models"MNRAS 265, 126-144 (1993).*
5. *Chamorow, A., R. Gregory, et al. "Static axisymmetric discs and gravitational collapse." Proc R. Soc. Lond. 413, 251-262 (1987).*
6. *Curzon,H. Proc.Lond.Math.Soc. 23, 477-480 (1924).*
7. *Dietz, W. & C. Hoenselaers "Stationary system of two masses kept apart by their gravitational spin spin interaction." Phys Rev Lett 48, 778-780 (1982).*
8. *Dietz, W. and C. Hoenselaers "Two mass Solutions of Einstein's Vacuum Equations: The double Kerr solution." Ann Phys 165, 319-383 (1985).*
9. *Evans, N. and P. de Zeeuw "Potential-density Pairs for Flat Galaxies." MNRAS 257, 152-176 (1992).*
10. *Fackerell, E. ApJ 153, 643-660 (1968).*
11. *Katz, J. Horwitz, G & Klapish, M. ApJ 199, 307-321 (1975).*
12. *Kerr,R. Phys.Rev.Let. 11, 237-238 (1963).*
13. *Hoenselaers, C., W. Kinnersley, et al. "Symmetries of the stationary Einstein-Maxwell equations, VI Transformations which generate asymptotically flat spacetimes with arbitrary multipole moments." J Math Phys 20, 2530-2536 (1979).*
14. *Hoenselaers, C. and W. Dietz "The rank N HKX Transformations: New stationary Axisymmetric Gravitational fields." Gen Rel Grav 16, 71-78 (1984).*
15. *Ipser,J. ApJ 158, 17-43 (1969).*
16. *Israel, W. Nuovo-Cimento 33, 331-335 (1964).*
17. *Lemos, J. "Self Similar relativistic Discs with Pressure." Class Q Grav 6, 1219-1230 (1989).*
18. *Morgan,T, Morgan L. Phys.Rev. 183, 1097-1102 (1969).*
19. *Misner, C.,Thorne, K. & Wheeler, J. , Gravitation,Freeman,(1973).*
20. *Pichon, C, & Lynden-Bell, D"Equilibria of flat and round disks"(1995) to appear in MNRAS.*
21. *Synge,J. The Relativistic Gas, North Holand (1957).*

22. *Ipser, J. & Thorne ApJ 154, 251- (1968).*
23. *Tolman, R. "Relativity, Thermodynamics and Cosmology.", Oxford University Press, (1934).*
24. *Toomre, A. "On the Gravitational Stability of a Disc of Stars." ApJ 139, 1217-1238 (1964).*
25. *Voorhess, B. Phys. Rev.* **D**. *2, 2119 (1970).*
26. *Weyl, H. Ann.Phys. 54, 117-118 (1917).*
27. *Yamazaki, M. "On the Hoenselaers-Kinnersley-Xanthopoulos spinning mass fields. J Math. Phys. 22, 133-135 (1981).*

A. Equation of state for a relativistic 2D adiabatic flow

The equation of state of a planar adiabatic flow is constructed here by relating the perfect fluid stress energy tensor of the flow to the most probable distribution function which maximises the Boltzmann entropy. Synge [21] gives an extensive derivation of the corresponding equation of state for a 3D flow. These properties are local characteristics of the flow. It is therefore assumed that all tensorial quantities introduced in this section are expressed in the local Vierbein frame.

Consider a infinitesimal volume element $d\vartheta$ defined in the neighbourhood of a given event, and assume that the particles entering this volume element are subject to molecular chaos. The distribution function F of particles is defined so that $F(\mathbf{R},\mathbf{P})\; d\vartheta d^2P$ gives the number of particles in the volume ϑ centered on $\mathbf{R}$ with 2-momentum pointing to $\mathbf{P}$ within d^2P.

The most probable distribution function $F^\star$ for these particles is then given by that which maximises Boltzmann entropy S subject to the constraints imposed by the conservation of the total energy momentum and by the conservation of the number of particles within that volume. This entropy reads in terms of the distribution F

$$S = -d\vartheta \int F \log F \, d^2P \,. \tag{A.1}$$

The stress energy tensor corresponds to the instantaneous flux density of energy momentum through the elementary volume $d\vartheta$ (here a surface)

$$T^{\alpha b} = \int F^\star P^\alpha P^\beta \, \frac{d^2P}{|\mathcal{E}|} \,, \tag{A.2}$$

where the $1/|\mathcal{E}|$ factor accounts for the integration over energy-momentum space to be restricted to the pseudo-sphere $P^\alpha P_\alpha = m^2$. Indeed the detailed energy-momentum conservation requires the integration to be carried along the volume element

$$\int \delta\left(P^\alpha P_\alpha - m^2\right)\, d^3P = \int \delta\left({P^0}^2 - \mathcal{E}^2\right)\, d^2P dP^0 = \frac{d^2P}{|\mathcal{E}|} \,, \tag{A.3}$$

where $\mathcal{E} = \sqrt{m^2 + \mathbf{P}^2}$. It is assumed here that momentum space is locally flat. Similarly the numerical flux vector reads

$$\phi^\alpha_\star = \int F^\star P^\alpha \, \frac{d^2P}{|\mathcal{E}|} \,. \tag{A.4}$$

The conservation of energy-momentum of the volume element $d\vartheta$ implies that the flux of energy momentum across that volume should be conserved; this flux reads

$$T^{\alpha\beta}\, n_\beta \, d\vartheta = d\vartheta \int F^\star P^\alpha \, d^2P = \text{Const.} \,, \tag{A.5}$$

where n_β is the unit time axis vector. Keeping the population number constant provides the last constraint on the possible variations of S

$$\phi^\alpha_\star n_\alpha d\vartheta = d\vartheta \int F^\star d^2P = \text{Const.} \,. \tag{A.6}$$

Varying Eq. $(A.1)$ subject to the constraints $(A.5)$ $(A.6)$, and putting δS to zero leads to

$$(\log F^\star + 1)\, \delta F^\star = a \delta F^\star + \lambda_\alpha P^\alpha \delta F^\star \,, \tag{A.7}$$

where a and λ_α are Lagrangian multipliers corresponding resp. to $(A.5)$ $(A.6)$. These multipliers are independent of P^a but in general will be a function of position. The distribution which extremises S therefore reads

$$F^\star = C \exp\left(\lambda_\alpha P^\alpha\right) \,. \tag{A.8}$$

The 4 constants C and λ_a are in principle fixed by Eqs. (A.5) and (A.6). The requirement for $F^\star$ to be Lorentz invariant – that is independent of the choice of normal n_α – and self consistent, is met instead by demanding that $F^\star$ obeys Eq. (A.2) and (A.4) , namely

$$C \int P^\alpha \exp\left(\lambda_\mu P^\mu\right) \frac{d^2P}{|\mathcal{E}|} = \phi^\alpha_\star \,, \tag{A.9}$$

$$C \int P^\alpha P^\beta \exp\left(\lambda_\mu P^\mu\right) \frac{d^2P}{|\mathcal{E}|} = T^{\alpha\beta} \,, \tag{A.10}$$

where $\phi^\alpha_\star$ and $T^{\alpha\beta}$ satisfy in turn the covariant constraints

$$\frac{\partial T^{\alpha\beta}}{\partial x^\beta} = 0 \quad \text{and} \tag{A.11a}$$

$$\frac{\partial \phi^\alpha_\star}{\partial x^\alpha} = 0 \,. \tag{A.11b}$$

Equations (A.9)-(A.11) provide a set of thirteen equations to constraint the thirteen functions $C, \lambda_\alpha, \phi^\alpha_\star$, and $T^{\alpha\beta}$. Equations (A.9) and (A.10) may be rearranged as

$$\phi^\alpha_\star = C\frac{\partial \Phi}{\partial \lambda^\alpha} \,, \quad T^{\alpha\beta} = C\frac{\partial^2 \Phi}{\partial\lambda^\alpha \partial\lambda^\beta} \,, \tag{A.12}$$

where the auxiliary function Φ is defined as $\Phi = \int \exp(\lambda_\alpha P^\alpha)\, d^2P/|\mathcal{E}|$; Φ is best evaluated using pseudo polar coordinates corresponding to the symmetry imposed by the energy momentum conservation $P^\alpha P_\alpha - m^2 = 0$; these are

$$\begin{aligned} P^1 &= m \sinh\chi \cos\phi \,, \\ P^2 &= m \sinh\chi \sin\phi \,, \\ P^0 &= im \cosh\chi \,, \end{aligned} \tag{A.13}$$

where the coordinate χ is chosen so that the normal n_α lies along $\chi = 0$. In terms of these variables, $d^2P/|\mathcal{E}|$ then reads

$$d^2P/|\mathcal{E}| = dP^1 dP^2/m\cosh\chi = m \sinh\chi d\chi d\phi \,. \tag{A.14}$$

Moving to a temporary frame in which λ^0 is the time axis ($\lambda^0 = i\lambda = i(-\lambda_\alpha\lambda^\alpha)^{1/2}$, $\lambda^k = 0$ $k = 1, 2$), Φ becomes

$$\Phi = 2\pi m \int_0^\infty \exp\left(-m\lambda\cosh\chi\right) \sinh\chi d\chi = \frac{2\pi}{\lambda} \exp\left(-\lambda\right) \,. \tag{A.15}$$

From Eq. (A.9)-(A.10) and (A.15), it follows that

$$T^{\alpha\beta} = \frac{2\pi C}{\lambda^3} \exp\left(-\lambda\right) \left[\left\{\lambda^2 + 3\lambda + 3\right\} \frac{\lambda^\alpha}{\lambda}\frac{\lambda^\beta}{\lambda} + \left\{\lambda + 1\right\} \delta^{\alpha\beta} \right] \,, \tag{A.16}$$

$$\phi^\alpha_\star = \frac{2\pi C}{\lambda^3} \exp\left(-\lambda\right) \left\{\lambda + 1\right\} \lambda^\alpha \,. \tag{A.17}$$

On the other hand, the stress energy tensor of a perfect fluid is

$$T^{\alpha\beta} = \left(\varepsilon_0 + p_0\right) U^\alpha U^\beta + p_0\, \delta^{\alpha\beta} \,, \tag{A.18}$$

while the numerical surface density of particles measured in the rest frame of the fluid Σ is related to $\phi^\alpha_\star$ via

$$\Sigma = -\phi^\alpha_\star U_\alpha \,. \tag{A.19}$$

Eq. (A.16) has clearly the form of Eq. (A.18) when identifying

$$U^\alpha = \lambda^\alpha/\lambda \,, \tag{A.20a}$$

$$\varepsilon_0 + p_0 = \frac{2\pi C}{\lambda^3} \exp\left(-\lambda\right) \left\{\lambda^2 + 3\lambda + 3\right\} \,, \tag{A.20b}$$

$$p_0 = \frac{2\pi C}{\lambda^3} \exp\left(-\lambda\right) \left\{\lambda + 1\right\} \,. \tag{A.20c}$$

Eliminating λ,C between Eqs. $(A.17)$–$(A.20c)$ yields the sought after equation of state

$$\varepsilon_0 = 2\,p_0 + \frac{\Sigma}{1+p_0/\Sigma}\,. \tag{A.21}$$

where $p_0 = \Sigma/\lambda$. This is the familiar gas law given that $1/\lambda$ is the absolute temperature. The equation of state Eq. $(A.21)$ corresponds by construction to an isentropic flow. Indeed, using the conservation equations Eq. $(A.11a)$ dotted with U^α, and Eq. $(A.11b)$ together with $U^\alpha U_\alpha = -1$ yields after some algebra to the identity

$$\lambda\frac{d}{ds}\left[\frac{\left(\lambda^2+3\lambda+3\right)}{\lambda\left(\lambda+1\right)}\right] + \frac{1}{\lambda} = -\frac{\partial U^\alpha}{\partial x^\alpha} = \frac{1}{\Sigma}\frac{d\Sigma}{ds}\,, \tag{A.22}$$

where $d/ds = (dx^\alpha/dx^\alpha)(\partial/\partial x^\alpha)$ is the covariant derivative following the stream lines. Writing the $r.h.s$ of Eq. $(A.22)$ as an exact covariant derivative leads to the first integral

$$\frac{d}{ds}\left[\frac{1}{1+\lambda} - 2\,\log\left(\lambda\right) + \log\left(1+\lambda\right) - \log\left(\Sigma\right)\right] = 0\,. \tag{A.23}$$

Given that $p_0 = \Sigma/\lambda$, it follows

$$\left(1+\frac{p_0}{\Sigma}\right)\frac{p_0}{\Sigma}\,\exp\left(\frac{1}{1+\Sigma/p_0}\right)\frac{1}{\Sigma} = \text{Const.} \tag{A.24}$$

which in the low temperature limit gives $\Sigma^{-2}p_0 = \text{Const}$. This corresponds to the correct adiabatic index $\gamma = (2+2)/2$.

B. Distribution functions for counter-rotating relativistic disks

For counter rotating disks in the absence of gravomagnetic forces, the inversion for distribution functions given in section 4.1 can be carried in close analogy to the Newtonian method given by Pichon & Lynden-Bell (1995) [20], and is sketched here. The relativistic flow is characterised by its stress energy tensor, $T^{(\alpha\beta)}$, which, in Vierbein components, reads

$$T^{(\alpha\beta)} = \int\int \frac{f_\star\left(\epsilon,h\right)\,P^{(\alpha)}\,P^{(\beta)}}{P^{(t)}}\,dP^{(R)}dP^{(\phi)}\,. \tag{B.1}$$

From the geodesic equation it follows that

$$P^\mu P_\mu = -1 \quad \Rightarrow \quad P^{(R)} = \frac{1}{\sqrt{\gamma_{tt}}}\left[\epsilon^2 - h^2\,\gamma_{tt}/\gamma_{\phi\phi} - g_{tt}\right]^{1/2}\,, \tag{B.2}$$

where the line element in the disk is taken to be

$$ds^2 = -\gamma_{tt}\,dt^2 + \gamma_{RR}\,dR^2 + \gamma_{\phi\phi}\,d\phi^2\,. \tag{B.3}$$

Differentiating Eq. $(B.2)$ implies

$$\frac{dP^{(R)}}{P^{(t)}} = \frac{d\epsilon}{\left[\epsilon^2 - h^2\,\gamma_{tt}/\gamma_{\phi\phi} - \gamma_{tt}\right]^{1/2}}\,, \quad \text{while} \quad dP^{(\phi)} = \frac{dh}{\sqrt{\gamma_{\phi\phi}}}\,, \tag{B.4}$$

where the differentiation is done at constant R and h , and R and ϵ respectively. Combinations of Eqs. $(B.1)$ lead to

$$\Lambda = {\gamma_{\phi\phi}}^{1/2}\,\left(T^{(tt)} - T^{(\phi\phi)} - T^{(RR)}\right) = \int\int \frac{f_\star\left(\epsilon,h\right)\,dh\,d\epsilon}{\sqrt{\epsilon^2 - h^2\gamma_{tt}/\gamma_{\phi\phi} - \gamma_{tt}}}\,, \tag{B.5a}$$

$$\Delta = {\gamma_{\phi\phi}}^{3/2}\,T^{(\phi\phi)} = \int\int \frac{h^2\,f_\star\left(\epsilon,h\right)\,dhd\epsilon}{\sqrt{\epsilon^2 - h^2\gamma_{tt}/\gamma_{\phi\phi} - \gamma_{tt}}}\,. \tag{B.5b}$$

Note that Eq. ($B.5a$) corresponds to Tolman's formula [23] which yields be integration the total gravitating mass of the disk. Introducing

$$\mathcal{R}^2 = \gamma_{\phi\phi}/\gamma_{tt}\,, \quad e = \frac{1}{2}\left(\epsilon^2 - 1\right)\,, \quad \Psi = \frac{1}{2}\left(1 - \gamma_{tt}\right) \quad \text{and} \quad \hat{f}_\star\left(e, h\right) = \frac{f\left(\epsilon, h\right)}{\epsilon}\,, \tag{B.6}$$

gives, for Eqs. ($B.5$):

$$\Lambda = \int\int \frac{\hat{f}_\star\left(e,h\right)\, dhde}{\left[2\left(e+\psi\right) - h^2/\mathcal{R}^2\right]^{1/2}} \quad \text{and} \quad \Delta = \int\int \frac{h^2\, \hat{f}_\star\left(e,h\right)\, dhde}{\left[2\left(e+\psi\right) - h^2/\mathcal{R}^2\right]^{1/2}}\,. \tag{B.7}$$

Eq. ($B.7$) is formally identical to Eq.(2.9) of Pichon & Lynden-Bell [20], replacing $(\Lambda, \Delta, \hat{f}_\star, \mathcal{R}, e, \Psi)$ by $(R\,\Sigma, R^3\, p_\phi,\ f, R, \epsilon, \psi)$. In fact $(\Lambda, \Delta, \hat{f}_\star, \mathcal{R}, e, \Psi)$ tends to $(R\,\Sigma, R^3\, p_\phi,\ f, R, \epsilon, \psi)$ in the classical regime. Introducing the intermediate functions $\hat{F}(h, \mathcal{R})$, which is chosen so that its moments satisfy Eqs. ($B.5$), and following the classical prescription of Pichon & Lynden-Bell [20] yields

$$\hat{f}\left(e,h\right) = \frac{1}{\pi}\int_{\mathcal{R}_e}^{\mathcal{R}_p} \frac{\left(\partial\hat{F}/\partial\mathcal{R}\right)_h\, d\mathcal{R}}{\sqrt{h^2/\mathcal{R}^2 - 2\Psi - 2e}} - \frac{1}{\pi}\int_{\mathcal{R}_a}^{\infty} \frac{\left(\partial\hat{F}/\partial\mathcal{R}\right)_h\, d\mathcal{R}}{\sqrt{h^2/\mathcal{R}^2 - 2\Psi - 2e}}\,, \tag{B.8}$$

where $\mathcal{R}_p(h,e)$, and $\mathcal{R}_a(h,e)$ are respectively the apogee and perigee of the star with invariants (h,e), and $\mathcal{R}_e(h)$ is the inner radius of a star on a "parabolic" (zero e energy) orbit with momentum h. Eq. ($B.8$) provides direct and systematic means to construct families of distribution function for counter-rotating disks characterised by their stress-energy tensor in the plane. Note that in contrast the dragging of inertial frames requires to fix three moments of the velocity distribution to account for the given energy density, pressure law and rotation law.

C. Distribution functions for rotating disks: Lorentzian in momentum

A possible choice for $\bar{F}$ is a Lorenzian parametrised in width, p_2, mean, p_1 and amplitude, p_0 such that

$$\bar{F}\left(v_\phi, R\right) dv_\phi = \frac{p_0\, p_2\, \pi^{-1}\, dp}{p_2^2 + \left(p - p_1\right)^2}\,, \quad \text{where} \quad p = \frac{v_\phi}{\sqrt{1 - v_\phi^2}} \quad \text{and} \quad v_\phi = e^\nu\left(\chi - \omega\right)/R_c\,. \tag{C.1}$$

The explicit function of v_ϕ is found using $dp = dv_\phi/(1 - v_\phi^2)^{3/2}$. In this instance, Eq. (4.12) becomes

$$T^{(tt)}\, e^{4\nu} = \frac{p_0\, p_2}{\pi}\int_{-\infty}^{\infty} \frac{dp}{\left({p_2}^2 + \left(p - p_1\right)^2\right)} = p_0\,, \tag{C.2a}$$

$$T^{(t\phi)}\, e^{4\nu} = \frac{p_0\, p_2}{\pi}\int_{-\infty}^{\infty} \frac{p\, dp}{\sqrt{1+p^2}\,\left({p_2}^2 + \left(p - p_1\right)^2\right)} = \mathcal{G}\left(p_0, p_1, p_2\right)\,, \tag{C.2b}$$

$$T^{(\phi\phi)}\, e^{4\nu} = \frac{p_0\, p_2}{\pi}\int_{-\infty}^{\infty} \frac{p^2\, dp}{\left(1+p^2\right)^2\,\left({p_2}^2 + \left(p - p_1\right)^2\right)} = \frac{p_0\left(p_2 + {p_2}^2 + {p_1}^2\right)}{\left(1 + p_2\right)^2 + {p_1}^2} \tag{C.2c}$$

where $\mathcal{G}(p_0, p_1, p_2)$ is given by Eq. ($C.4$) bellow. The inversion of Eqs. ($C.2$) for (p_0, p_1, p_2), together with Eqs. ($C.1$), (4.14) and Eq. ($4.3c$) yields the distribution function of a Lorenzian flow compatible with the energy distribution imposed by the metric (ν, ζ, ω) and the cut $z = f(R)$. This inversion is always achievable provided the energy conditions Eq. (3.12) are satisfied.

More generally, families of distributions functions corresponding to azimuthal momentum distribution such as $2p_2^3\, p_0\, \pi^{-1}/(p_2^2 + (p-p_1)^2)^2, 8p_2^5\, p_0\, (3\pi)^{-1}/(p_2^2 + (p-p_1)^2)^3 \cdots$ are readily derived in a similar manner while differentiating the *r.h.s.* of Eq. ($C.2$) with respect to p_2^2. These higher order distributions have all vanishing number of stars with azimuthal velocity close to the velocity of light. This parametrisation is illustrated for the Kerr disk on Fig. 7.5.

C.1. The quadrature for $\mathcal{G}(p_0, p_1, p_2)$

Changing variables to u such that $p = (u - 1/u)/2$ Eq. $(C.2b)$ becomes

$$\mathcal{G}\left(p_0, p_1, p_2\right) = \frac{2p_0\, p_2}{\pi} \int_0^\infty \frac{\left(u^2-1\right)\, du}{4{p_2}^2\, u^2 + \left(u^2 - 1 - 2p_1\, u\right)^2} \tag{C.3}$$

This integral is then carried and yields

$$\begin{aligned}\mathcal{G}\left(p_0, p_1, p_2\right) = &\frac{p_0\left(p_2 + i\, p_1\right)\, \log\left(-2\, i\, p_2 + 2\, p_1 - 2\sqrt{1 + \left(-i\, p_2 + p_1\right)^2}\right)}{2\sqrt{1 + \left(-i\, p_2 + p_1\right)^2}\, \pi} + \\ &\frac{p_0\, \left(i\, p_2 - p_1\right)\, \log\left(-2\, i\, p_2 + 2\, p_1 + 2\sqrt{1 + \left(-i\, p_2 + p_1\right)^2}\right)}{2\sqrt{1 + \left(-i\, p_2 + p_1\right)^2}\, \pi} + \frac{p_0(p_2 - i\, p_1)\, \log\left(2\, i\, p_2 + 2\, p_1 - 2\sqrt{1 + \left(i\, p_2 + p_1\right)^2}\right)}{2\sqrt{1 + \left(i\, p_2 + p_1\right)^2}\, \pi} + \\ &\frac{p_0\, \left(i\, p_1 - p_2\right)\, \log\left(2\, i\, p_2 + 2\, p_1 + 2\sqrt{1 + \left(i\, p_2 + p_1\right)^2}\right)}{2\sqrt{1 + \left(i\, p_2 + p_1\right)^2}\, \pi}\end{aligned} \tag{C.4}$$

D. The relativistic epicyclic frequency

The equation for the radial oscillations follows from the Lagrangian

$$\mathcal{L} = -\sqrt{e^{2\nu}\, \left(\dot{t} - \omega\dot{\phi}\right)^2 - e^{2\zeta - 2\nu}\, \left(1 + f'^2\right)\, \dot{R}^2 - \, e^{-2\nu}\, \dot{\phi}^2 R^2}, \tag{D.1}$$

where $\dot{(\ )}$ stands here for derivation with respect to the proper time τ for the star describing its orbit. In Eq. $(D.1)$, ϕ and t are ignorable which leads to the invariants:

$$\frac{\partial \mathcal{L}}{\partial \dot{\phi}} = h \qquad \frac{\partial \mathcal{L}}{\partial \dot{t}} = -\epsilon. \tag{D.2}$$

The integral of the motion for the radial motion follows from Eqs. $(D.2)$ and $U^\mu U_\mu = -1$, namely:

$$e^{2\zeta - 2\nu}\, \left(1 + f'^2\right)\, \dot{R}^2 + \frac{e^{2\nu}}{R^2}\left(h - \epsilon\, \omega\right)^2 - \epsilon^2 e^{-2\nu} = -1$$

This equation, together with its total derivative with respect to proper time provides the radial equation of motion, having solved for the angular momentum h and the energy ϵ of circular orbits as a function of radius when equating both $\dot{R}$ and $\ddot{R}$ to zero. the relativistic generalisation of the classical epicyclic frequency is defined here to be the frequency of the oscillator calling back linear departure from circular orbits. Hence the equation for radial perturbation reads

$$\delta\ddot{R} + \kappa^2 \delta R = 0, \tag{D.3}$$

which gives for κ^2 :

$$\begin{aligned}\kappa^2 = &e^{-2Z}\left(Z'' - 2Z'^2\right) - \epsilon^2 e^{-2L}\left(L'' - 2L'^2\right) - \\ &e^{2K}\left[\, \left(h - \epsilon\omega\right)^2\left(K'' + 2K'^2\right) - \epsilon\left(h - \epsilon\omega\right)\left(4K'\omega' + \omega''\right) + \epsilon^2\omega'^2\,\right],\end{aligned} \tag{D.4}$$

where $(\quad)'$ stands in this Appendix for $d/dR \equiv \partial/\partial R + f'\,\partial/\partial z$ and L, K, and Z are given in terms of the potential ζ and ν by:

$$L = \zeta + \log\sqrt{1+f'^2}, \tag{D.5a}$$

$$Z = \zeta + \log\sqrt{1+f'^2} - \nu, \tag{D.5b}$$

$$K = 2\nu - \zeta - \log\sqrt{1+f'^2} - \log R. \tag{D.5c}$$

Here ϵ and h are known functions of R given by the roots of:

$$\dot{R} = 0 \quad \Rightarrow \quad e^{-2L}\epsilon^2 = (h - \epsilon\,\omega)^2\, e^{2N} + e^{-2Z}, \tag{D.6a}$$

$$\ddot{R} = 0 \quad \Rightarrow \quad e^{-2Z}Z' = e^{-2L}L'\epsilon^2 + (h-\epsilon\omega)\, e^{2N}\left[(h-\epsilon\,\omega)\,N' - \epsilon\,\omega'\right]. \tag{D.6b}$$

E. Correction to Lemos' Self-Similar Disk

The result given in section 6.1 agrees with that of Lemos, having made the following agreed corrections to his solution:

- Eq.(L 3.14) should read: $(k+n)\cot\frac{1}{2}(k+n)\pi = -4\pi p_{*rr}$ with a minus sign, because the integration of θ is carried downwards. This gives $n + k \geq 1$ for the disks with positive pressures.
- Lemos gives the stress energy tensor integrated through the plane using coordinate increment rather than proper length. Our result gives the latter which has an extra factor $\exp(\zeta - \nu)$ and gives the physical energy tensor per unit area.
- The exponent of $\cos[(n+k)\pi/2]$ is $2n(k-n)/(n+k)^2$ rather than $4n(1-2n)/(k+n)^2$.

New sources for Kerr and other metrics: rotating relativistic disks with pressure support.

C. Pichon[1,2], **& D. Lynden-Bell**[1]

1 Institute of Astronomy, Madingley Road, Cambridge CB3 0HA
2 CITA,McLennan Labs,University of Toronto,
60 St. George Street,Toronto,Ontario M5S 1A7.

ABSTRACT

Complete sequences of new analytic solutions of Einstein's equations which describe thin super massive disks are constructed. These solutions are derived geometrically. The identification of points across two symmetrical cuts through a vacuum solution of Einstein's equations defines the gradient discontinuity from which the properties of the disk can be deduced. The subset of possible cuts which lead to physical solutions is presented. At large distances, all these disks become Newtonian, but in their central regions they exhibit relativistic features such as velocities close that of light, and large redshifts. Sections with zero extrinsic curvature yield cold disks. Curved sections may induce disks which are stable against radial instability. The general counter rotating flat disk with planar pressure tensor is found. Owing to gravomagnetic forces, there is no systematic method of constructing vacuum stationary fields for which the non-diagonal component of the metric is a free parameter. However, all static vacuum solutions may be extended to fully stationary fields via simple algebraic transformations. Such disks can generate a great variety of different metrics including Kerr's metric with any ratio of a to m. A simple inversion formula is given which yields all distribution functions compatible with the characteristics of the flow, providing formally a complete description of the stellar dynamics of flattened relativistic disks. It is illustrated for the Kerr disk.

keywords: Relativity – methods: analytical – stellar dynamics, disks – quasars
accepted by the Monthly Notices of the Royal Astronomical Society

1. Introduction

The general-relativistic theory of rapidly rotating objects is of great intrinsic interest and has potentially important applications in astrophysics. Following Einstein's early work on relativistic collisionless spherical shells, Fackerell (1968) [10], Ipser (1969) [15] and Ipser & Thorne (1968) [22] have developed the general theory of relativistic collisionless spherical equilibria. The stability of such bodies has been further expanded by Katz (1975) [11]. Here the complete dynamics of flat disk equilibria is developed and illustrated, extending these results to differentially rotating configurations with partial pressure support. A general inversion method for the corresponding distribution functions is presented, yielding a coherent model for the stellar dynamics of these disks. Differentially rotating flat disks in which centrifugal force almost balances gravity can also give rise to relatively long lived configurations with large binding energies. Such objects may therefore correspond to possible models for the latest stage of the collapse of a proto-quasar. Analytic calculations of their structure have been carried into the post Newtonian régime by Chandrasekhar. Strongly relativistic bodies have been studied numerically following the pioneering work on uniformly rotating cold disks by Bardeen & Wagoner [1]. An analytic vacuum solution to the Einstein equations, the Kerr metric [12],

which is asymptotically flat and has the general properties expected of an exterior metric of a rotating object, has been known for thirty years, but attempts to fit an interior solution to its exterior metric have been unsatisfactory. A method for generating families of self-gravitating rapidly rotating disks purely by geometrical methods is presented. Known vacuum solutions of Einstein's equations are used to produce the corresponding relativistic disks. One family includes interior solutions for the Kerr metric.

1.1. Background

In 1919 Weyl [26] and Levi-Civita gave a method for finding all solutions of the axially symmetric Einstein field equations after imposing the simplifying conditions that they describe a static vacuum field. Bìcák, Lynden-Bell and Kalnajs (1993) [3]– here-after refered as BLK – derived complete solutions corresponding to counter rotating pressure-less axisymmetric disks by matching exterior solutions of the Weyl- Levi-Civita type on each side of the disk. For static metrics, the vacuum solution was obtained via line superposition of fictitious sources placed symmetrically on each side of the disk by analogy with the classical method of images. The corresponding solutions describe two counter-rotating stellar streams. This method will here be generalised, allowing *true rotation* and radial pressure support for solutions describing self-gravitating disks. These solutions provide physical sources (interior solutions) for stationary axisymmetric gravitational fields.

1.1.1. Pressure Support via Curvature

In Newtonian theory, once a solution for the vacuum field of Laplace's equation is known, it is straightforward to build solutions to Poisson's equation for disks by using the method of mirror images. In general relativity, the overall picture is similar. In fact, it was pointed out by Morgan & Morgan (1969) [18] that for pressureless counter rotating disks in Weyl's co-ordinates, the Einstein equation reduces essentially to solving Laplace's equation. When pressure is present, no global set of Weyl co-ordinates exists. The condition for the existence of such a set of co-ordinates is that $T_{RR} + T_{zz} = 0$. On the disk itself, this is satisfied only if the radial eigenvalue of the pressure tensor, p_R, vanishes (T_{zz} vanishes provided the disk is thin). When p_R is non-zero, vacuum co-ordinates of Weyl's type still apply both above and below the disk, but as two separate co-ordinate patches. Consider global axisymmetric co-ordinates (R', ϕ', z') with $z' = 0$ on the disk itself. For $z' > 0$, Weyl's co-ordinates R, ϕ, z may be used. In terms of these variables, the upper boundary of the disk $z' = 0^+$ is mapped onto a given surface $z = f(R)$. On the lower patch, by symmetry, the disk will be located on the surface $z = -f(R)$. Thus in Weyl co-ordinates, the points $z = f(R)$ on the upper surface of the disk must be identified with the points $z = -f(R)$ on the lower surface. The intrinsic curvature of the two surfaces that are identified match by symmetry. The jump in the extrinsic curvature gives the surface distribution of stress-energy on the disk. A given metric of Weyl's form is a solution of the empty space Einstein equations, and does not give a complete specification of its sources (for example, a Schwarzschild metric of any given mass can be generated by a static spherical shell of any radius). With this method, all physical properties of the source are entirely characterised once it is specified that the source lie on the surface $z = \pm f(R)$ and the corresponding extrinsic curvature (i.e. its relative layout within the embedding vacuum spacetime) is known. The freedom of choice of ν in the Weyl metric corresponds to the freedom to choose the density of the disk as a function of radius. The supplementary degree of freedom involved in choosing the surface of section $z = f(R)$ corresponds classically to the choice of the radial pressure profile.

1.1.2. Rotating Disks

For rotating disks, the dragging of inertial frames induces strongly non-linear fields outside the disk which prohibit the construction of a vacuum solution by superposition of the line densities of fictitious sources. nevertheless, in practise quite a few vacuum stationary solutions have been given in the literature, the most famous being the Kerr metric. Hoenselaers, Kinnersley & Xanthopoulos (1979) [13,14](HKX hereafter) have also given a discrete method of generating rotating solutions from known static Weyl solutions. The disks are derived by taking a cut through such a field above all singularities or sources and identifying it with a symmetrical cut through a reflection of the source field. This method applies directly to the non-linear fields such as those generated by a rotating metric of the Weyl-Papapetrou type describing stationary axisymmetric vacuum solutions. The analogy with electromagnetism is then to consider the field associated with a known azimuthal vector potential A_ϕ, the analog of $g_{t\phi}/g_{tt}$. The jump in the tangential component of the corresponding B-field gives the electric current in the plane, just as the jump in the t,ϕ component of the extrinsic curvature gives the matter current.

The procedure is then the following: for a given surface embedded in curved space-time and a given field outside the disk, the jump in the extrinsic curvature on each side of the mirror images of that surface is determined in order to specify the matter distribution within the disk. The formal relationship between extrinsic curvatures and surface energy tensor per unit area was introduced by Israel and is described in details by Misner Thorne Wheeler (1973) p 552. [19] Plane surfaces and non-rotating vacuum fields (*i.e.*the direct counterpart of the classical case) were investigated by BLK and led to pressureless counter-rotating disks. Any curved surface will therefore produce disks with some radial pressure support. Any vacuum metric with $g_{t\phi} \neq 0$ outside the disk will induce rotating disks.

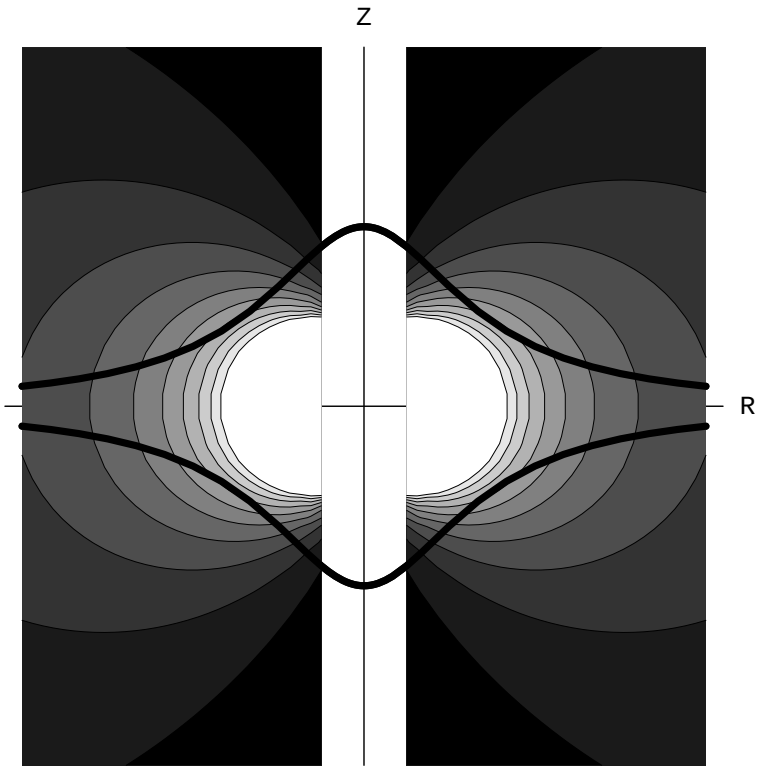

Figure 1.1: Symbolic representation of a section $z = \pm f(R)$ through the $g_{t\phi}$ field representing the upper and lower surface of the disk embedded in two Weyl-Papapetrou fields. The isocontours of $\omega(R,z)$ correspond to a measure of the amount of rotation in the disk.

In section 2, the construction scheme for rotating disks with pressure support is presented. In section 3, the properties of these disks are analysed, and a reasonable cut, $z = f(R)$, is suggested. Section 4 describes stellar equilibria which have the corresponding anisotropic stress energy tensors, while section 5 derives the properties of the limiting counter-rotating disks. This method is then first applied to warm counter rotating disks in section 6; the dominant energy condition given for Curzon disks by Chamorow *et. al.*(1987) [5], and Lemos ' solution for the self - similar Mestel disk with pressure support are recovered. In section 7, the Kerr disk is studied and the method for producing general HKX disks is sketched.

2. Derivation

The jump in extrinsic curvature of a given profile is calculated and related to the stress energy tensor of the matter distribution in the corresponding self gravitating relativistic disk.

2.1. The Extrinsic Curvature

The line element corresponding to an axisymmetric stationary vacuum gravitational field is given by the Weyl-Papapetrou (WP) metric

$$ds^2 = -e^{2\nu}\left(dt - \omega\, d\phi\right)^2 + e^{2\zeta - 2\nu}\left(dR^2 + dz^2\right) + R^2 e^{-2\nu}\, d\phi^2, \tag{2.1}$$

where (R, ϕ, z) are standard cylindrical co-ordinates, and ν, ζ and ω are functions of (R, z) onlygeometric units $G = c = 1$ are used throughout this paper. Note that this form is explicitly symmetric under simultaneous change of ϕ and t. The vacuum field induces a natural metric on a 3-space-like $z = f(R)$ surface

$$\begin{aligned} d\sigma^2 = g_{\alpha\beta}\frac{\partial x^\alpha}{\partial x^a}\frac{\partial x^\beta}{\partial x^b}dx^a dx^b &\equiv g_{\alpha\beta}\, h^\alpha_a h^\beta_b\, dx^a dx^b, \\ &\equiv \gamma_{ab}\, dx^a\, dx^b, \end{aligned} \tag{2.2}$$

where $\{x^a\}$ are the co-ordinates on the embedded hypersurface $z = f(R)$, $\{x^a\} = (t, R, \phi)$, and $\{x^\alpha\} = (t, R, z, \phi)$ are Weyl's co-ordinates for the embedding spacetime. Here, γ_{ab} stands for the embedded metric, and h^α_a is given by

$$h^\alpha_a = \frac{\partial x^\alpha}{\partial x^a} = \begin{bmatrix} 1 & 0 & 0 & 0 \\ 0 & 1 & 0 & f' \\ 0 & 0 & 1 & 0 \end{bmatrix}, \tag{2.3}$$

where hereafter a prime, $(\ )'$, represents the derivative with respect to R. The line element is then

$$d\sigma^2 = -e^{2\nu}\left(dt - \omega\, d\phi\right)^2 + R^2 e^{-2\nu} d\phi^2 + e^{2\zeta - 2\nu}\left(1 + f'^2\right) dR^2. \tag{2.4}$$

Let the upward pointing normal N_μ to the surface $z = f(R)$ be

$$N_\mu = \frac{\partial}{\partial x^\mu}\left[z - f\left(R\right)\right] = \left(0, -f', 0, 1\right). \tag{2.5}$$

The normalised normal is therefore

$$n_\mu = \frac{N_\mu}{\sqrt{N_\alpha N^\alpha}} = \frac{N_\mu}{\sqrt{g^{\alpha\beta} N_\beta N_\alpha}} = \frac{N_\mu}{\sqrt{1 + f'^2}} e^{\zeta - \nu}. \tag{2.6}$$

The extrinsic curvature tensor K is given in its covariant form by

$$K_{ab} = n_\mu \left(\partial_a h^\mu_b + \Gamma^\mu_{\alpha\,\beta}\, h^\alpha_a\, h^\beta_b\right), \tag{2.7}$$

where $\partial_a h^\mu_b = \partial h^\mu_b / \partial x^a$. Eq. (2.6) and (2.3) together with the Christoffel symbols for the Weyl metric lead to the computation of K , the extrinsic curvature of that surface embedded in the Weyl Papapetrou metric:

$$K_{tt} = -\frac{e^{\nu-\zeta}}{\sqrt{1+f'^2}}\left(\frac{\partial \nu}{\partial N}\right) e^{4\nu-2\zeta}, \tag{2.8a}$$

$$K_{RR} = -\frac{e^{\nu-\zeta}}{\sqrt{1+f'^2}}\left(\frac{f''}{1+f'^2} + \frac{\partial\left(\nu-\zeta\right)}{\partial N}\right)\left(1+f'^2\right), \tag{2.8b}$$

$$K_{\phi t} = -\frac{e^{\nu-\zeta}}{\sqrt{1+f'^2}}\left[\frac{\partial\left[\nu+\frac{1}{2}\log\left(\omega\right)\right]}{\partial N}\right]\omega e^{4\nu-2\zeta}, \tag{2.8c}$$

$$K_{\phi\phi} = -\frac{e^{\nu-\zeta}}{\sqrt{1+f'^2}}\left[\left(\frac{f'}{R}+\frac{\partial \nu}{\partial N}\right)R^2 e^{-2\zeta} + e^{4\nu-2\zeta}\omega^2\frac{\partial\left[\nu-\log\left(\omega\right)\right]}{\partial N}\right], \tag{2.8d}$$

where the notation $\partial/\partial N \equiv (\partial/\partial z - f'\partial/\partial R)$ has been used.

2.2. The Stress Energy Tensor

The stress energy tensor per unit surface τ^a_b is the integral of of the stress energy tensor carried along the normal to the surface $z = f(R)$. In a locally Minkowskian frame co-moving with the mean flow of the disk, the corresponding orthonormal tetrad is

$$e^{(0)}_i = e^{\nu}\left(1,0,-\omega\right), \tag{2.9a}$$

$$e^{(1)}_i = e^{\zeta-\nu}\sqrt{1+f'^2}\left(0,1,0\right), \tag{2.9b}$$

$$e^{(2)}_i = Re^{-\nu}\left(0,0,1\right), \tag{2.9c}$$

so that

$$d\,s^2 = \eta_{(a)(b)}\left(e^{(a)}_i d\,x^i\right)\left(e^{(b)}_j d\,x^j\right), \tag{2.10}$$

with $\eta_{(a)(b)} = \mathrm{Diag}(-1,1,1)$. In that frame,

$$\left[\tau^{(a)(b)}\right]_0 = \begin{bmatrix} \varepsilon & 0 & 0 \\ 0 & p_{_R} & 0 \\ 0 & 0 & p_\phi \end{bmatrix}. \tag{2.11}$$

After a Lorentz transformation to a more general frame in which the flow is rotating with relative velocity V in the ϕ direction, this stress becomes

$$\tau^{(a)(b)} = \frac{1}{1-V^2}\begin{bmatrix} \varepsilon + p_\phi V^2 & 0 & \left(p_\phi+\varepsilon\right)V \\ 0 & \left(1-V^2\right)p_R & 0 \\ \left(p_\phi+\varepsilon\right)V & 0 & p_\phi + \varepsilon V^2 \end{bmatrix}. \tag{2.12}$$

2.3. The Discontinuity Equations

Israel (1964) [16] has shown that Einstein's equations integrated through a given surface of discontinuity can be re-written in terms of the jump in extrinsic curvature, namely

$$\tau_b^a = \frac{1}{8\pi}\,[K_b^a - K_a^a\,\delta_b^a]_-^+ \equiv \mathcal{L}_b^a. \tag{2.13}$$

where $[\quad]_-^+$ stands for $(\quad)$ taken on $z = f(R)$ minus $(\quad)$ taken on $z = -f(R)$. This tensor $\mathcal{L}_b^a$ is known as the Lanczos tensor.

In the tetrad frame (2.9), the Lanczos tensor given by Eqs. (2.13) and (2.8) reads

$$\mathcal{L}^{(a)(b)} = \frac{e^{\nu-\zeta}}{4\pi\sqrt{1+f'^2}} \begin{bmatrix} \frac{f''}{1+f'^2} + \frac{f'}{R} + \frac{\partial(2\nu-\zeta)}{\partial N} & 0 & \frac{\partial\omega}{\partial N}\frac{e^{2\nu}}{2R} \\ 0 & -\frac{f'}{R} & 0 \\ \frac{\partial\omega}{\partial N}\frac{e^{2\nu}}{2R} & 0 & -\frac{f''}{1+f'^2} + \frac{\partial\zeta}{\partial N} \end{bmatrix}. \tag{2.14}$$

Identifying the stress energy tensor $\tau^{(a)(b)}$ with the tetrad Lanczos tensor $\mathcal{L}^{(a)(b)}$ according to Eq. (2.13), and solving for $p_{_R}\,, p_\phi\,, \varepsilon$ and V yields

$$V = \frac{R\,e^{-2\nu}}{\partial\omega/\partial N}\left[\left(\frac{f'}{R} + 2\frac{\partial\nu}{\partial N}\right) - Q\right], \tag{2.15a}$$

$$\varepsilon = \frac{e^{\nu-\zeta}}{4\pi\sqrt{1+f'^2}}\left[\frac{Q}{2} + \left(\frac{f''}{1+f'^2} + \frac{f'}{2R} + \frac{\partial\,(\nu-\zeta)}{\partial N}\right)\right], \tag{2.15b}$$

$$p_\phi = \frac{e^{\nu-\zeta}}{4\pi\sqrt{1+f'^2}}\left[\frac{Q}{2} - \left(\frac{f''}{1+f'^2} + \frac{f'}{2R} + \frac{\partial\,(\nu-\zeta)}{\partial N}\right)\right], \tag{2.15c}$$

$$p_{_R} = \frac{e^{\nu-\zeta}}{4\pi\sqrt{1+f'^2}}\left(\frac{-f'}{R}\right), \tag{2.15d}$$

where

$$Q \equiv \sqrt{\left(\frac{f'}{R} + 2\frac{\partial\nu}{\partial N}\right)^2 - \frac{e^{4\nu}}{R^2}\left(\frac{\partial\omega}{\partial N}\right)^2}. \tag{2.16}$$

All quantities are to be evaluated along $z = f(R)$. Eq. (2.15) gives the form of the most general solution to the relativistic rotating thin disk problem provided the expressions for $\varepsilon, p_\phi, p_{_R}$ are physically acceptable.

3. Physical properties of the warm disks

Physical properties of interest for these disks are derived and related to the choice of profile $z = f(R)$ compatible with their dynamical stability.

Defining the circumferential radius R_c, proper radial length $\tilde{R}$, and a synchronised proper time τ_* by

$$R_c = R\,e^{-\nu}\,, \tag{3.1a}$$

$$\tilde{R} = \int \sqrt{1+f'^2}\,e^{\zeta-\nu}\,dR\,, \tag{3.1b}$$

$$\tau_* = \int_{(\mathcal{T})} e^{\nu}\left(1 - \omega\frac{d\phi}{dt}\right)dt\,, \tag{3.1c}$$

where the integral over dR is performed at $z = f(R)$ and that over dt is performed along a given trajectory $(\mathcal{T})$, the line element on the disk (2.4) reads

$$d\,\sigma^2 = -\not{d}\tau_*^2 + d\tilde{R}^2 + R_c^2 d\phi^2\,. \tag{3.2}$$

For circular flows ($\not{d}\tau_* = e^\nu [1 - \omega d\phi/dt]\, dt$), V may be re-written as

$$V = R_c \frac{d\phi}{\not{d}\tau_*}. \tag{3.3}$$

Equation (3.3) is inverted to yield the angular velocity of the flow as measured at infinity:

$$\Omega \equiv \frac{d\phi}{dt} = \frac{V e^\nu / R_c}{1 + \omega V e^\nu / R_c}. \tag{3.4}$$

Similarly, the covariant specific angular momentum h of a given particle reads in terms of these variables

$$h \equiv \frac{p_\phi}{\mu} = \gamma_{t\,\phi} u^t + \gamma_{\phi\,\phi} u^\phi = \frac{1}{\sqrt{1 - V^2}} \left(R_c V + \omega\, e^\nu \right) , \tag{3.5}$$

where μ is the rest mass of the particle. The covariant specific energy ϵ of that particle reads

$$\epsilon \equiv -\frac{p_t}{\mu} = -\gamma_{t\,\phi} u^\phi - \gamma_{t\,t} u^t = \frac{e^\nu}{\sqrt{1 - V^2}} . \tag{3.6}$$

which gives the central redshift, $1 + z_c = \exp(-\nu)$. The velocity of zero angular momentum observers (so called ZAMOs) follows from Eq. (3.5):

$$V_z = -\frac{\omega e^\nu}{R_c} . \tag{3.7}$$

With these observers, the cuts $z = f(R)$ may be extended inside ergoregions where the dragging of inertial frames induces apparent superluminous motions as measured by locally static observers. The circumferential radius R_z as measured by ZAMOs is Lorentz contracted with respect to R_c, becoming

$$R_z \equiv \sqrt{g_{\phi\phi}} = R_c \left[1 - V_z^2 \right]^{1/2} , \tag{3.8}$$

while the velocity flow measured by ZAMOs is

$$V_{/z} = \frac{V - V_z}{1 - V V_z} . \tag{3.9}$$

The total angular momentum of the disk H follows from the asymptotic behaviour of the vacuum field ω at large radii, $\omega \to -2H/r$. Define the binding energy of the disk ΔE as the difference between the baryonic rest mass M_0 and the total mass-energy of the disk M as measured from infinity given by $\nu \to -M/r$:

$$\Delta E = M_0 - M. \tag{3.10}$$

M is also given by the Tolman formula, but corresponds, by construction, to the mass of the line source for the vacuum field. The baryonic rest mass can be expressed as

$$M_0 \equiv \int \Sigma \sqrt{-g}\, U^\mu dS_\mu = \int \frac{\left[1 - \omega\Omega \right]^{-1}}{\sqrt{1 - V^2}} \Sigma\, 2\pi R_c d\tilde{R} , \tag{3.11}$$

where the baryonic energy density Σ can be related to the energy density ε through some yet unspecified equation of state or the knowledge of a distribution function.

3.1. Constraints on the internal solutions

The choice of the profile $z = f(R)$ is open, provided that it leads to meaningful physical quantities. Indeed it must lead to solutions which satisfy $\varepsilon \geq 0$, $p_{_R} \geq 0$, $p_\phi \geq 0$, and $V \leq 1$ while the dominant energy condition implies also that $\varepsilon \geq p_\phi$ and $\varepsilon \geq p_{_R}$. These translate into the following constraints on f

$$\varepsilon \geq 0 \quad \Rightarrow \quad \sqrt{\mathcal{N}^2 - \mathcal{O}^2} + (\mathcal{N} - 2\mathcal{Z}) \geq 0\,; \tag{3.12a}$$

$$0 \leq V \leq 1 \quad \Rightarrow \quad \mathcal{N} \geq \mathcal{O} \text{ and } \mathcal{O} \geq 0\,; \tag{3.12b}$$

$$0 \leq p_\phi \leq \varepsilon \quad \Rightarrow \quad 4\mathcal{Z}\,\mathcal{N} \geq \left(\mathcal{O}^2 + 4\mathcal{Z}^2\right) \text{ and } \mathcal{N} \geq 2\mathcal{Z}\,; \tag{3.12c}$$

$$0 \leq p_{_R} \leq \varepsilon \quad \Rightarrow \quad f' \leq 0 \text{ and } -2f'/R \leq \sqrt{\mathcal{N}^2 - \mathcal{O}^2} + (\mathcal{N} - 2\mathcal{Z})\,; \tag{3.12d}$$

given

$$\mathcal{N} \equiv \frac{f'}{R} + 2\frac{\partial \nu}{\partial N}\,, \quad \mathcal{O} \equiv \frac{e^{2\nu}}{R}\frac{\partial \omega}{\partial N}\,, \quad \text{and} \quad \mathcal{Z} \equiv \left(\frac{\partial \zeta}{\partial N} - \frac{f''}{1+f'^2}\right)\,. \tag{3.13}$$

The existence of a solution satisfying this set of constraints can be demonstrated as follows: in the limit of zero pressure and counter-rotation (*i.e.* $\mathcal{O} \to 0, \mathcal{N} \to 2\partial\nu/\partial z$, and $\mathcal{Z} \to \partial\zeta/\partial z$), any cut $z = \text{Const} \equiv b \gg m$ satisfies Eqs. (3.12). By continuity, there exist solutions with proper rotation and partial pressure support. In practise, all solutions given in sections 6 and 7 satisfy the constraints (3.12). Note that in the limit of zero radial pressure, Eq. (3.12b) implies $\partial/\partial z\,[\omega/R + \exp 2\nu] \leq 0$.

3.2. Ansatz for the profile

In the following discussion, the section $z = f(R)$ is chosen so that the corresponding radial pressure gradient balances a given fraction of the gravitational field which would have occurred had there been no radial pressure within the disk. This choice 'bootstraps' calculations for all relevant physical quantities in terms of a single degree of freedom (*i.e.* this fraction η), rather than a complete functional. This gives

$$\frac{\partial p_{_R}}{\partial \tilde{R}} = -\frac{\eta}{(1-V^2)}\frac{\partial \nu}{\partial \tilde{R}}\left[\varepsilon + p_{_R} + V^2\left(p_\phi - p_{_R}\right)\right]\,. \tag{3.14}$$

On the r.h.s. of Eq. (3.14), $p_{_R}$ is put to zero and V, p_ϕ, ε are re-expressed in terms of ζ, ν, ω via Eqs. (2.15) with $f' = f'' = 0$ and $z = \text{Const}$. On the l.h.s. of Eq. (3.14), $p_{_R}$ is chosen according to Eq. (2.15d). In practise, this Ansatz for f is a convenient way to investigate a parameter space which is likely to be stable with respect to ring formation as discussed in the next subsection. In principle, a cut, f, could be chosen so as to provide a closed bounded symmetrical surface containing all fictitious sources. Indeed, by symmetry no flux then crosses the $z = 0$ plane beyond the cut, and the energy distribution is therefore bound to the edge of that surface: this corresponds to a finite pressure supported disk. It turns out that in general this choice is not compatible with all the constraints enumerated in the previous section. More specifically, the positivity of p_ϕ fails for all finite disk models constructed. The Ansatz described above gives for instance an upper bound on the height of that surface when assuming that all the support is provided by radial pressure. This height is in turn not compatible with positive azimuthal pressure at all radii.

3.3. Stability

To what extent are the equilibria studied in the previous sections likely to be stable under the action of disturbances? The basic instabilities can be categorised as follows:

dynamical instabilities, which are intrinsic to the dynamical parameters of the disks, grow on an orbital time scale, and typically have drastic effects on the structure of the system.

secular instabilities, which arise owing to dissipative mechanisms such as viscosity or gravitational radiation, grow on a time scale which depends on the strength of the dissipative mechanism involved, and slowly drive the system along a sequence of dynamical equilibria.

Amongst dynamical instabilities, kinematical instabilities correspond to the instability of circular orbits to small perturbations, and collective instabilities arises from the formation of growing waves triggered by the self-gravity of the disk. Rings, for instance, will be generated spontaneously in the disk if the local radial pressure is insufficient to counteract the self-gravity of small density enhancements. Even dynamically stable non-axisymmetric modes may drive the system away from its equilibrium by radiation of gravitational waves which will slowly remove angular momentum from the disk. For gaseous disks, viscosity and photon pressure will affect the equilibria. Radiative emission may disrupt or broaden the disk if the radiation pressure exceeds the Eddington limit. The energy loss by viscosity may induce a radial flow in the disk. However, the disks discussed in this paper have anisotropic pressures inappropriate for gaseous disks and the accurate description of the latter two processes requires some prescription for the dissipative processes in the gas. The scope of this section is therefore restricted to a simple analysis of the dynamical instabilities.

Turning briefly to the corresponding Newtonian problem, Toomre (1963) [24] gave the local criterion for radial collective instability of stellar disks,

$$\sigma_{_R} \geq \frac{3.36 G \Sigma_0}{\kappa}, \tag{3.15}$$

where Σ_0 is the local surface density, σ_R^2 the radial velocity dispersion, and κ the epicyclic frequency of the unperturbed stars. This criterion is derived from the first critical growing mode of the dispersion relation for radial waves. The corresponding critical wavelength is Jeans length $\sim 2\sigma_R^2/G\Sigma_0$.

For the relativistic disks described in this paper, spacetime is locally flat, which suggests a direct translation of Eq. (3.15) term by term. The constraints that stability against ring formation places on these models will then be addressed at least qualitatively via the Newtonian approach. The proper relativistic analysis is left to further investigation. The relativistic surface density generalising Σ_0 is taken to be the co-moving energy density ε given by Eq. (2.15b). The radial velocity dispersion $\sigma_{_R}^2$ is approximated by $p_{_R}/\varepsilon$. The epicyclic frequency is calculated in the appendix. Putting Eqs. (D.4) and (D.5) into Eq. (3.15) give another constraint on f for local radial stability of these disks. Note that the kinematical stability of circular orbits follows from Eq. (D.3) by requiring κ^2 to be positive.

4. Stellar dynamical equilibria for rotating super-massive disks

The method described in section 2 will generally induce rotating disks with anisotropic pressures ($p_\phi \neq p_R$). These objects may therefore be described in the context of stellar dynamics. It should be then checked that there exist a stellar equilibria compatible with a given vacuum field and a given cut $z = f(R)$.

4.1. Distribution functions for rotating super-massive disks

Here a general procedure to derive all distribution functions corresponding to a specified stress energy tensor is presented for disks with non-zero mean rotation (a more direct derivation for counter-rotating disk is given in Appendix B). The detailed description of the dynamics of the disk follows.
In Vierbein components, the stress energy tensor reads

$$T^{(\alpha\beta)} = \int\int \frac{f_\star\,(\epsilon,h)\; P^{(\alpha)}\,P^{(\beta)}}{P^{(t)}}\, dP^{(R)} dP^{(\phi)}\,, \tag{4.1}$$

where $f_\star(\epsilon,h)$ is the distribution of stars at position R,ϕ with momentum $P^{(R)}, P^{(\phi)}$. For a stationary disk, it is a function of the invariant of the motion ϵ, h. Now for the line element (2.4):

$$d\sigma^2 = -\,e^{2\,\nu}\,(dt-\omega\;d\phi)^2 + e^{2\,\zeta-2\,\nu}\,\left(1+f'^2\right)\,dR^2 + R^2 e^{-2\,\nu}\,d\phi^2, \tag{4.2}$$

the Vierbein momenta read

$$P^{(\phi)} = e^{\nu}\,R^{-1}\,(h-\omega\,\epsilon)\;, \tag{4.3a}$$
$$P^{(t)} = e^{-\nu}\,\epsilon\;, \tag{4.3b}$$
$$P^{(R)} = \left[\epsilon^2 e^{-2\nu} - e^{2\nu}\,R^{-2}\;(h-\omega\,\epsilon)^2 - 1\right]^{1/2}\;. \tag{4.3c}$$

Calling $\chi = h/\epsilon$ and $\vartheta = 1/\epsilon^2$, Eqs. (4.3) becomes

$$P^{(\phi)} = e^{\nu}\,R^{-1}\,\vartheta^{-1/2}\;(\chi-\omega)\;, \tag{4.4a}$$
$$P^{(t)} = e^{-\nu}\,\vartheta^{-1/2}\,, \tag{4.4b}$$
$$P^{(R)} = \vartheta^{-1/2}\,\left[e^{-2\nu} - e^{2\nu}\,R^{-2}\;(\chi-\omega)^2 - \vartheta\right]^{1/2}\;. \tag{4.4c}$$

In terms of these new variables, the integral element $dP^{(\phi)}dP^{(R)}$ becomes

$$dP^{(\phi)}dP^{(R)} = \left|\frac{\partial P^{(\phi)}\,\partial P^{(R)}}{\partial\chi\;\partial\vartheta}\right| d\chi\,d\vartheta = \frac{e^{-\nu}\,R^{-1}\,\vartheta^{-2}\,d\chi\,d\vartheta}{2\sqrt{e^{-2\nu} - e^{2\nu}\,R^{-2}\;(\chi-\omega)^2 - \vartheta}}\,. \tag{4.5}$$

Given Eq. (4.5) and Eq. (4.3b), Eq. (4.1) may be rewritten as

$$T^{(\alpha\beta)} = \int\int P^{(\alpha)}P^{(\beta)}\,\frac{f_\star\,(\epsilon,h)\;R^{-1}\,\vartheta^{-3/2}\,d\chi\,d\vartheta}{2\sqrt{e^{-2\nu} - e^{2\nu}\,R^{-2}\;(\chi-\omega)^2 - \vartheta}}\,. \tag{4.6}$$

In particular,

$$R\,T^{(tt)}\,e^{2\nu} = \int\int \frac{f_\star\,(\epsilon,h)\;\vartheta^{-5/2}\,d\chi\,d\vartheta}{2\sqrt{e^{-2\nu} - e^{2\nu}\,R^{-2}\;(\chi-\omega)^2 - \vartheta}}\,, \tag{4.7a}$$
$$R^2\,T^{(t\phi)} = \int\int (\chi-\omega)\;\frac{f_\star\,(\epsilon,h)\;\vartheta^{-5/2}\,d\chi\,d\vartheta}{2\sqrt{e^{-2\nu} - e^{2\nu}\,R^{-2}\;(\chi-\omega)^2 - \vartheta}}\,, \tag{4.7b}$$
$$R^3\,T^{(\phi\phi)}\,e^{-2\nu} = \int\int (\chi-\omega)^2\;\frac{f_\star\,(\epsilon,h)\;\vartheta^{-5/2}\,d\chi\,d\vartheta}{2\sqrt{e^{-2\nu} - e^{2\nu}\,R^{-2}\;(\chi-\omega)^2 - \vartheta}}\,. \tag{4.7c}$$

Note that given Eqs. (4.7), $T^{(RR)}$ follows from the equation of radial support. Note also that

$$R_c\left(T^{(tt)} - T^{(\phi\phi)} - T^{(RR)}\right) = \int\int \frac{f_\star\,(\epsilon,h)\;e^{-\nu}\,\vartheta^{-3/2}\,d\chi\,d\vartheta}{2\sqrt{e^{-2\nu} - e^{2\nu}\,R^{-2}\;(\chi-\omega)^2 - \vartheta}}\,, \tag{4.8}$$

or equivalently,

$$T^{(tt)} - T^{(\phi\phi)} - T^{(RR)} = \int\int \frac{f_\star\,(\epsilon, h)}{P^{(t)}}\, dP^{(\phi)}\, dP^{(R)}\,. \tag{4.9}$$

Equation (4.9) yields the total gravitating mass. It is known as Tolman's formulae and can be derived directly from the relation $P^\mu P_\mu = -1$ and Eq. (4.1).
Let

$$F\,(\chi, R) = \frac{1}{2}\int \frac{f_\star\,(\epsilon, h)\,\vartheta^{-5/2}\,d\vartheta}{\sqrt{e^{-2\nu} - e^{2\nu}\,R^{-2}\,(\chi-\omega)^2 - \vartheta}} = \int_1^{\mathcal{Y}} \frac{f_*\,(\chi,\vartheta)\;d\vartheta}{2\sqrt{\mathcal{Y}-\vartheta}}\,, \tag{4.10}$$

$$\text{where}\quad f_*\,(\chi,\vartheta) = f_\star\,(\epsilon, h)\,\vartheta^{-5/2}\,,\quad \text{and}\quad \mathcal{Y}\,(R,\chi) = e^{-2\nu} - e^{2\nu}\,R^{-2}\,(\chi-\omega)^2\,. \tag{4.11}$$

The set of Eqs. (4.7) becomes

$$R\,T^{(tt)}\,e^{2\nu} = \int F\,(\chi, R)\;d\chi = Re^{-2\nu}\int \bar{F}\,(v_\phi, R)\;dv_\phi\,, \tag{4.12a}$$

$$R^2\,T^{(t\phi)} = \int F\,(\chi, R)\;(\chi-\omega)\;d\chi = R^2 e^{-4\nu}\int v_\phi\,\bar{F}\,(v_\phi, R)\;dv_\phi\,, \tag{4.12b}$$

$$R^3\,T^{(\phi\phi)}\,e^{-2\nu} = \int F\,(\chi, R)\;(\chi-\omega)^2\;d\chi = R^3 e^{-6\nu}\int v_\phi^2\,\bar{F}\,(v_\phi, R)\;dv_\phi\,. \tag{4.12c}$$

The *r.h.s* of Eqs. (4.12) was re-expressed convinienlty in terms of the new variable $v_\phi \equiv e^\nu(\chi-\omega)/R_c$, and the new function $\bar{F}(v_\phi, R) \equiv F(\chi = R_c v_\phi e^{-\nu}+\omega, R)$ in order to stress the analogy with the classical identities. Note that in the limit of zero pressures, v_ϕ reduces to V, the geodesic velocity of stars on circular orbits. In Eq. (4.12), the dragging of inertial frames requires to fix simultaneously three moments of the velocity distribution to account for the given energy density, pressures and rotation law. This third constraint does not hold in the corresponding Newtonian problem, nor for static relativistic disks as described in appendix B. Any positive function $F(\chi, R)$ satisfying the moment constraints Eqs. (4.12) corresponds to a possible choice. For instance the parametrisation is carried in Appendix C for $\bar{F}$ distributions corresponding to powers of Lorentzians in azimuthal momenta. Let $\tilde{F}(\chi, \mathcal{Y}) = F(\chi, R)$, where $\mathcal{Y}(R, \chi)$ is given by Eq. (4.11). Written in terms of $\tilde{F}$, the integral equation Eq. (4.10) is solved for f_* by an Abel transform

$$f_*\,(\chi,\vartheta) = \frac{2}{\pi}\int_1^{\vartheta}\left(\frac{\partial\tilde{F}}{\partial\mathcal{Y}}\right)_\chi \frac{d\mathcal{Y}}{\sqrt{\vartheta-\mathcal{Y}}}\,. \tag{4.13}$$

The latter integration may be carried in R space and yields

$$f_\star\,(\epsilon, h) = \frac{2}{\epsilon^4\pi}\int_{\mathcal{R}_\epsilon}^{\mathcal{R}_p}\left(\frac{\partial F}{\partial R}\right)_\chi \frac{dR}{\sqrt{-\left(P^{(R)}\right)^2}} - \frac{2}{\epsilon^4\pi}\int_{\mathcal{R}_a}^{\infty}\left(\frac{\partial F}{\partial R}\right)_\chi \frac{dR}{\sqrt{-\left(P^{(R)}\right)^2}}\,, \tag{4.14}$$

where $P^{(R)}$ is given by Eq. (4.3*c*) as a function of R, ϵ, and h. Here F is chosen to satisfy Eq. (4.12) which specifies the stress energy components $T^{(\alpha\beta)}$. The integration limits correspond to two branches: the first branch is to be carried between $\mathcal{R}_e(h)$, the inner radius of a star on a "parabolic" orbit with momentum h, and $\mathcal{R}_p(h,\epsilon)$, the perigee of a star with invariants (h,ϵ); the second branch contributes negatively to Eq. (4.14) and corresponds to radii larger than $\mathcal{R}_a(h,\epsilon)$, the apogee of a star with invariants (h,ϵ). Note that the derivative in Eq. (4.14) is taken at constant reduced momentum $\chi = h/\epsilon$. This inversion procedure is illustrated on Fig. 7.5. All properties of the flow follow in turn from $f_\star(\epsilon, h)$. For instance, the rest mass surface density, Σ, may be evaluated from the detailed "microscopic" behaviour of the stars, leading to an estimate of the binding energy of the stellar cluster.

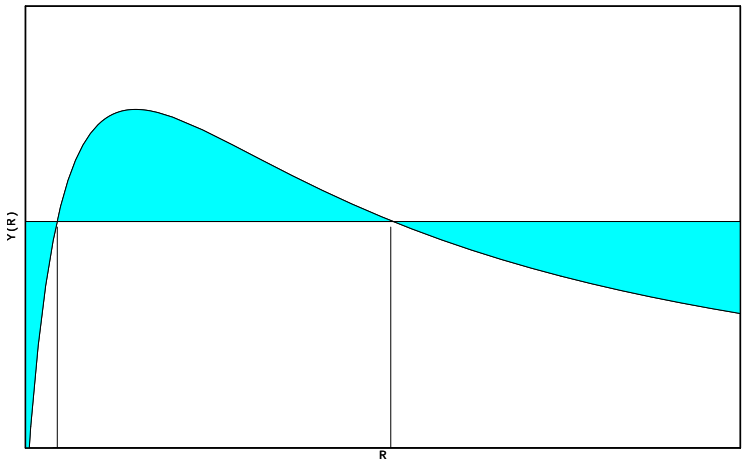

Figure 4.1: sketch for the effective potential $Y(R)$ as a function of radius. The horizontal line corresponds to the energy level $1/\epsilon^2$, the absisse line corresponds to the escape energy $1/\epsilon^2 = 1$. The ordinate axis corresponds to $\mathcal{R}_e(h,\epsilon)$, the inner radius of a star on a "parabolic" orbit with momentum h, the left vertical line corresponds to $\mathcal{R}_p(h,\epsilon)$, the perigee of a star with invariants (h,ϵ); the right vertical line corresponds to $\mathcal{R}_a(h,\epsilon)$, the apogee of a star with invariants (h,ϵ). The area between the curve $Y = Y(R)$ and the lines $Y = 1/\epsilon^2$ and $R = \mathcal{R}_e$ are shaded, defining three regions from left to right. The middle region does not contribute to Eq. (4.14). The equation $Y = 1/\epsilon^2$ has two roots corresponding to $\mathcal{R}_p(h,\epsilon)$ and $\mathcal{R}_a(h,\epsilon)$, while $Y = 1$ has two roots corresponding to infinity and $\mathcal{R}_e$. The sign of the slope of $Y(R)$ gives the sign of the contribution for each branch in Eq. (4.14).

4.2. A simple equation of state

An equation of state for these rotating disks with planar anisotropic pressure tensors is alternatively found directly while assuming (somewhat arbitrarily) that the fluid corresponds to the superposition of two isotropic flows going in opposite directions. In other words, the anisotropy of the pressures measured in the frame co-moving with the mean flow V is itself induced by the counter rotation of two isotropic streams. (These counter rotating streams are described in more details in the next section.) In each stream, it is assumed that the pressure is isotropic and that the energy is exchanged adiabatically between each volume element. The detailed derivation of the corresponding relationship between the surface density and the pressure of each stream is given in Appendix A. The above set of assumption yields the following prescription for Σ :

$$\Sigma = \frac{\varepsilon - p_\phi - p_R + \sqrt{(\varepsilon - p_\phi - p_R)\,(\varepsilon - p_\phi + 3p_R)}}{2\sqrt{1-V_0^2}}, \tag{4.15}$$

where $V_0 = \sqrt{(p_\phi - p_R)/(\varepsilon + p_R)}$ is the counter rotating velocity measured in the frame co-moving with V which induces $p_\phi \neq p_R$. In the classical limit, $\Sigma \to (\varepsilon - p_\phi)/\sqrt{1-V_0^2}$. The binding energy of these rotating disks is computed from Eq. (4.15) together with Eqs. (3.11) and (2.15).

5. Application: warm counter-rotating disks

For simplicity, warm counter-rotating solutions are presented first, avoiding the non-linearities induced by the dragging of inertial frames. These solutions generalise those of BLK, while implementing partial pressure support within the disk. Formally this is achieved by putting $\omega(R,z)$ identically to zero in Eq. (4.2); the metric for the axisymmetric static vacuum solutions given by Weyl is then recovered:

$$ds^2 = -e^{2\,\nu}\,dt^2 + e^{2\,\zeta-2\,\nu}\,\left(dR^2+dz^2\right) + R^2\,e^{-2\,\nu}d\phi^2, \tag{5.1}$$

where the functions $\zeta(R,z)$ and $\nu(R,z)$ are generally of the form (cf. Eq. (BLK 2.21))

$$\nu = -\int \frac{W\,(b)\;db}{\sqrt{R^2+(|z|+b)^2}}, \tag{5.2a}$$

$$\zeta = \int\int W\,(b_1)\,W\,(b_2)\,Z\,(b_1,b_2)\;db_1\,db_2, \tag{5.2b}$$

with Z given by

$$Z = -\frac{1}{2r_1r_2}\left\{1-\left(\frac{r_2-r_1}{b_2-b_1}\right)^2\right\} \geq 0\,. \tag{5.3}$$

Here b_1 and b_2 are the distances of two points below the disk's center and r_1 and r_2 are the distances measured from these points to a point above the disk. Below the disk, Z is given by reflection with respect to the plane $z=0$. When the line density of fictitious sources is of the form $W(b) \propto b^{-m}$ (Kuzmin-Toomre), or $W(b) \propto \delta^{(m)}\,(b)$ (Kalnajs-Mestel), the corresponding functions ζ,ν have explicitly been given in Bìcák, Lynden-Bell & Pichon (1994) [4]. For the metric of Eq. (5.1), the Lanczos tensor (2.14) reads

$$\begin{bmatrix} \mathcal{L}^{(t)(t)} \\ \mathcal{L}^{(R)(R)} \\ \mathcal{L}^{(\phi)(\phi)} \end{bmatrix} = \frac{e^{\nu-\zeta}}{4\pi\sqrt{1+f'^2}} \begin{bmatrix} \frac{f''}{1+f'^2}+\frac{f'}{R}+\frac{\partial(2\nu-\zeta)}{\partial N} \\ \frac{-f'}{R} \\ \frac{-f''}{1+f'^2}+\frac{\partial\zeta}{\partial N} \end{bmatrix}. \tag{5.4}$$

Consider again counter-rotating disks made of two equal streams of stars circulating in opposite directions around the disk center. The stress energy tensor is then the sum of the stress energy tensor of each stream:

$$\tau^{(a)(b)} = \begin{bmatrix} \varepsilon & 0 & 0 \\ 0 & p_{_R} & 0 \\ 0 & 0 & p_\phi \end{bmatrix} = \frac{2}{1-V_0^2} \begin{bmatrix} \varepsilon_0+p_0\,V_0^2 & 0 & 0 \\ 0 & \left(1-V_0^2\right)\,p_0 & 0 \\ 0 & 0 & p_0+\varepsilon_0 V_0^2 \end{bmatrix}, \tag{5.5}$$

the pressure p_0 in each stream being chosen to be isotropic in the plane. Subscript $(\quad)_0$ represents quantities measured for one stream. Expressions for ε, p_ϕ and $p_{_R}$ follow from identifying Eqs. (5.5) and (5.4) according to Eq. (2.13). Solving for ε_0, V_0, and p_0 in Eq. (5.5), given Eq. (5.4) and (2.13) gives

$$\varepsilon_0 = \frac{e^{\nu-\zeta}}{4\pi\sqrt{1+f'^2}}\left[\frac{f''}{1+f'^2}+\frac{\partial\,(\nu-\zeta)}{\partial N}\right], \tag{5.6a}$$

$$p_0 = \frac{e^{\nu-\zeta}}{8\pi\sqrt{1+f'^2}}\left[\frac{-f'}{R}\right], \tag{5.6b}$$

$$V_0^2 = \left(\frac{\partial\zeta}{\partial N}-\frac{f''}{1+f'^2}+\frac{f'}{R}\right)\left(\frac{f''}{1+f'^2}+\frac{\partial\,(2\nu-\zeta)}{\partial N}\right)^{-1}. \tag{5.6c}$$

The above solution provides the most general counter rotating disk model with pressure support. Indeed, any physical static disk will be characterised entirely by its vacuum field ν and its radial pressure profile $p_{_R}$, which in turn defines $W(b)$ and $f(R)$ uniquely according to Eqs. (5.6b) and (BLK 2.33). The other properties of the disk are then readily derived.

The angular frequency and angular momentum of these disks follow from Eq. (3.5), (3.4) on putting ω to zero and V to V_0. The epicyclic frequency κ given by Eq. $(D.4)$ may be recast as

$$\kappa^2 = \frac{e^\nu}{R_c^3}\frac{dh^2}{d\tilde{R}}, \tag{5.7}$$

which relates closely to the classical expression $\kappa^2 = R^{-3}dh^2/dR$.

The Ansatz given by Eq. (3.14) for $z = f(R)$ becomes, after the substitutions $\varepsilon \rightarrow \varepsilon_0$, $V \rightarrow V_0$, $p_\phi \rightarrow 0$,

$$(f'/R)' = -\eta\frac{\partial\nu}{\partial R}\left[\frac{\partial\nu}{\partial z} - \frac{1}{2}\frac{\partial\zeta}{\partial z}\right], \tag{5.8a}$$

$$= \eta\frac{\partial\nu}{\partial R}\frac{\partial\nu}{\partial z}\left[R\frac{\partial\nu}{\partial R} - 1\right], \tag{5.8b}$$

where z is to be evaluated at b. Equation (5.8b) follows from Eq. (5.8a) given the $\binom{R}{z}$ component of the Einstein equation outside the disk.

The equation of state for a relativistic isentropic 2D flow of counter-rotating identical particles is derived in appendix A while relating the perfect fluid stress energy tensor of the flow to the most probable distribution function which maximises the Boltzmann entropy. It reads

$$\varepsilon_0 = 2\,p_0 + \frac{\Sigma}{1 + p_0/\Sigma}\,. \tag{5.9}$$

Solving for Σ gives

$$\Sigma = \frac{1}{2}\left[\varepsilon_0 - 2\,p_0 + \sqrt{\varepsilon_0 - 2\,p_0}\,\sqrt{\varepsilon_0 + 2\,p_0}\right], \tag{5.10}$$

which in the classical limit gives $\Sigma \rightarrow \varepsilon_0 - p_0$. The binding energy of these counter rotating disks is computed here from Eq. (5.10) together with Eqs. (3.11) and (5.6). Alternatively, it could be computed by constructing distribution functions using the inversion described in Appendix B.

6. Examples of warm counter-rotating disks

6.1. Example 1 : The Self-similar disk

The symmetry of the self-similar disk allows one to reduce the partial differential equations corresponding to Einstein's field equations to an ordinary differential equation with respect to the only free parameter $\theta = \arctan(R/z)$ (Lemos, 89 [17]). Lemos' solution may be recovered and corrected by the method presented in sections 2 and 4. Weyl's metric in spherical polar co-ordinates (ρ, χ, ϕ) defined in terms of (R, z, ϕ) by $\rho = \sqrt{(R^2 + z^2)}$ and $\cot(\chi) = z/R$ is

$$d\sigma^2 = -e^{2\nu}d\tau^2 + \rho^2\left[e^{-2\nu}\,\sin^2(\chi)\,d\phi^2 + e^{2\zeta-2\nu}\left(\frac{d\rho^2}{\rho^2} + d\chi^2\right)\right]. \tag{6.1}$$

A self-similarity argument led Lemos to the metric

$$ds^2 = -r^{2n}e^N dt^2 + r^{2k}\left[e^{2P-N}\,d\phi^2 + e^{Z-N}\left(\frac{dr^2}{r^2} + d\theta^2\right)\right], \tag{6.2}$$

where P, N, and Z are given by

$$P(\theta) = \log\left[\sin(k+n)\,\theta\right], \tag{6.3a}$$

$$N(\theta) = \frac{4n}{k+n}\log\left[\cos(k+n)\,\theta/2\right], \tag{6.3b}$$

$$Z(\theta) = \frac{8n^2}{(k+n)^2}\log\left[\cos(k+n)\,\theta/2\right] + 2\log(k+n)\,. \tag{6.3c}$$

Here the ϕ's in both metrics have already been identified since they should in both case vary uniformly in the range $[0, 2\pi[$. The rest of the identification between the two metrics follows from the transformation

$$\chi = (n+k)\ \theta, \tag{6.4a}$$
$$\rho = r^{n+k}, \tag{6.4b}$$
$$\tau = t, \tag{6.4c}$$

with the result that ν and ζ take the form:

$$2\nu = N + 2n\log(r)\,, \tag{6.5a}$$
$$2\zeta = Z - 2\log(n+k)\,. \tag{6.5b}$$

This can be written in terms of the new variables given in Eqs. (6.4) as

$$\zeta = \frac{4n^2}{(k+n)^2}\log\left(\frac{\chi}{2}\right), \tag{6.6a}$$
$$\nu = \frac{2n}{(k+n)^2}\log\left(\frac{\chi}{2}\right) + \frac{n}{k+n}\log(\rho)\,. \tag{6.6b}$$

The procedure described earlier may now be applied. In order to preserve the self-similarity of the solution and match Lemos' solution, $f(R)$ is chosen so that

$$f'(R) = \text{const.} = \cot(\bar{\eta}) \quad \text{say.} \tag{6.7}$$

Then

$$\frac{\partial}{\partial N} \equiv \left(\frac{\partial}{\partial z} - f'\frac{\partial}{\partial R}\right) = -\frac{1}{\rho\,\sin(\bar{\eta})}\frac{\partial}{\partial\bar{\eta}}. \tag{6.8}$$

Putting Eqs. (6.6) and Eq. (6.8) into Eq. (2.15) gives

$$\begin{bmatrix}\varepsilon\\ p_{_R}\\ p_\phi\end{bmatrix} = \frac{r^{-k}}{4\pi}\left[\cos\left(\frac{\bar{\eta}}{2}\right)\right]^{\frac{2n(k-n)}{(k+n)^2}} \begin{bmatrix}\cot(\bar{\eta}) + \frac{2nk}{(k+n)^2}\tan(\eta/2)\\ -\cot(\bar{\eta})\\ \frac{2n^2}{(k+n)^2}\tan(\bar{\eta}/2)\end{bmatrix}, \tag{6.9}$$

with $\bar{\eta}$ to be evaluated at $(n+k)\,\pi/2$. The above equations are in accordance with the solution found by Lemos by directly integrating the Einstein field equations.

6.2. Example 2: The Curzon disk

The Curzon disk is characterised by the following pair of Weyl functions:

$$\nu = -\alpha/r, \qquad \zeta = -\alpha^2 R^2/\left(2\,r^4\right), \tag{6.10}$$

with $r = \sqrt{R^2+f^2}$, given the dimensionless parameter $\alpha = M/b$ (recall that $G \equiv c \equiv 1$), all lengths being expressed in units of b. This disk is the simplest example of the Kuzmin-Toomre family, where $W(b) \propto \delta(b)$. It also corresponds to the building block of the expansion given in Eqs. (5.2). Equations (5.4) and (5.5) then imply

$$\begin{bmatrix}\varepsilon\\ p_{_R}\\ p_\phi\end{bmatrix} = \frac{e^{-\frac{\alpha}{r}\left(1-\frac{\alpha R^2}{2r^3}\right)}}{4\pi b\sqrt{1+f'^2}} \begin{bmatrix}\frac{f''}{1+f'^2} + \frac{f'}{R} + \frac{\alpha}{r^6}\left\{2f\left(r^3-\alpha R^2\right) + \left[\alpha\left(R^2-f^2\right) - 2r^3\right]Rf'\right\}\\ \frac{-f'}{R}\\ -\frac{f''}{1+f'^2} + \frac{\alpha^2}{r^6}\left[2R^2 f - \left(R^2-f^2\right)Rf'\right]\end{bmatrix}. \tag{6.11}$$

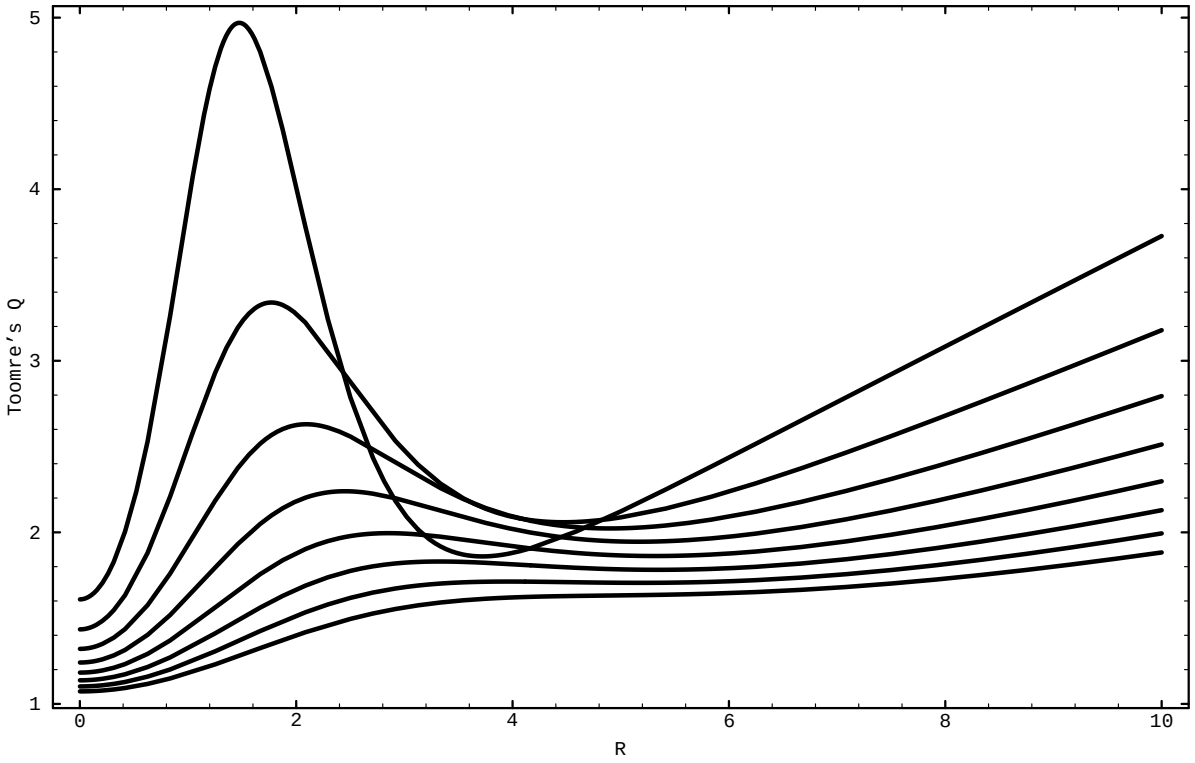

Figure 6.1: the "Toomre Q number" $Q = \sigma_{_R}\kappa/(3.36\Sigma_0)$ is plotted here as a function of circumferential radius R_c for different compactness parameter $\alpha = b/M$ when $\eta = 1/25$.

The weak energy conditions $\varepsilon \geq 0$, $\varepsilon + p_{_R} \geq 0$, and $\varepsilon + p_\phi \geq 0$ which follow are in agreement with those found by Chamorow *et al.*(1987) [5]. Their solution was derived by direct integration of Einstein's static equations using the harmonic properties of the supplementary unknown needed to avoid the patch of Weyl metric above and below the disk. The cut $z = f(R)$ corresponds to the imaginary part of the complex analytic function, the existence of which follows from the harmonicity of that new function.

The Ansatz (3.14) leads here to the cut

$$f\,(R) = b\, + \frac{\eta}{2}\left[\frac{b\,m^2}{4\,(b^2+R^2)} - \frac{2b\,m^3\,\left(4b^2+7\,R^2\right)}{105\,\left(b^2+R^2\right)^{5/2}}\right]\,. \tag{6.12}$$

In Fig. 6.1, the ratio of the binding energy of these Curzon disks (which is derived from Eqs. (3.11), (5.10),(6.11) and (6.12)) over the corresponding rest mass M_0 is plotted with respect to the compactness parameter b/M_0 for different ratios p_0/ε_0 measured at the origin. The relative binding energy decreases in the most compact configurations because these contain too many unstable orbits ($\kappa^2 < 0$). A maximum ratio of about 5 % is reached.

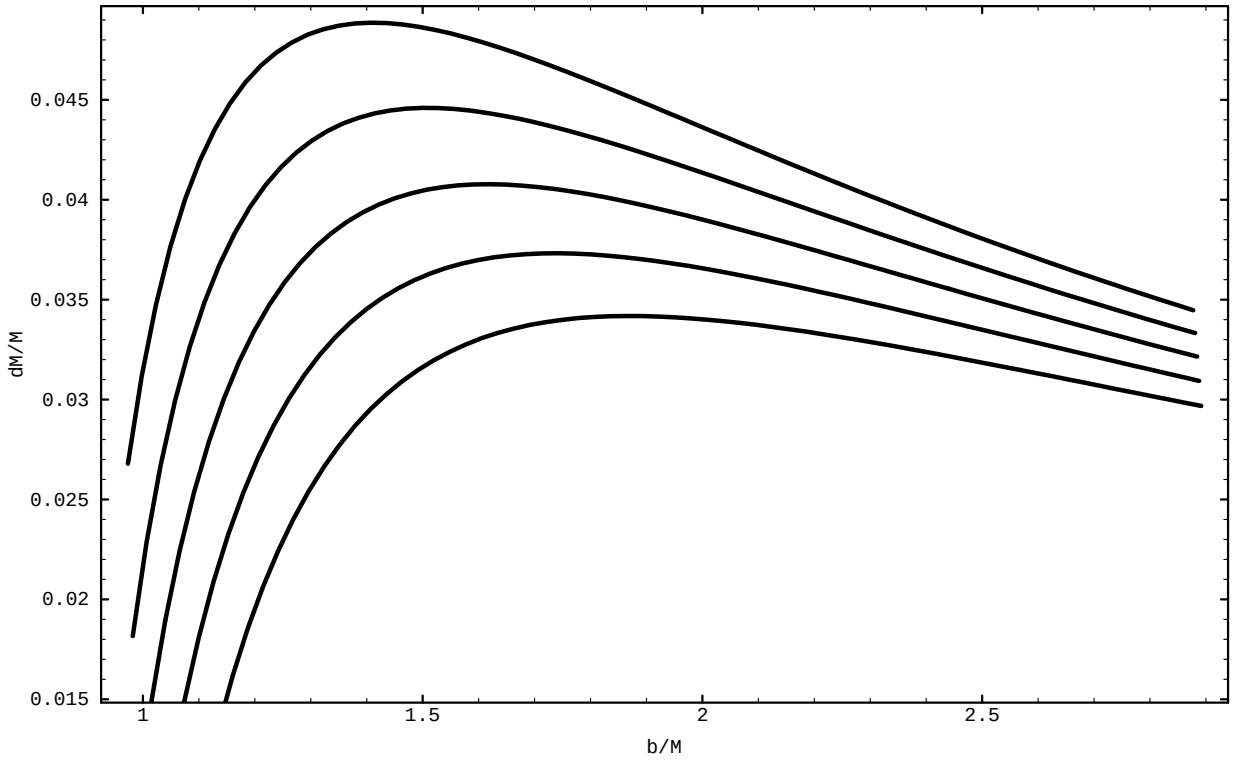

Figure 6.2: the binding energy over the rest mass $\Delta E/M_0$ for Curzon disks, plotted against the compactness parameter $\alpha = b/M$ for different ratios p_0/ε_0 fixed by $\eta = 0.01, 0.16, \cdots, 0.7$.

7. Examples of rotating disks and an internal solution for the Kerr metric

The problem of constructing disks with proper rotation and partial pressure support is more complicated but physically more appealing than that of counter rotating solutions. It is now illustrated on an internal solution for the Kerr metric, and a generalisation of the solutions constructed by BLK and BLP to *warm rotating* solutions is sketched.

7.1. A Kerr internal solution

The functions (ν, ζ, ω) for the Kerr metric in Weyl-Papapetrou form expressed in terms of spheroidal co-ordinates ($R = s\sqrt{(x^2 \mp 1)(1 - y^2)}$, $z = sxy$) are given by

$$e^{2\nu} = \frac{-m^2 + s^2\, x^2 + a^2\, y^2}{(m + s\, x)^2 + \ a^2\, y^2}, \tag{7.1}$$

$$e^{2\zeta} = \frac{-m^2 + s^2\, x^2 + a^2\, y^2}{s^2\ (x^2 \mp y^2\ )}, \tag{7.2}$$

and

$$\omega = -\frac{2\, a\, m\ (m + s\, x)\ \left(1 - y^2\right)}{-m^2 + \ s^2\, x^2 + a^2\, y^2}, \tag{7.3}$$

where $s = (\pm(m^2 - a^2))^{1/2}$. Here $\pm$ corresponds to the choice of prolate $(+)$, or oblate $(-)$ spheroidal co-ordinates corresponding to the cases $a < m$ and $a > m$ respectively. In this set of co-ordinates, the prescription given in section 2 leads to completely algebraic solutions. The normal derivative to the surface $z = f(R)$ reads (when $a > m$)

$$(\partial/\partial N) = N\,(x, y)\,(\partial/\partial x) + N\,(y, x)\,(\partial/\partial y)\,, \tag{7.4}$$

where

$$N(x,y) = \left(x^2-1\right)\left[y/s + x\ \left(y^2-1\right)\ f'/R\right]/\left(x^2-y^2\right).$$

Differentiating Eqs. (7.1) through (7.3) with respect to x and y together with Eq. (7.4) leads via Eqs. (2.15) to all physical characteristics of the Kerr disk in terms of the Kerr metric parameters m and a, and the function $z = f(R)$ which must be chosen so as to provide relevant pressures and energy distributions according to Eqs. (3.12). (Bìcák & Ledvinka (1993) [2] have constructed independently a cold Kerr solution when $a < m$.) On the axis $R = 0$, $f \equiv b$, and $f'' \equiv -c$, while Eqs. (3.12) imply $f' = 0$ at $(x = b/s,\ y = 1)$. This in turn implies

$$(p_\phi)_0 = (p_{_R})_0 = \frac{c}{4\pi}\sqrt{\frac{a^2+b^2-m^2}{a^2+(b+m)^2}}, \tag{7.5a}$$

$$(\varepsilon)_0 = \frac{1}{4\pi}\sqrt{\frac{a^2+b^2-m^2}{a^2+(b+m)^2}}\left[\frac{2m\left[(b+m)^2-a^2\right]}{\left(a^2+(b+m)^2\right)\left(a^2+b^2-m^2\right)} - c\right], \tag{7.5b}$$

where $(\quad)_0$ stands for $(\quad)$ taken at $R = 0$. The constraint that all physical quantities should remain positive implies

$$b \geq \sqrt{m^2-a^2}, \tag{7.6a}$$

$$c \leq 2m\frac{(b+m)^2-a^2}{\left(a^2+(b+m)^2\right)\left(a^2+b^2-m^2\right)}. \tag{7.6b}$$

Equation (7.6a) is the obvious requirement that the surface of section should not enter the horizon of the fictitious source. Similarly, ergoregions will arise when the cut $z = f(R)$ enter the torus

$$\left(\frac{z}{m}\right)^2 + \left(\frac{R}{m} - \frac{a}{m} + \frac{1}{2}\frac{m}{a}\right)^2 = \left(\frac{1}{2}\frac{m}{a}\right)^2. \tag{7.7}$$

The analysis may be extended beyond the ergoregion via the ZAMO frame. The characteristics of these frames are given by Eq. (3.7), (3.8) and (3.9). The central redshift

$$1 + z_c = e^{-\nu} = \frac{(m+b)^2+a^2}{b^2+a^2-m^2}, \tag{7.8}$$

can be made very large for such models constructed when $b \to \sqrt{m^2-a^2}$.

On Fig. 7.1, Fig. 7.2 and Fig. 7.3, some characteristics of these Kerr disks with both $a > m$ and $a < m$ are illustrated. For simplicity, pressure is implemented via the cut (6.12). These disks present anisotropy of the planar pressure tensor ($p_\phi \neq p_{_R}$). The anisotropy follows from the properties of the ω vacuum field which gives rise to the circular velocity curve. Indeed, in the outer part of the disk, the specific angular momentum h tends asymptotically to a constant. The corresponding centrifugal force is therefore insufficient to counter-balance the field generated by the ν function. As this construction scheme generates such equilibria, the system compensates by increasing its azimuthal pressure away from isotropy. When $a > m$, and $\eta = 0$ the height of the critical cut corresponding to the last disk with positive pressures everywhere scales like $a\,(a^2-m^2)^{1/2}$ in the range $2 \leq a/m \leq 20$. Note that this limit is above that of the highly relativistic motions which only occurs when b tends asymptotically to the Kerr horizon $(a^2-m^2)^{1/2}$. The binding energy which follows Eq. (4.15) reaches values as high as one tenth of the rest mass for the most compact configurations. The inversion method described in section 4.1 was carried for the Kerr disks and yields distribution functions which characterise completely the equilibria as illustrated on Fig. 7.5. It was assumed that the velocity distribution of stars at radius R was a modified squared Lorentzian, as discussed in Appendix C and shown on Fig. 7.4. Note that disks with low rotation support present in their outer parts two distinct maxima, one of which is counter rotating, in agreement with the assumptions yielding the equation of state Eq. (4.15).

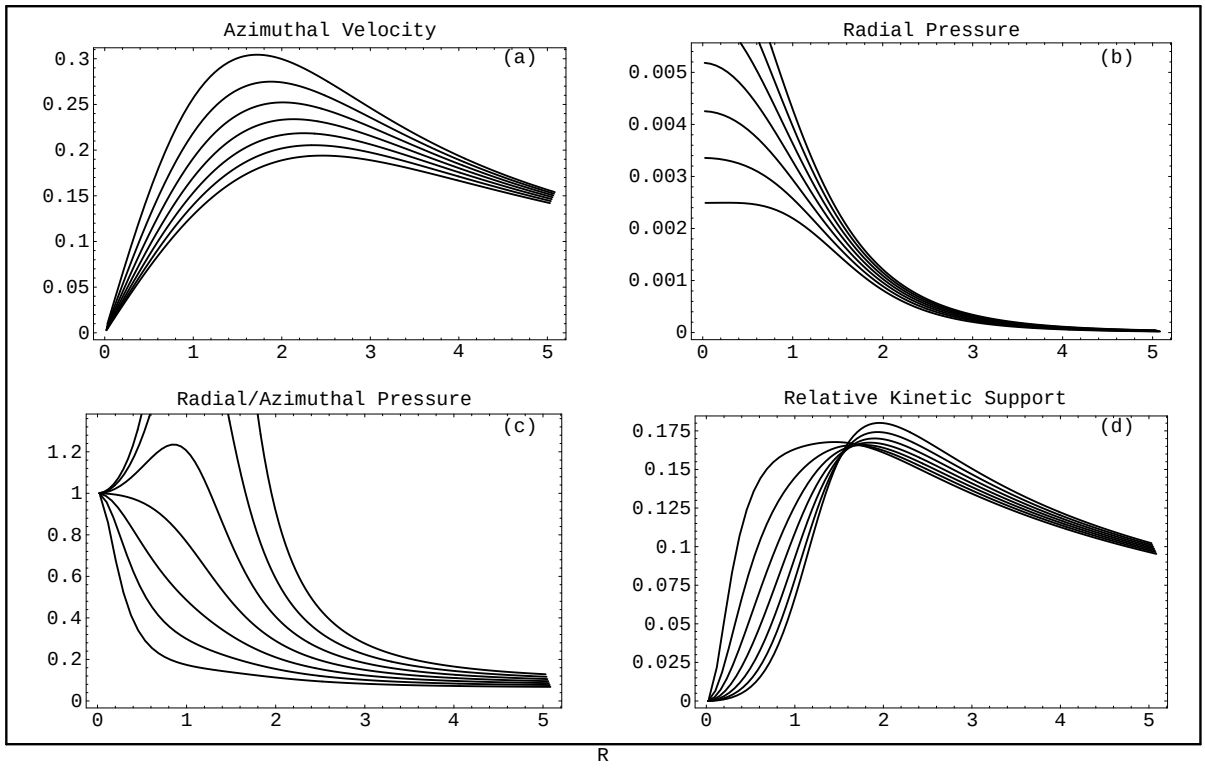

Figure 7.1: the azimuthal velocity (a), the radial pressure (b), the ratio of radial over azimuthal pressure and the relative fraction of Kinetic Support (d) namely $\varepsilon V^2/(\varepsilon V^2 + p_\phi + p_{_R})$ for the $a/m = 0.5$ Kerr disk as a function of circumferential radius R_c, for a class of solutions with decreasing potential compactness, $b/m = 1.1, 1.2 \cdots 1.7$, and relative radial pressure support $\eta/m = 1/5 + 2(b/m - 1)/5$.

7.2. Other rotating solutions

The rotating disk models given in section 2 require prior knowledge of the corresponding vacuum solutions. However, while studying the symmetry group of the stationary axially symmetric Einstein Maxwell equations, Hoenselaers, Kinnersley & Xanthopoulos (1979) [13,14] found a method of generating systematically complete families of stationary Weyl-Papapetrou vacuum metrics from known static Weyl solutions. Besides, the decomposition of the Weyl potential ν_0 into line densities provides a direct and compact method of finding solutions to the static field. The N+1 rank zero HKX transform is defined as follows: let ν_0 and ζ_0 be the seed Weyl functions given by Eqs. (5.2). HKX define the $N \times N$ matrix $\mathbf{\Gamma}$ parameterised by N twist parameters α_k and N poles, a_k, $k = 1, \cdots N$ as

$$\left(\Gamma^{\pm}\right)_{k,k'} = i\,\alpha_k\,\frac{e^{\beta_k}}{r_k}\left[\frac{r_k - r_{k'}}{a_k - a_{k'}} \pm 1\right], \tag{7.9}$$

with $r_k = r(a_k) = \sqrt{R^2 + (z - a_k)^2}$ and $\beta_k = \beta(a_k)$, β being a function satisfying (7.11a) below. Defining $\mathbf{r} = \mathrm{Diag}(r_k)$, they introduce the auxiliary functions

$$D^{\pm} = \left|\mathbf{1} + \mathbf{\Gamma}^{\pm}\right|, \text{ and } L_{\pm} = 2D^{\pm}\,\mathrm{tr}\left[\left(\mathbf{1} + \mathbf{\Gamma}^{\pm}\right)^{-1}\mathbf{\Gamma}^{\pm}\,\mathbf{r}\right],$$
$$\omega_{\pm} = D^{+} \pm e^{2\nu_0} D^{-}, \text{ and } \mathcal{M}_{\pm} = \varpi\,\omega_{\pm} + 2\left(L_{+} \mp e^{2\nu_0} L_{-}\right),$$

which lead to the Weyl-Papapetrou potentials

$$e^{2\nu} = e^{2\nu_0}\,\Re\left[\frac{D^{-}}{D^{+}}\right], \tag{7.10a}$$

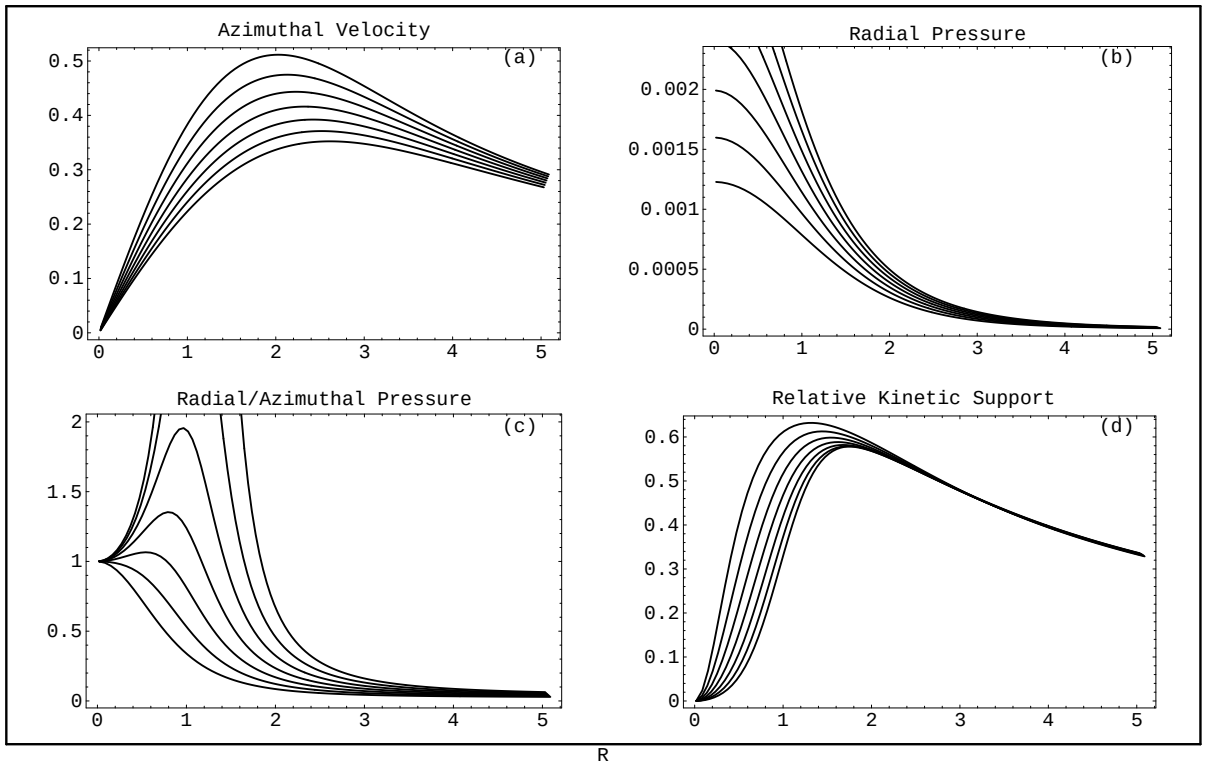

Figure 7.2: as in Fig. 7.1 with $a/m = 0.95$, $\eta/m = 1/15 + (b-1)/5$. Note the large relative kinetic support.

$$e^{2\zeta} = k e^{2\zeta_0} \Re\left[D^- D^{+*}\right], \tag{7.10b}$$

$$\omega = 2\Im\left[\frac{\mathcal{M}_+^* (\omega_+ + \omega_-) - \mathcal{M}_- (\omega_+ + \omega_-)^*}{|\omega_+|^2 - |\omega_-|^2}\right], \tag{7.10c}$$

where $\Re$ and $\Im$ stand respectively for the real part and the imaginary part of the argument and $(\quad)^*$ represents the complex conjugate of $(\quad)$. k is a constant of integration which is fixed by the boundary conditions at infinity. The two yet unspecified function β and ϖ satisfy:

$$\nabla\beta(a_k) = \frac{1}{r_k}\left(\left[z - a_k\right]\nabla + R\,\mathbf{e}_\phi \times \nabla\right)\nu_0, \tag{7.11a}$$

$$\nabla\varpi = R\,\mathbf{e}_\phi \times \nabla\nu_0, \tag{7.11b}$$

where $\nabla = (\partial/\partial R, \partial/\partial z)$ and $\mathbf{e}_\phi$ is the unit vector in the ϕ direction. The linearity of these equations suggests again that solutions should be sought in terms of the line density, $W(b)$, characterising ν_0, namely

$$\beta(a_k) = \int \frac{W(b)}{a_k}\left[\frac{R^2 + (z - b - a_k)^2}{R^2 + (z-b)^2}\right]^{\frac{1}{2}} db, \tag{7.12a}$$

$$\varpi = \int \frac{W(b)\,(b-z)}{\sqrt{R^2 + (z-b)^2}}\, db. \tag{7.12b}$$

It is therefore a matter of algebraic substitution to apply the above procedure and construct all non-linear stationary vacuum fields of the Papapetrou form from static Weyl fields. Following the prescription described in section 2, the corresponding disk in real rotation is then constructed. The requirement for the physical

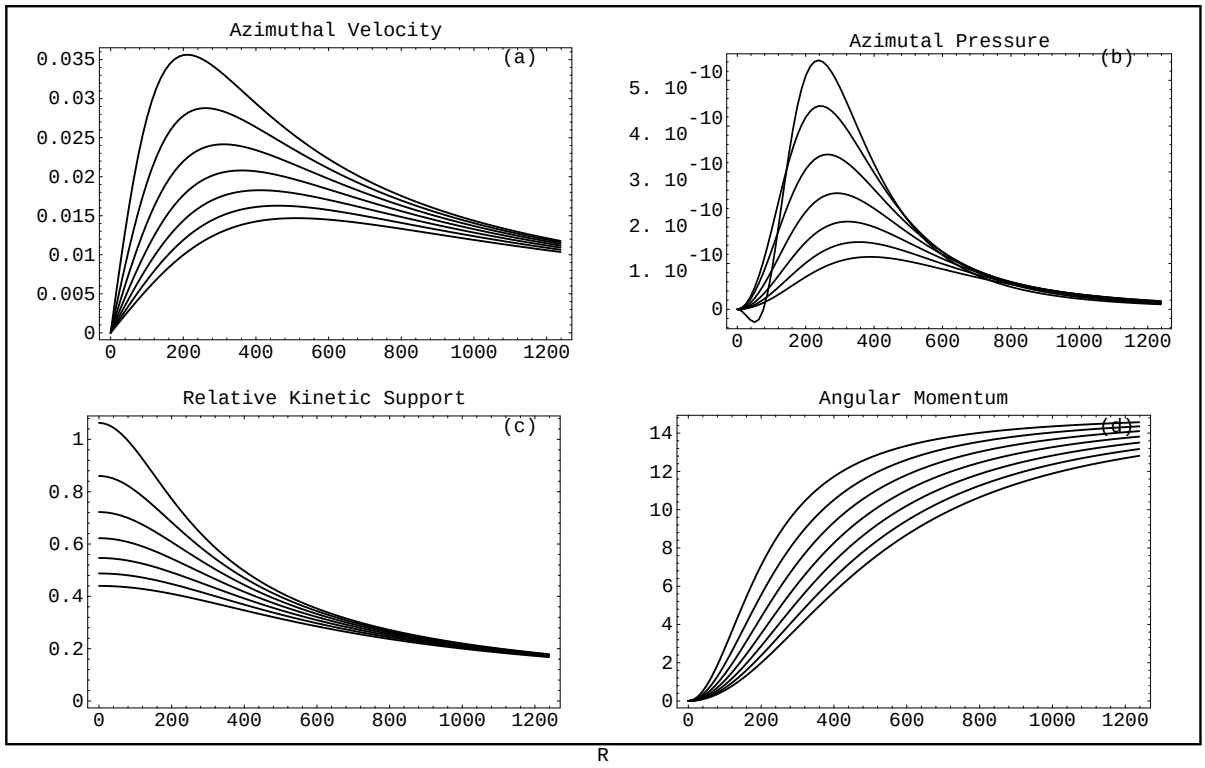

Figure 7.3: the azimuthal velocity (a), the azimuthal pressure (b), the relative fraction of Kinetic Support (c), namely $\varepsilon V^2/(\varepsilon V^2 + p_\phi)$ and the angular momentum (d) for the $a/m = 10$ zero radial pressure Kerr disk as a function of circumferential radius R_c, for a class of solutions with decreasing potential compactness $b/m = 210, 260 \cdots 510$. The first curve corresponds to a cut which induces negative azimuthal pressure (tensions).

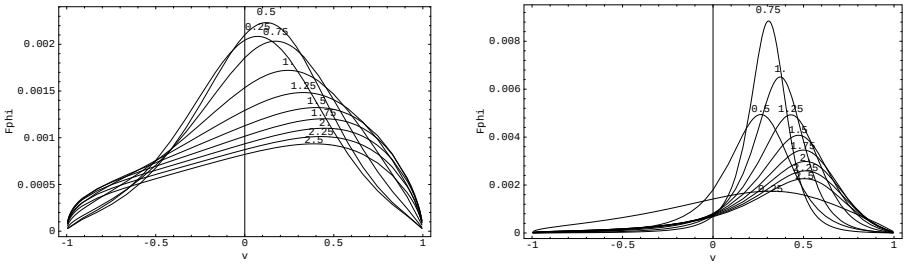

Figure 7.4: Parametrization of the number of star with velocity v_ϕ at radius R as a squared Lorentzian (as discussed in Appendix C) for the Kerr disk. The corresponding radius is appended on each curve. The left panel correspond to $a = 0.2$ while the right panel corresponds to $a = 0.8$. The pressure law is given in the caption of Fig. 7.5 where the corresponding distribution function is illustrated.

source to be a disk is in effect a less stringent condition on the regularity of the vacuum metric in the neighbourhood of its singularity because only the half space which does not contain these singularities is

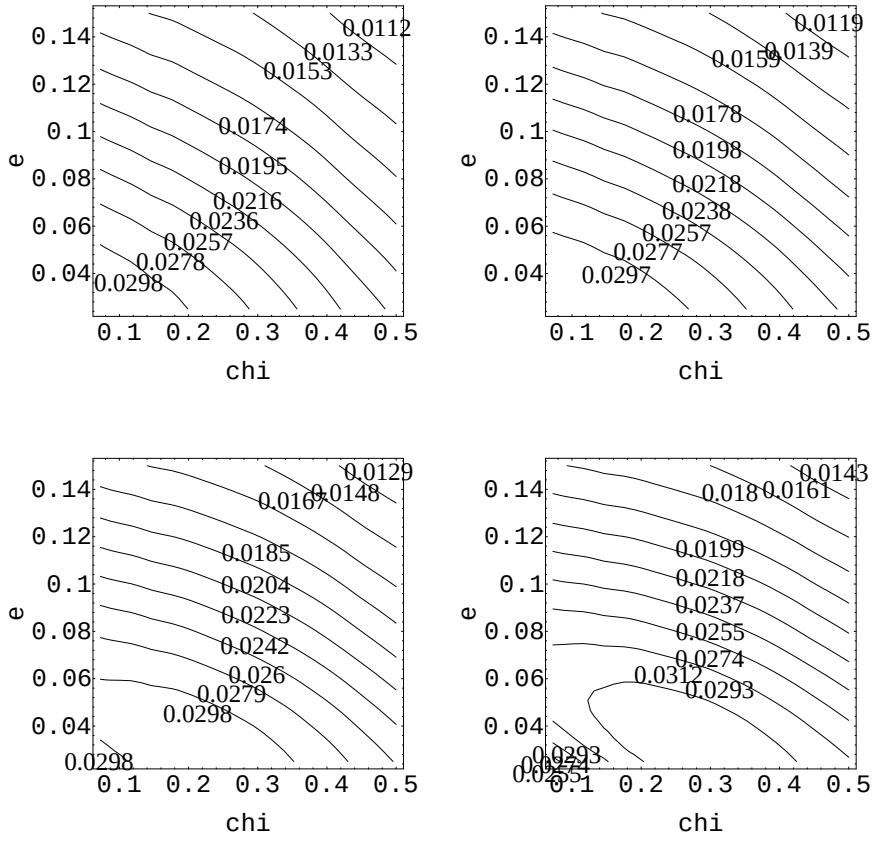

Figure 7.5: the isocontours of the distribution function for the Kerr disk as a function of the reduced momentum $\chi = h/\epsilon$, and the relative eccentricity of the orbit $\bar{e}_c = (\epsilon - \epsilon_\chi)/(1-\epsilon_\chi)$ where ϵ_χ is the energy of circular orbits with reduced momentum χ. The four panels correspond to $a = 0, 0.1, 0.2, 0.3, 0.4$ from left to right and top to bottom, while the pressure law was chosen to correspond to the cut $f(R) = -4(4+7R^2)/(525(1+R^2)^{5/2}) + (16+15R^2)/(10(1+R^2))$ corresponding to a tepid disk. The figures are centered on the inner parts of the disk to illustrate the relative shift of the maximum number of stars towards larger angular momentum for faster rotating disks. The inversion assumed a squared Lorentzian for the distribution in angular velocity as discussed in Appendix C and illustrated on Fig. 7.4.

physically meaningful. A suitable Ehlers transformation on $D_-/D+$ ensures asymptotic flatness at large distance from the source.

To illustrate this prescription consider the vacuum field given by Yamazaki (1981) [27]. This field arises from 2 HKX rank zero transformation on the Zipoy-Voorhess [25] static metric given by

$$\nu_0 = \tfrac{1}{2}\delta \log \frac{(x-1)}{(x+1)}, \tag{7.13a}$$

$$\zeta_0 = \tfrac{1}{2}\delta^2 \log \frac{(x-1)}{(x^2-y^2)}, \tag{7.13b}$$

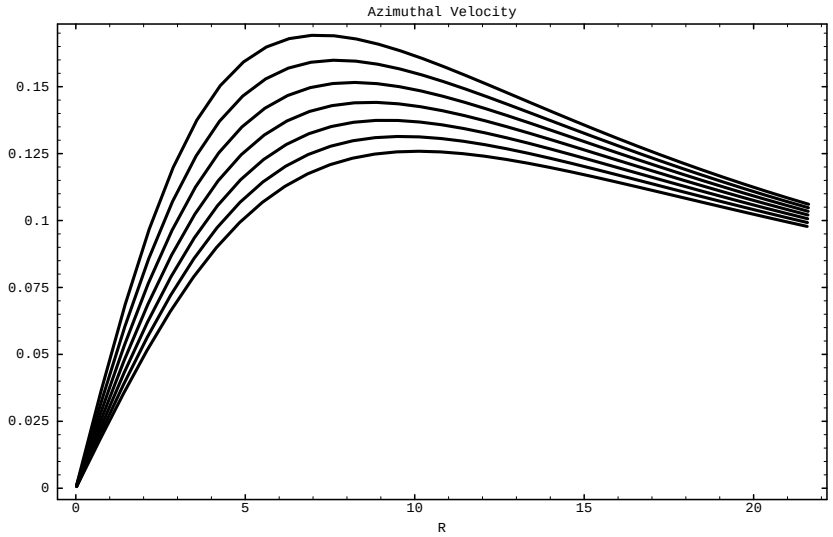

Figure 7.6: the azimuthal velocity for the a/κ_Y zero radial pressure Yamazaki disk as a function of circumferential radius R_c, for a class of solutions with decreasing potential compactness $b/\kappa_Y = 3.6, 3.8, \cdots 5$. κ_Y is the natural unit of distance in these disks as defined by Yamazaki's Eq. (Y-2) [27].

in prolate spheroidal co-ordinates. It corresponds to a uniform line density between $\pm\delta$. The functions β and ϖ follow from Eqs. (7.12). Choosing poles $a_k,\ k = 1, 2$ at the end of the rod $\pm\delta$, leads to

$$\beta\left(a_{\pm}\right) = \tfrac{1}{2}\delta \log \frac{x^2 - 1}{\left[x \mp y\right]^2}, \tag{7.14a}$$

$$\varpi = 2\delta y. \tag{7.14b}$$

Equations (7.10) together with (7.13) and (7.11) characterize completely the three Weyl-Papapetrou metric functions ν, ζ, and ω; all physical properties of the corresponding disks follow. For instance, Fig. 7.6 gives the zero radial pressure velocity curve of the Yamazaki disk spanning from the Schwarzschild ($\delta = 1/2$) metric when $\alpha_1 = \alpha_2$.

More generally, the extension of this work to the construction of disks with planar *isotropic* pressures should be possible by requiring that Eq. (2.15c) is identically equal to Eq. (2.15d) given Eq. (7.10).

8. Conclusion

The general counter rotating disk with partial pressure support has been presented. The suggested method for implementing radial pressure support also applies to the construction of stationary axisymmetric disk with rotation but requires prior knowledge of the corresponding vacuum solution. In this manner, a disk-like source for the Kerr field has been constructed orbit by orbit. The corresponding distribution reduces to a Keplerian flow in the outer part of the disk and presents strong relativistic features in the inner regions such as azimuthal velocities close to that of light, large central redshift and ergoregions. The disk itself is likely to be stable against ring formation and the ratio of its binding energy to rest mass can be as large as 1:10. The broad lines of how to construct all rotating disks arising from HKX-transforming the corresponding counter rotating model into a fully self-consistent model with proper rotation and partial pressure support has been sketched. It should be a simple matter to implement this method with the additional requirement that the pressure remains isotropic with a sensible polytropic index. One could then analyse the fate of a sequence of gaseous disks of increasing compactness and relate it to the formation and evolution of quasars

at high redshift. Alternatively, the inversion method described in section 4.1 yields a consistent description of the detailed dynamics for all disks in terms of stellar dynamics.

References

1. Bardeen, J. *"A variational principle for rotating stars in general relativity."* ApJ 162, 71-95 (1970).
2. Bìcák, J. & Ledvinka, T. *"Relativistic disks as sources of the Kerr metric."* Phys Rev D 71, 1669-1672 (1993).
3. Bìcák, J. Lynden-Bell, D. et al. *"Relativistic disks as sources of static vacuum spacetimes." Phys Rev D 47, 4334-4343 (1993).*
4. *Bìcák J, Lynden-Bell, D & Pichon C."Relativistic discs and flat galaxy models"MNRAS 265, 126-144 (1993).*
5. *Chamorow, A., R. Gregory, et al. "Static axisymmetric discs and gravitational collapse." Proc R. Soc. Lond. 413, 251-262 (1987).*
6. *Curzon,H. Proc.Lond.Math.Soc. 23, 477-480 (1924).*
7. *Dietz, W. & C. Hoenselaers "Stationary system of two masses kept apart by their gravitational spin spin interaction." Phys Rev Lett 48, 778-780 (1982).*
8. *Dietz, W. and C. Hoenselaers "Two mass Solutions of Einstein's Vacuum Equations: The double Kerr solution." Ann Phys 165, 319-383 (1985).*
9. *Evans, N. and P. de Zeeuw "Potential-density Pairs for Flat Galaxies." MNRAS 257, 152-176 (1992).*
10. *Fackerell, E. ApJ 153, 643-660 (1968).*
11. *Katz, J. Horwitz, G & Klapish, M. ApJ 199, 307-321 (1975).*
12. *Kerr,R. Phys.Rev.Let. 11, 237-238 (1963).*
13. *Hoenselaers, C., W. Kinnersley, et al. "Symmetries of the stationary Einstein-Maxwell equations, VI Transformations which generate asymptotically flat spacetimes with arbitrary multipole moments." J Math Phys 20, 2530-2536 (1979).*
14. *Hoenselaers, C. and W. Dietz "The rank N HKX Transformations: New stationary Axisymmetric Gravitational fields." Gen Rel Grav 16, 71-78 (1984).*
15. *Ipser,J. ApJ 158, 17-43 (1969).*
16. *Israel, W. Nuovo-Cimento 33, 331-335 (1964).*
17. *Lemos, J. "Self Similar relativistic Discs with Pressure." Class Q Grav 6, 1219-1230 (1989).*
18. *Morgan,T, Morgan L. Phys.Rev. 183, 1097-1102 (1969).*
19. *Misner, C.,Thorne, K. & Wheeler, J. , Gravitation,Freeman,(1973).*
20. *Pichon, C, & Lynden-Bell, D"Equilibria of flat and round disks"(1995) to appear in MNRAS.*
21. *Synge,J. The Relativistic Gas, North Holand (1957).*
22. *Ipser, J. & Thorne ApJ 154, 251- (1968).*
23. *Tolman, R. "Relativity, Thermodynamics and Cosmology.", Oxford University Press, (1934).*
24. *Toomre, A. "On the Gravitational Stability of a Disc of Stars." ApJ 139, 1217-1238 (1964).*
25. *Voorhess, B. Phys. Rev.* **D**. *2, 2119 (1970).*
26. *Weyl, H. Ann.Phys. 54, 117-118 (1917).*
27. *Yamazaki, M. "On the Hoenselaers-Kinnersley-Xanthopoulos spinning mass fields. J Math. Phys. 22, 133-135 (1981).*

A. Equation of state for a relativistic 2D adiabatic flow

The equation of state of a planar adiabatic flow is constructed here by relating the perfect fluid stress energy tensor of the flow to the most probable distribution function which maximises the Boltzmann entropy. Synge [21] gives an extensive derivation of the corresponding equation of state for a 3D flow. These properties are local characteristics of the flow. It is therefore assumed that all tensorial quantities introduced in this section are expressed in the local Vierbein frame.

Consider a infinitesimal volume element $d\vartheta$ defined in the neighbourhood of a given event, and assume that the particles entering this volume element are subject to molecular chaos. The distribution function F of particles is defined so that $F(\mathbf{R},\mathbf{P})\; d\vartheta d^2P$ gives the number of particles in the volume ϑ centered on $\mathbf{R}$ with 2-momentum pointing to $\mathbf{P}$ within d^2P.

The most probable distribution function $F^\star$ for these particles is then given by that which maximises Boltzmann entropy S subject to the constraints imposed by the conservation of the total energy momentum and by the conservation of the number of particles within that volume. This entropy reads in terms of the distribution F

$$S = -d\vartheta \int F \log F \, d^2P \, . \tag{A.1}$$

The stress energy tensor corresponds to the instantaneous flux density of energy momentum through the elementary volume $d\vartheta$ (here a surface)

$$T^{\alpha b} = \int F^\star P^\alpha P^\beta \, \frac{d^2P}{|\mathcal{E}|} \, , \tag{A.2}$$

where the $1/|\mathcal{E}|$ factor accounts for the integration over energy-momentum space to be restricted to the pseudo-sphere $P^\alpha P_\alpha = m^2$. Indeed the detailed energy-momentum conservation requires the integration to be carried along the volume element

$$\int \delta\left(P^\alpha P_\alpha - m^2\right)\, d^3P = \int \delta\left(P^{0\,2} - \mathcal{E}^2\right)\, d^2P dP^0 = \frac{d^2P}{|\mathcal{E}|} \, , \tag{A.3}$$

where $\mathcal{E} = \sqrt{m^2 + \mathbf{P}^2}$. It is assumed here that momentum space is locally flat. Similarly the numerical flux vector reads

$$\phi^\alpha_\star = \int F^\star P^\alpha \, \frac{d^2P}{|\mathcal{E}|} \, . \tag{A.4}$$

The conservation of energy-momentum of the volume element $d\vartheta$ implies that the flux of energy momentum across that volume should be conserved; this flux reads

$$T^{\alpha\beta}\, n_\beta \, d\vartheta = d\vartheta \int F^\star P^\alpha \, d^2P = \text{Const.} \, , \tag{A.5}$$

where n_β is the unit time axis vector. Keeping the population number constant provides the last constraint on the possible variations of S

$$\phi^\alpha_\star n_\alpha d\vartheta = d\vartheta \int F^\star d^2P = \text{Const.} \, . \tag{A.6}$$

Varying Eq. $(A.1)$ subject to the constraints $(A.5)$ $(A.6)$, and putting δS to zero leads to

$$(\log F^\star + 1)\, \delta F^\star = a \delta F^\star + \lambda_\alpha P^\alpha \delta F^\star \, , \tag{A.7}$$

where a and λ_α are Lagrangian multipliers corresponding resp. to $(A.5)$ $(A.6)$. These multipliers are independent of P^a but in general will be a function of position. The distribution which extremises S therefore reads

$$F^\star = C \exp\left(\lambda_\alpha P^\alpha\right) \, . \tag{A.8}$$

The 4 constants C and λ_a are in principle fixed by Eqs. $(A.5)$ and $(A.6)$. The requirement for $F^\star$ to be Lorentz invariant – that is independent of the choice of normal n_α – and self consistent, is met instead by demanding that $F^\star$ obeys Eq. $(A.2)$ and $(A.4)$, namely

$$C \int P^\alpha \exp\left(\lambda_\mu P^\mu\right) \frac{d^2P}{|\mathcal{E}|} = \phi^\alpha_\star \,, \tag{A.9}$$

$$C \int P^\alpha P^\beta \exp\left(\lambda_\mu P^\mu\right) \frac{d^2P}{|\mathcal{E}|} = T^{\alpha\beta} \,, \tag{A.10}$$

where $\phi^\alpha_\star$ and $T^{\alpha\beta}$ satisfy in turn the covariant constraints

$$\frac{\partial T^{\alpha\beta}}{\partial x^\beta} = 0 \quad \text{and} \tag{A.11a}$$

$$\frac{\partial \phi^\alpha_\star}{\partial x^\alpha} = 0 \,. \tag{A.11b}$$

Equations $(A.9)$-$(A.11)$ provide a set of thirteen equations to constraint the thirteen functions $C, \lambda_\alpha, \phi^\alpha_\star$, and $T^{\alpha\beta}$. Equations $(A.9)$ and $(A.10)$ may be rearranged as

$$\phi^\alpha_\star = C\frac{\partial \Phi}{\partial \lambda^\alpha} \,, \quad T^{\alpha\beta} = C\frac{\partial^2 \Phi}{\partial \lambda^\alpha \partial \lambda^\beta} \,, \tag{A.12}$$

where the auxiliary function Φ is defined as $\Phi = \int \exp(\lambda_\alpha P^\alpha)\, d^2P/|\mathcal{E}|$; Φ is best evaluated using pseudo polar coordinates corresponding to the symmetry imposed by the energy momentum conservation $P^\alpha P_\alpha - m^2 = 0$; these are

$$\begin{aligned} P^1 &= m \sinh\chi \cos\phi \,, \\ P^2 &= m \sinh\chi \sin\phi \,, \\ P^0 &= im \cosh\chi \,, \end{aligned} \tag{A.13}$$

where the coordinate χ is chosen so that the normal n_α lies along $\chi = 0$. In terms of these variables, $d^2P/|\mathcal{E}|$ then reads

$$d^2P/|\mathcal{E}| = dP^1 dP^2/m\cosh\chi = m \sinh\chi d\chi d\phi \,. \tag{A.14}$$

Moving to a temporary frame in which λ^0 is the time axis ($\lambda^0 = i\lambda = i(-\lambda_\alpha\lambda^\alpha)^{1/2}$, $\lambda^k = 0$ $k = 1,2$), Φ becomes

$$\Phi = 2\pi m \int_0^\infty \exp\left(-m\lambda\cosh\chi\right) \sinh\chi d\chi = \frac{2\pi}{\lambda}\exp\left(-\lambda\right) \,. \tag{A.15}$$

From Eq. $(A.9)$-$(A.10)$ and $(A.15)$, it follows that

$$T^{\alpha\beta} = \frac{2\pi C}{\lambda^3}\exp\left(-\lambda\right)\left[\left\{\lambda^2+3\lambda+3\right\}\frac{\lambda^\alpha}{\lambda}\frac{\lambda^\beta}{\lambda} + \left\{\lambda+1\right\}\delta^{\alpha\beta}\right] \,, \tag{A.16}$$

$$\phi^\alpha_\star = \frac{2\pi C}{\lambda^3}\exp\left(-\lambda\right)\left\{\lambda+1\right\}\lambda^\alpha \,. \tag{A.17}$$

On the other hand, the stress energy tensor of a perfect fluid is

$$T^{\alpha\beta} = \left(\varepsilon_0 + p_0\right) U^\alpha U^\beta + p_0\, \delta^{\alpha\beta} \,, \tag{A.18}$$

while the numerical surface density of particles measured in the rest frame of the fluid Σ is related to $\phi^\alpha_\star$ via

$$\Sigma = -\phi^\alpha_\star U_\alpha \,. \tag{A.19}$$

Eq. $(A.16)$ has clearly the form of Eq. $(A.18)$ when identifying

$$U^\alpha = \lambda^\alpha/\lambda \,, \tag{A.20a}$$

$$\varepsilon_0 + p_0 = \frac{2\pi C}{\lambda^3}\exp\left(-\lambda\right)\left\{\lambda^2+3\lambda+3\right\} \,, \tag{A.20b}$$

$$p_0 = \frac{2\pi C}{\lambda^3}\exp\left(-\lambda\right)\left\{\lambda+1\right\} \,. \tag{A.20c}$$

Eliminating λ,C between Eqs. $(A.17)$–$(A.20c)$ yields the sought after equation of state

$$\varepsilon_0 = 2\,p_0 + \frac{\Sigma}{1+p_0/\Sigma}\,. \tag{A.21}$$

where $p_0 = \Sigma/\lambda$. This is the familiar gas law given that $1/\lambda$ is the absolute temperature. The equation of state Eq. $(A.21)$ corresponds by construction to an isentropic flow. Indeed, using the conservation equations Eq. $(A.11a)$ dotted with U^α, and Eq. $(A.11b)$ together with $U^\alpha U_\alpha = -1$ yields after some algebra to the identity

$$\lambda\frac{d}{ds}\left[\frac{(\lambda^2+3\lambda+3)}{\lambda\,(\lambda+1)}\right] + \frac{1}{\lambda} = -\frac{\partial U^\alpha}{\partial x^\alpha} = \frac{1}{\Sigma}\frac{d\Sigma}{ds}\,, \tag{A.22}$$

where $d/ds = (dx^\alpha/dx^\alpha)(\partial/\partial x^\alpha)$ is the covariant derivative following the stream lines. Writing the $r.h.s$ of Eq. $(A.22)$ as an exact covariant derivative leads to the first integral

$$\frac{d}{ds}\left[\frac{1}{1+\lambda} - 2\,\log(\lambda) + \log(1+\lambda) - \log(\Sigma)\right] = 0\,. \tag{A.23}$$

Given that $p_0 = \Sigma/\lambda$, it follows

$$\left(1+\frac{p_0}{\Sigma}\right)\frac{p_0}{\Sigma}\,\exp\left(\frac{1}{1+\Sigma/p_0}\right)\frac{1}{\Sigma} = \text{Const.} \tag{A.24}$$

which in the low temperature limit gives $\Sigma^{-2}p_0 = \text{Const}$. This corresponds to the correct adiabatic index $\gamma = (2+2)/2$.

B. Distribution functions for counter-rotating relativistic disks

For counter rotating disks in the absence of gravomagnetic forces, the inversion for distribution functions given in section 4.1 can be carried in close analogy to the Newtonian method given by Pichon & Lynden-Bell (1995) [20], and is sketched here. The relativistic flow is characterised by its stress energy tensor, $T^{(\alpha\,\beta)}$, which, in Vierbein components, reads

$$T^{(\alpha\beta)} = \int\int \frac{f_\star\,(\epsilon,h)\;P^{(\alpha)}\,P^{(\beta)}}{P^{(t)}}\,dP^{(R)}dP^{(\phi)}\,. \tag{B.1}$$

From the geodesic equation it follows that

$$P^\mu P_\mu = -1 \quad \Rightarrow \quad P^{(R)} = \frac{1}{\sqrt{\gamma_{tt}}}\left[\epsilon^2 - h^2\,\gamma_{tt}/\gamma_{\phi\phi} - g_{tt}\right]^{1/2}\,, \tag{B.2}$$

where the line element in the disk is taken to be

$$ds^2 = -\gamma_{tt}\,dt^2 + \gamma_{RR}\,dR^2 + \gamma_{\phi\phi}\,d\phi^2\,. \tag{B.3}$$

Differentiating Eq. $(B.2)$ implies

$$\frac{dP^{(R)}}{P^{(t)}} = \frac{d\epsilon}{\left[\epsilon^2 - h^2\,\gamma_{tt}/\gamma_{\phi\phi} - \gamma_{tt}\right]^{1/2}}\,, \quad \text{while} \quad dP^{(\phi)} = \frac{dh}{\sqrt{\gamma_{\phi\phi}}}\,, \tag{B.4}$$

where the differentiation is done at constant R and h , and R and ϵ respectively. Combinations of Eqs. $(B.1)$ lead to

$$\Lambda = {\gamma_{\phi\phi}}^{1/2}\,\left(T^{(tt)} - T^{(\phi\phi)} - T^{(RR)}\right) = \int\int \frac{f_\star\,(\epsilon,h)\;dh\,d\epsilon}{\sqrt{\epsilon^2 - h^2\gamma_{tt}/\gamma_{\phi\phi} - \gamma_{tt}}}\,, \tag{B.5a}$$

$$\Delta = {\gamma_{\phi\phi}}^{3/2}\,T^{(\phi\phi)} = \int\int \frac{h^2\,f_\star\,(\epsilon,h)\;dhd\epsilon}{\sqrt{\epsilon^2 - h^2\gamma_{tt}/\gamma_{\phi\phi} - \gamma_{tt}}}\,. \tag{B.5b}$$

Note that Eq. $(B.5a)$ corresponds to Tolman's formula [23] which yields be integration the total gravitating mass of the disk. Introducing

$$\mathcal{R}^2 = \gamma_{\phi\phi}/\gamma_{tt}\,, \quad e = \frac{1}{2}\left(\epsilon^2 - 1\right)\,, \quad \Psi = \frac{1}{2}\left(1 - \gamma_{tt}\right) \quad \text{and} \quad \hat{f}_\star\left(e,h\right) = \frac{f\left(\epsilon,h\right)}{\epsilon}\,, \tag{B.6}$$

gives, for Eqs. $(B.5)$:

$$\Lambda = \int\int \frac{\hat{f}_\star\left(e,h\right)\,dhde}{\left[2\left(e+\psi\right) - h^2/\mathcal{R}^2\right]^{1/2}} \quad \text{and} \quad \Delta = \int\int \frac{h^2\,\hat{f}_\star\left(e,h\right)\,dhde}{\left[2\left(e+\psi\right) - h^2/\mathcal{R}^2\right]^{1/2}}\,. \tag{B.7}$$

Eq. $(B.7)$ is formally identical to Eq.(2.9) of Pichon & Lynden-Bell [20], replacing $(\Lambda, \Delta, \hat{f}_\star, \mathcal{R}, e, \Psi)$ by $(R\,\Sigma, R^3\,p_\phi,\ f, R, \epsilon, \psi)$. In fact $(\Lambda, \Delta, \hat{f}_\star, \mathcal{R}, e, \Psi)$ tends to $(R\,\Sigma, R^3\,p_\phi,\ f, R, \epsilon, \psi)$ in the classical regime. Introducing the intermediate functions $\hat{F}(h, \mathcal{R})$, which is chosen so that its moments satisfy Eqs. $(B.5)$, and following the classical prescription of Pichon & Lynden-Bell [20] yields

$$\hat{f}\left(e,h\right) = \frac{1}{\pi}\int_{\mathcal{R}_e}^{\mathcal{R}_p} \frac{\left(\partial\hat{F}/\partial\mathcal{R}\right)_h\,d\mathcal{R}}{\sqrt{h^2/\mathcal{R}^2 - 2\Psi - 2e}} - \frac{1}{\pi}\int_{\mathcal{R}_a}^{\infty} \frac{\left(\partial\hat{F}/\partial\mathcal{R}\right)_h\,d\mathcal{R}}{\sqrt{h^2/\mathcal{R}^2 - 2\Psi - 2e}}\,, \tag{B.8}$$

where $\mathcal{R}_p(h,e)$, and $\mathcal{R}_a(h,e)$ are respectively the apogee and perigee of the star with invariants (h,e), and $\mathcal{R}_e(h)$ is the inner radius of a star on a "parabolic" (zero e energy) orbit with momentum h. Eq. $(B.8)$ provides direct and systematic means to construct families of distribution function for counter-rotating disks characterised by their stress-energy tensor in the plane. Note that in contrast the dragging of inertial frames requires to fix three moments of the velocity distribution to account for the given energy density, pressure law and rotation law.

C. Distribution functions for rotating disks: Lorentzian in momentum

A possible choice for $\bar{F}$ is a Lorenzian parametrised in width, p_2, mean, p_1 and amplitude, p_0 such that

$$\bar{F}\left(v_\phi, R\right)dv_\phi = \frac{p_0\,p_2\,\pi^{-1}\,dp}{p_2^2 + \left(p - p_1\right)^2}\,, \quad \text{where} \quad p = \frac{v_\phi}{\sqrt{1 - v_\phi^2}} \quad \text{and} \quad v_\phi = e^\nu\left(\chi - \omega\right)/R_c\,. \tag{C.1}$$

The explicit function of v_ϕ is found using $dp = dv_\phi/(1 - v_\phi^2)^{3/2}$. In this instance, Eq. (4.12) becomes

$$T^{(tt)}\,e^{4\nu} = \frac{p_0\,p_2}{\pi}\int_{-\infty}^{\infty} \frac{dp}{\left({p_2}^2 + \left(p - p_1\right)^2\right)} = p_0\,, \tag{C.2a}$$

$$T^{(t\phi)}\,e^{4\nu} = \frac{p_0\,p_2}{\pi}\int_{-\infty}^{\infty} \frac{p\,dp}{\sqrt{1+p^2}\,\left({p_2}^2 + \left(p - p_1\right)^2\right)} = \mathcal{G}\left(p_0, p_1, p_2\right)\,, \tag{C.2b}$$

$$T^{(\phi\phi)}\,e^{4\nu} = \frac{p_0\,p_2}{\pi}\int_{-\infty}^{\infty} \frac{p^2\,dp}{\left(1+p^2\right)^2\,\left({p_2}^2 + \left(p - p_1\right)^2\right)} = \frac{p_0\left(p_2 + {p_2}^2 + {p_1}^2\right)}{\left(1 + p_2\right)^2 + {p_1}^2} \tag{C.2c}$$

where $\mathcal{G}(p_0, p_1, p_2)$ is given by Eq. $(C.4)$ bellow. The inversion of Eqs. $(C.2)$ for (p_0, p_1, p_2), together with Eqs. $(C.1)$, (4.14) and Eq. $(4.3c)$ yields the distribution function of a Lorenzian flow compatible with the energy distribution imposed by the metric (ν, ζ, ω) and the cut $z = f(R)$. This inversion is always achievable provided the energy conditions Eq. (3.12) are satisfied.

More generally, families of distributions functions corresponding to azimuthal momentum distribution such as $2p_2^3\,p_0\,\pi^{-1}/(p_2^2 + (p-p_1)^2)^2, 8p_2^5\,p_0\,(3\pi)^{-1}/(p_2^2 + (p-p_1)^2)^3 \cdots$ are readily derived in a similar manner while differentiating the *r.h.s.* of Eq. $(C.2)$ with respect to p_2^2. These higher order distributions have all vanishing number of stars with azimuthal velocity close to the velocity of light. This parametrisation is illustrated for the Kerr disk on Fig. 7.5.

C.1. The quadrature for $\mathcal{G}(p_0, p_1, p_2)$

Changing variables to u such that $p = (u - 1/u)/2$ Eq. $(C.2b)$ becomes

$$\mathcal{G}\left(p_0, p_1, p_2\right) = \frac{2p_0\, p_2}{\pi} \int_0^\infty \frac{\left(u^2-1\right)\, du}{4{p_2}^2\, u^2 + \left(u^2 - 1 - 2p_1\, u\right)^2} \tag{C.3}$$

This integral is then carried and yields

$$\begin{aligned}\mathcal{G}\left(p_0, p_1, p_2\right) = & \frac{p_0\left(p_2 + i\, p_1\right)\, \log\left(-2\, i\, p_2 + 2\, p_1 - 2\sqrt{1 + \left(-i\, p_2 + p_1\right)^2}\right)}{2\sqrt{1 + \left(-i\, p_2 + p_1\right)^2}\, \pi} + \\ & \frac{p_0\, \left(i\, p_2 - p_1\right)\, \log\left(-2\, i\, p_2 + 2\, p_1 + 2\sqrt{1 + \left(-i\, p_2 + p_1\right)^2}\right)}{2\sqrt{1 + \left(-i\, p_2 + p_1\right)^2}\, \pi} + \frac{p_0(p_2 - i\, p_1)\, \log\left(2\, i\, p_2 + 2\, p_1 - 2\sqrt{1 + \left(i\, p_2 + p_1\right)^2}\right)}{2\sqrt{1 + \left(i\, p_2 + p_1\right)^2}\, \pi} + \\ & \frac{p_0\, \left(i\, p_1 - p_2\right)\, \log\left(2\, i\, p_2 + 2\, p_1 + 2\sqrt{1 + \left(i\, p_2 + p_1\right)^2}\right)}{2\sqrt{1 + \left(i\, p_2 + p_1\right)^2}\, \pi}\end{aligned} \tag{C.4}$$

D. The relativistic epicyclic frequency

The equation for the radial oscillations follows from the Lagrangian

$$\mathcal{L} = -\sqrt{e^{2\nu}\, \left(\dot{t} - \omega\dot{\phi}\right)^2 - e^{2\zeta - 2\nu}\, \left(1 + f'^2\right)\, \dot{R}^2 - \, e^{-2\nu}\, \dot{\phi}^2 R^2}, \tag{D.1}$$

where $\dot{(\quad)}$ stands here for derivation with respect to the proper time τ for the star describing its orbit. In Eq. $(D.1)$, ϕ and t are ignorable which leads to the invariants:

$$\frac{\partial \mathcal{L}}{\partial \dot{\phi}} = h \qquad \frac{\partial \mathcal{L}}{\partial \dot{t}} = -\epsilon. \tag{D.2}$$

The integral of the motion for the radial motion follows from Eqs. $(D.2)$ and $U^\mu U_\mu = -1$, namely:

$$e^{2\zeta - 2\nu}\, \left(1 + f'^2\right) \dot{R}^2 + \frac{e^{2\nu}}{R^2} \left(h - \epsilon\, \omega\right)^2 - \epsilon^2 e^{-2\nu} = -1$$

This equation, together with its total derivative with respect to proper time provides the radial equation of motion, having solved for the angular momentum h and the energy ϵ of circular orbits as a function of radius when equating both $\dot{R}$ and $\ddot{R}$ to zero. the relativistic generalisation of the classical epicyclic frequency is defined here to be the frequency of the oscillator calling back linear departure from circular orbits. Hence the equation for radial perturbation reads

$$\delta\ddot{R} + \kappa^2 \delta R = 0, \tag{D.3}$$

which gives for κ^2 :

$$\begin{aligned}\kappa^2 = & e^{-2Z}\, \left(Z'' - 2Z'^2\right) - \epsilon^2 e^{-2L}\, \left(L'' - 2L'^2\right) - \\ & e^{2K}\, \left[\, \left(h - \epsilon\omega\right)^2 \left(K'' + 2K'^2\right) - \epsilon\, \left(h - \epsilon\omega\right)\, \left(4K'\omega' + \omega''\right) + \epsilon^2 \omega'^2\, \right],\end{aligned} \tag{D.4}$$

where $(\quad)'$ stands in this Appendix for $d/dR \equiv \partial/\partial R + f'\,\partial/\partial z$ and L, K, and Z are given in terms of the potential ζ and ν by:

$$L = \zeta + \log\sqrt{1+f'^2}, \tag{D.5a}$$

$$Z = \zeta + \log\sqrt{1+f'^2} - \nu, \tag{D.5b}$$

$$K = 2\nu - \zeta - \log\sqrt{1+f'^2} - \log R. \tag{D.5c}$$

Here ϵ and h are known functions of R given by the roots of:

$$\dot{R} = 0 \quad \Rightarrow \quad e^{-2L}\epsilon^2 = (h - \epsilon\,\omega)^2\, e^{2N} + e^{-2Z}, \tag{D.6a}$$

$$\ddot{R} = 0 \quad \Rightarrow \quad e^{-2Z}Z' = e^{-2L}L'\epsilon^2 + (h-\epsilon\omega)\, e^{2N}\left[(h-\epsilon\,\omega)\,N' - \epsilon\,\omega'\right]. \tag{D.6b}$$

E. Correction to Lemos' Self-Similar Disk

The result given in section 6.1 agrees with that of Lemos, having made the following agreed corrections to his solution:

- Eq.(L 3.14) should read: $(k+n)\cot\frac{1}{2}(k+n)\pi = -4\pi p_{*rr}$ with a minus sign, because the integration of θ is carried downwards. This gives $n + k \geq 1$ for the disks with positive pressures.
- Lemos gives the stress energy tensor integrated through the plane using coordinate increment rather than proper length. Our result gives the latter which has an extra factor $\exp(\zeta - \nu)$ and gives the physical energy tensor per unit area.
- The exponent of $\cos[(n+k)\pi/2]$ is $2n(k-n)/(n+k)^2$ rather than $4n(1-2n)/(k+n)^2$.